Orientation-Indepedent Wireless Charging of Multiple Mobile Devices At a Distance

by

Lixin Shi

Submitted to the Department of Electrical Engineering and Computer Science
in partial fulfillment of the requirements for the degree of

Doctor of Philosophy

at the

MASSACHUSETTS INSTITUTE OF TECHNOLOGY

February 2016

Signature redacted

Author .....
Department of Electrical Engineering and Computer Science
September 18, 2015

Signature redacted

Certified by .....
Dina Katabi
Andrew and Erna Viterbi Professor
Thesis Supervisor

Signature redacted

Accepted by .....
Leslie A. Kolodziejsk
Chairman, Department Committee on Graduate Theses

Orientation-Indepedent Wireless Charging of Multiple Mobile Devices At a Distance

by

Lixin Shi

Submitted to the Department of Electrical Engineering and Computer Science
on September 18, 2015, in partial fulfillment of the
requirements for the degree of
Doctor of Philosophy

Abstract

Each year, consumers carry an increasing number of mobile devices on their person: mobile phones, tablets, smartwatches, etc. As a result, users must remember to recharge each device, every day. Wireless charging promises to free users from this burden, allowing devices to remain permanently unplugged. Today's wireless charging, however, is either limited to a single device, or is highly cumbersome, requiring the user to remove all of her wearable and handheld gadgets and place them on a charging pad.

This thesis proposes MultiSpot, a new wireless charging technology that can charge multiple devices, even as the user is wearing them or carrying them in her pocket. A MultiSpot charger acts as an access point for wireless power. When a user enters the vicinity of the MultiSpot charger, all of her gadgets start to charge automatically. It achieves this by tracking multiple receivers and focusing the magnetic field from multiple transmit coils in a provably optimal way. We have prototyped MultiSpot and evaluated it using off-the-shelf mobile phones, smartwatches, and tablets. Our results show that MultiSpot can charge six devices at distances of up to 50 cm.

Thesis Supervisor: Dina Katabi
Title: Andrew and Erna Viterbi Professor

Acknowledgments

First and foremost, I would like to thank my adviser Prof. Dina Katabi. Without her guidance I would not have been able to finish this thesis. She provided me with invaluable guidance and generous help; whenever I felt lost or had problems, I would turn to her and she would always give me prompt and helpful feedback. Her guidance and help have gone beyond research and include career advice and suggestions on how to become a better collaborator. I have thoroughly enjoyed working with her and learning from her. The past four years that I worked with her have shaped me as a research and as a person and I am sure what I have learned here will continue to positively affect my future life.

I am grateful to Prof. David Perreault. Before I started the project that led to this thesis, I knew very little about power electronics. He taught me with great patience and clarity. He shared his incredible passion for efficient circuits and elegant system design with me for which I am very grateful. Furthermore he was willing to walk through the detailed design and implementation of key circuits with me which helped make this thesis possible.

I would also want to thank my thesis committee, Prof. Dina Katabi, Prof. David Perreault, and Prof. Hari Balakrishnan, for the inspiring discussion and comments on my thesis. I am in debt to my collaborators in the projects contained in this thesis: Zach Kabelac, thanks for tolerating me blowing up the circuits from time to time due to my unsteady hands; John MacDonald, thanks for revising my drafts and listening to my random and sometimes meaningless ideas, and I look forward to the following years of working with you, which I am sure will be enjoyable and fruitful.

I also want to thank everyone in the NETMIT group, Omid Abari, Fadel Adib, Ezzeldin Hamed, Chen-Yu Hsu, Haitham Hassanieh, Zach Kabelac, Swarun Kumar, Hariharan Rahul, Deepak Vasisht, Jue Wang. And thanks Mary for feeding us before deadlines, and helping us over all the administrative hurdles that came up along the way.

And, I am deeply grateful to my parents and my sister, for supporting me in the

past 24 years in my life unconditionally. Even though some of my decisions surely sounded ridiculous, they have shown great patience; they have given me the freedom to do the things I want and pursue my dreams. The help and support they give me go far beyond what I can possibly repay in my lifetime.

And of course, Mia — I will for sure reserve a paragraph for you. I can not imagine what life would have been if I had not met with you 10 years ago. Your presence to me has been my greatest source of confidence to go forward.

Contents

List of Figures

List of Tables

List of Algorithms

Chapter 1

Introduction

1.1 Wireless Power Hotspot

Our daily lives rely on a multitude of personal mobile devices, such as phones, tablets, and wearables. While new devices have made our lives easier in many respects, having to remember and manage to charge all of our mobile devices is a recurring and increasingly significant burden. If we could wirelessly charge our devices, it would alleviate this daily anxiety, and may even allow such devices to be permanently unplugged. While previous work has taken initial steps towards this goal, it either remains limited to a single device at a time [55, 82, 3], or requires forms factor that are too large to fit within mobile devices [66], or is extremely cumbersome requiring the user to remove all of her wearable and handheld gadgets and place them physically on top of a charging pad [4, 5], as in Fig. 1-1.

Imagine, however, if one had a single wireless charger that was able to charge all of its surrounding devices simultaneously, even if they were on the user's body or in her purse. In some sense, this would be analogous to a short-range WiFi hotspot –i.e., the wireless charger would act as a power access point; once the user enters the vicinity of the charger, her devices start receiving power as needed, and if she moves away the charging stops. One could use such a charger as a desk mat. Whenever the user sits at her desk, the iPhone in her pocket, the tablet in her purse, and the smartwatch on her wrist would charge automatically without even thinking of them,

(a) Multi-Phone Charger (b) Smartwatch Charger

Figure 1-1: **Today's Wireless Charging:** Today's wireless chargers require careful placement of each device on the charging pad.

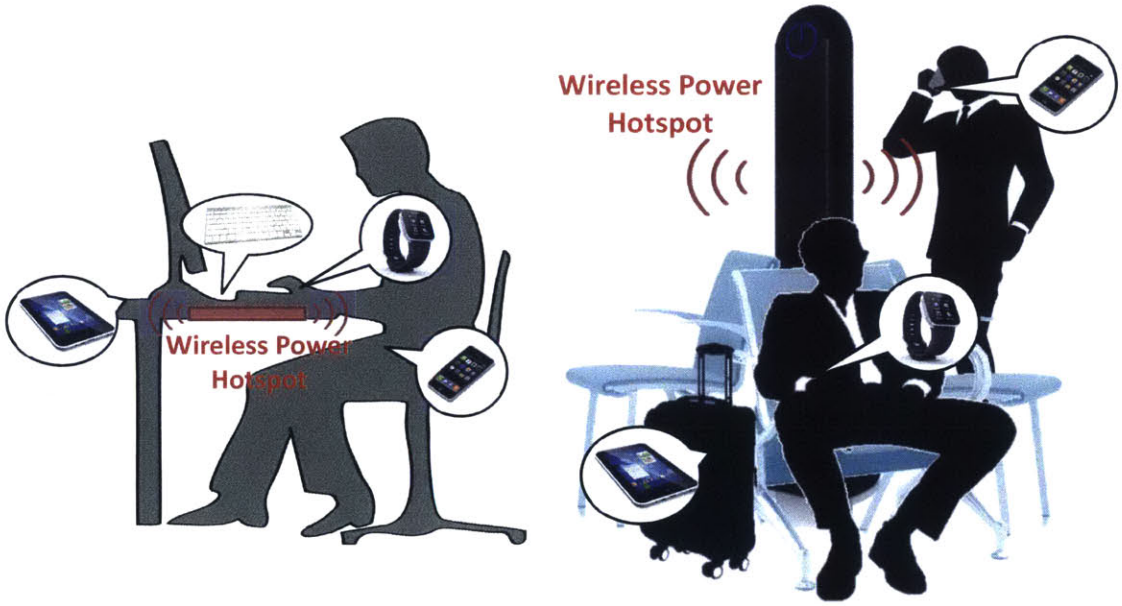

(a) Desktop Charging Hotspot (b) Airport Charging Hotspot

Figure 1-2: **Wireless Power Hotspot:** (a) MultiSpot acts as a wireless power hotspot. Mounted as a desk mat, it is able to charge all surrounding personal electronics, including cellphones, tablets, smartwatches, ereaders, wireless keyboards and touchpads. (b) Wireless power hub in an airport charges travelers' electronic devices in their pockets or suitcases. Furthermore it allows travelers to continue using their devices while simultaneously charging without the encumbrance of a cable.

as shown in Fig. 1-2a. Power hotspots could also be placed in airports and train stations to eliminate the struggle that users today have as they fight over the plug and are forced to stop using their favorite devices while they are tethered to the wall.

Specifically, an ideal wireless power hotspot should have the following properties:

1) it can charge multiple devices simultaneously; 2) it is able to charge the device in any location/orientation combination as they exist in the real world – on the user's wrist, in the user's pocket or tossed haphazardly on the table. In this thesis, we will show first that it is possible to create such a wireless power hotspot, second to explore the numerous challenges encountered in attempting to implement such a system in the real world and third and in depth examination of a system that addresses these challenges and delivers on the promise in real world environments – MultiSpot.

1.2 How to Deliver a Wireless Power Hotspot?

As we investigate the answer to this question, we focus on charging via magnetic coupling because it is the approach already adopted by the wireless power standards [25, 10], it is the base technology underlying all consumer implementations of wireless charging to date, and it is deemed safe and compliant with FCC rules [59].[1] In magnetic coupling, the power transmitter uses one or more coils. When an AC current traverses the transmitter's coil, it creates a variable magnetic field. If this magnetic field traverses a nearby coil, it generates an electric current, hence delivering power to that device. The stronger the magnetic field is at the receiver, the more power is delivered. The challenge, however, is that the magnetic field attenuates very quickly with distance, and hence typical wireless charging devices operate at very short distances of several centimeters [25, 17].

Our approach builds on a recent idea called magnetic beamforming [55], where multiple coils on the transmitter act as a multi-antenna system, shaping the magnetic field in a beam and focusing it on the receiver, in a manner similar to beamforming in MIMO (Multi-Input Multi-Output) systems.[2] This initial idea has been demon-

[1] In particular, we use magnetic resonance [10]. Some start-ups have advocated the use of RF radiation [15, 2], ultrasound [26], or lasers [16] for wireless power transfer. None of those approaches have made it into the standards for consumer electronics. Further, charging consumer electronics, e.g., phones, using RF or lasers raises safety concerns [48, 99] (for further details see §2).

[2] The term "magnetic beamforming" in [55] and this thesis refers to shaping the magnetic flux in the near field in the form of a beam (or multiple beams). In contrast, traditional beamforming in wireless communication systems operates over radiated waves in the far field. This difference is critical to understanding why it is a non-trivial difference in the fundamental physics upon which the respective systems rely.

strated for *a single receiver*, where beamforming of the magnetic field can increase the charging range up to 40 cm and allow for a flexible phone orientation [55].

At first blush, it might seem that one can beamform the magnetic field to multiple receivers by directly borrowing from multi-user MIMO. Unfortunately, there is an intrinsic difference between multi-user MIMO in RF communications and the physics of wireless charging. Specifically, consider the effect of introducing multiple receivers. In a conventional wireless communication system, each receiver is a passive listener that only receives signals. In contrast, in a wireless charging system, receivers interact with each other. A receiver not only accepts power, but also reflects power back to the transmitters and other receivers. The presence of a receiver affects the magnetic field observed by other receivers and transmitters. As a result, adding, removing, or moving just a single receiver in the system affects all of the other receivers, which is typically negligible in RF communication systems. In fact not accounting for these interactions can lead to large errors in shaping the magnetic field and consequent charging failures, as we show in §8.3. One therefore needs to account for these fundamental differences between the models of multi-user RF channels and multi-receiver magnetic channels, while formulating and solving the magnetic charging problem.

This thesis introduces MultiSpot, a multi-coil power transmitter that can beam its magnetic field toward multiple power receivers simultaneously and is able to cope with changing real-world environments in real time. MultiSpot formulates the multi-receiver magnetic charging problem and derives a provably optimal solution whose equations account for inter-receiver interactions. By shaping the magnetic field into beams and focusing them towards the receivers, MultiSpot can significantly increase the range of multi-receiver wireless charging. Further, by steering the beams with receiver motion and orientation, MultiSpot can accommodate a flexible charging pattern capable of charging a smartwatch on the user's wrist, a phone in her hand, and a tablet in her purse – simultaneously and even while some of the devices are in motion.

1.3 The MultiSpot System

As developed in this thesis, the MultiSpot system has the following key features:

1. MultiSpot is analytically proven to maximize the coil-to-coil power delivery efficiency to the receivers, by minimizing the power loss at the transmitters. Said differently, given a particular topology of the transmit and receive coils (and hence their resulting magnetic couplings), MultiSpot delivers a closed-form solution that sets the charging parameters to guarantee maximum power delivery to the receivers' coils. In the case that each receiver may require different amount of power, MultiSpot can maximize the efficiency (i.e., minimizing the power loss on the transmitters) while delivering the exact amount of power specified by each receiver.

2. MultiSpot's solution is adaptive. It adjusts to movements of the receivers and re-converges to the optimal solution. In our implementation, MultiSpot adapts to receivers' movements in just a few milliseconds.

3. A MultiSpot charger employs a non-interruptive channel estimation method. Like in the traditional MIMO system, beamforming requires the transmitter to know the channels. Communication systems use a channel estimation phase, where the transmitter pauses data transmission and the time is dedicated solely to estimating the channels[3]. In MultiSpot, we will show that this is no longer necessary. The transmitter can non-interruptedly beamform to the receiver, without having to stop and dedicate extra time to estimate the channel. This is critically important where time spent in channel estimate means time not delivering power and especially in the case of multiple and moving receivers could result in a dramatic lengthening of charging time.

4. MultiSpot can deliver power simultaneously to a large variety of devices, even if their power level is orders of magnitude different. For example, MultiSpot can

[3]In communication systems, there are commonly two ways: 1) the transmitter transmits known signals so that the receiver can measure the channel and send it back; 2) the receiver transmits known signals to the transmitter and transmitter infers reciprocal channels. [90]

deliver 10W to a tablet and 0.1W to a wearable sensor at the same time, without overloading the low-power device or underpowering the high-power device. This requires MultiSpot to have the ability to fine-tune and manipulate the strength of the magnetic field in space with reasonably high resolution, specifically forming high-density magnetic fields at a high-power device and low-density magnetic fields at a low-power device.

5. MultiSpot's design also features several innovative circuit designs.

    - Power converters with high efficiency and high reliability, delivering tens of watts at moderately high frequencies (MHz range frequency), which is generally considered to be particularly challenging [81].
    - Real-time high-accuracy sensing circuits to sense the circuit parameters in the Tx circuits. This is the key to the accuracy of the whole system. Specifically, since the circuits themselves are in the magnetic fields generated by the Tx coils, dealing with the electro-magnetic interferences that is created is a major challenge.

Implementation and Results: We built a prototype of MultiSpot and evaluated it with smart phones, a smartwatch, and a tablet. We also compared MultiSpot to multiple baselines: Duracell Powermat [4], Energizer Qi [5] and LUXA2 [12], and a reference design by WiTricity called WiT-5000 [17]. Our results show the following:

- MultiSpot can charge 6 devices at distances up to 50 cm, whereas the baselines are limited to 2 devices at 5cm.
- MultiSpot charges different types of devices simultaneously. When attached to an office desk, and with the user sitting at the desk, MultiSpot simultaneously charged a smartwatch on the user's wrist, an iPhone in her pocket, and a nearby tablet, keyboard, and touchpad.
- MultiSpot's charging time is lower than all wireless charging baselines, for the same distance. The charging time depends on distance. For distances less than

20 cm, MultiSpot charges two phones from dead batteries to full charge in less than 1.5x of the time taken for wired charging. The charging time increases to 3x when the phones are 35cm away from the charger, and 5x when they are 50cm away.

- We also examined MultiSpot's ability to control the amount of power delivered to each device. We show that MultiSpot can deliver the exact amount of power within $\pm 5\%$, across a large range of specified power for different kinds of devices from wearables ($<$1W) to tablets (10W).

- Interestingly, the presence of multiple receivers can increase the range of power transfer. We show that the maximal range is 10cm larger with two phones than it is with one phone, and 17cm larger with 4 phones.

- Finally, we compare MagMIMO [55] to MultiSpot in the presence of two phones. Our results show that MagMIMO's charging time is comparable to MultiSpot *only* when the two phones are co-located and hence can be considered as one device. Otherwise, MagMIMO takes an order of magnitude longer time or might fail to charge one of the phones altogether. This is because MagMIMO has no mechanism to disentangle the magnetic couplings of different receivers, and hence in the presence of multiple receivers it can fail to compute the correct beamforming solution.

1.4 Contributions & Organization

Contributions: This thesis presents theoretical analysis, algorithms, and power electronics that name MultiSpot to deliver the features explained in 1.3, including:

- A system that delivers the wireless power hotspot vision, which can charge multiple devices, including mobile phones and wearables, in any dynamic orientation within a half-meter range from the base.

- A set of provably optimal solutions to maximize coil-to-coil efficiency of wireless power delivery to multiple receivers by shaping the magnetic field of a multi-coil power transmitter. Considered scenarios include 1) maximizing total delivered power to the receivers; or 2) delivering to each receiver a specified amount of power that is not necessarily the same among receivers.

- Algorithmic designs and real-time implementations to allow the system to adapt gracefully to receiving devices' motion in a dynamic environment.

- The ability to deliver power to receiving devices with orders of magnitude different power requirements, which is enabled by MultiSpot's ability to strengthen or weaken the magnetic field at specific location in space and orientation combination with respect to the transmitter.

- Innovative power electronics circuit design, PCB layout and implementation of the underlying circuit, and empirical evaluation with off-the-shelf devices including smart phones, a smart watch, a Fitbit, a tablet, a wireless keyboard, and a wireless touchpad.

- Discussion about how to design transmitter and receiver coils to meet the requirements of range and use case desirable for the office-desk power hotspot vision.

Organization: The rest of this dissertation is organized as follows: §2 reviews the existing literature on wireless charging, and provides background to understand the rest of the thesis. §3 develops the most basic circuit equations and formulations that are used throughout this thesis. §4 and §5 describe the core system, however with different focuses: §4 explains the basic magnetic beamforming solution under the goal of maximizing total power delivered to all receivers; §5 extends this solution to be able to control the amount of power to each receiver – this is specifically useful when receivers with very different power requirements exist at the same time. §6 discusses issues and design choices related to transmitter and receiver coils. §7

describes the power electronics circuit implementation of the system. and §8 presents the experimental results.

Chapter 2

Background & Related Work

Wireless power transfer has spread across a vast array of fields expanding the capabilities of devices such as phones [4, 7, 82], wearables [46, 88], medical implants [69, 63, 64], electric vehicles [70, 54], sensors [89, 97, 28, 29, 83], etc. In this chapter, we will focus on describing the landscape of existing wireless charging technologies and how they are different from what is proposed in this thesis.

2.1 Wireless Charging via Magnetic Coupling

2.1.1 Basic Inductive & Resonant Charging

The most widespread approach for wireless charging of consumer devices is based on magnetic coupling. In fact, magnetic coupling is used in all commercial wireless chargers for phones and smartwatches [3, 9], as well as current industry standards [25, 10]. In this approach, the transmitter coil, made of copper or other conductive materials, is driven by an ac current to generate an oscillating magnetic field. When another conductive coil is placed within range of the transmitter, some of the magnetic field passes through the center of its coil. This field induces an ac current on the receiver, which can be used to power the device, as demonstrated by Fig. 2-1a.

This basic methodology of magnetic coupling, which we refer to as *magnetic induction*, is employed by most earlier products [7]. However, recent products are

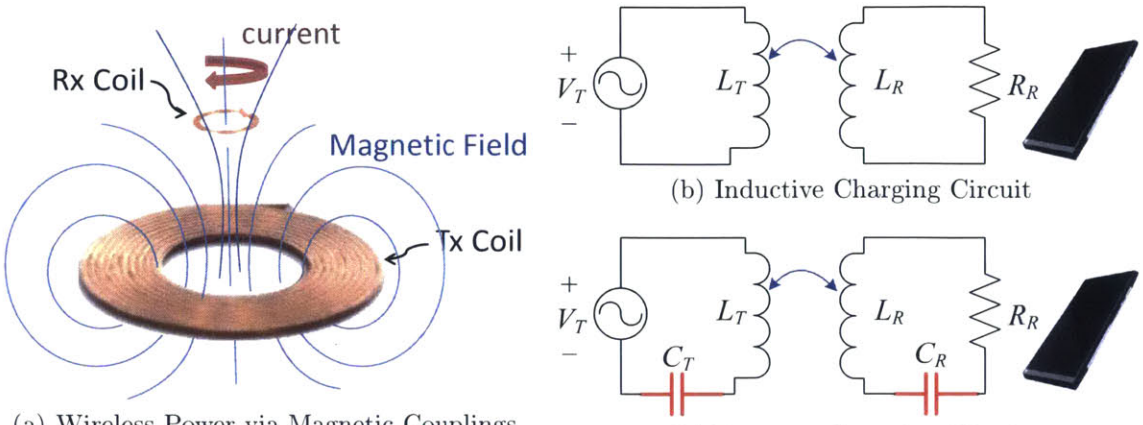

(a) Wireless Power via Magnetic Couplings

(b) Inductive Charging Circuit

(c) Resonant Charging Circuit

Figure 2-1: **Demonstrations of Basic Wireless Charging Systems:** a) demonstration of the physics of magnetic coupling; b) & c): resonant charging circuits have resonant capacitors in series which allows the energy to resonate back and forth between the coils and capacitors, thus improving the efficiency of the system.

moving towards a new technique called *magnetic resonance* [65], in which a capacitor is added to the transmitter and receiver circuits to make them resonate at the same frequency. The oscillations cause the circuits to resonate back and forth without consuming much energy. Specifically, this enables large leakage impedances as seen at the ports of the magnetic circuit to be nulled, and – in some cases – for magnetizing current for the magnetic circuit to be delivered using a simple capacitor rather than the external power electronics, improving efficiency. Fig. 2-1 shows the differences between inductive and resonant charging in terms of circuit schematics. Magnetic resonance is the underlying power transfer mechanism used in MultiSpot.

However, both inductive and resonant charging suffer from severe range and orientation limitations:

- Range: magnetic field attenuates cubically with distance [99], as shown by Fig. 2-2, where a receiver at any distance from the transmitter that is larger than the diameter of the transmit coil receives less than 10% of the magnetic field at the center of the coil. As a result, charging a receiver using the circuit shown in Fig. 2-1b and Fig. 2-1c will not yield an effective distance that is sufficient for most use cases. Practical systems to charge phones and similar consumer devices are limited to distances of a few centimeters [4, 5, 12]. Example of wireless

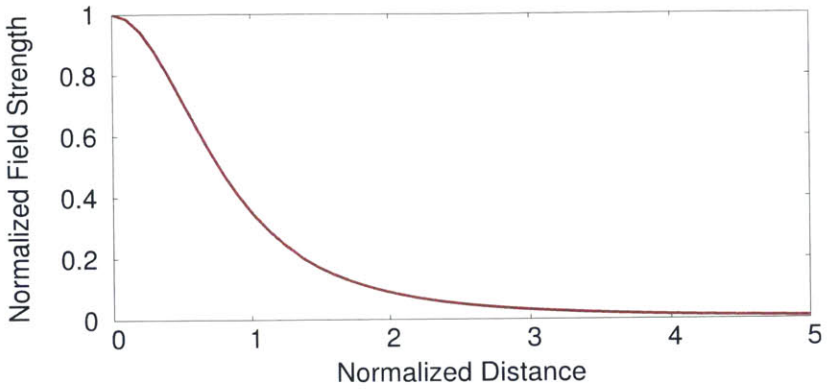

Figure 2-2: **Degradation of Magnetic Field vs. Distance:** The degradation of the strength of magnetic field, where the measurement point is vertically above the center of a current loop. The horizontal axis is the distance from the receiver to the current loop, normalized by the radius of the current loop; the vertical axis is the magnetic field strength normalized by the strength at the center of the loop.

power delivery over longer distances either requires a very big receiver coil that is impractical to fit in the back of a phone or the strap of a smartwatch [44, 45, 60, 61], or delivers very little power such that it is only useful for small LEDs [24] or sensors [68] that operate at tens to a couple hundred milliwatts. In contrast, a typical phone battery requires at least a few watts [22].

- Orientation: magnetic fields have its own directionalities that result in charging receivers in some particular directions very challenging. To see why, consider the cases presented in Fig. 2-3: in both cases the receiver is at the same location but with different orientations. In the case when the receiver is aligned with the transmitter (Fig. 2-3a), the magnetic flux goes through the receiver coil orthogonally thus maximizing the amount of power that the receiver could receive. However, in the case when the receiver is perpendicular (Fig. 2-3b), no magnetic flux will go through the receiver coil and hence no power will be delivered.

2.1.2 Charging Multiple Devices

Commercial product that can charge multiple devices today [12, 4, 17] all take a very simple approach: they concatenate different transmit coils together, and dedicate

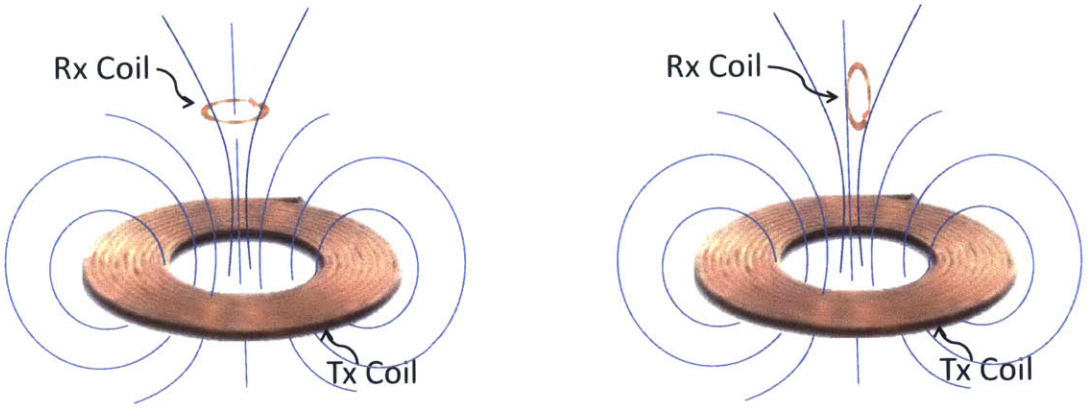

(a) Aligned Tx/Rx with Maximum Flux Linkage

(b) Orthogonal Tx/Rx with Almost Zero Flux Linkage

Figure 2-3: **Impact of Different Receiver Orientations:** (a) Receiver receives maximal power when it is aligned with the Tx; (b) Receiver cannot receive any at all due to perpendicular Tx/Rx coils.

each transmit coils to a single receiver. In practice, a user has to align each of her devices carefully to each transmit coil in order to charge her devices. This removes the key benefit of a wireless power hotspot which is that a user can have her devices passively charged without any direct actions on her part to bond a receiving device to a transmitter.

Academic research has taken important steps towards wirelessly delivering power to multiple receivers using magnetic coupling. We distinguish between two system classes:

- The first class can deal with a small receiver coil that fits in the back of a phone or the strap of a smartwatch and achieve a maximum distance of 10 cm [44, 45, 60, 61].

- The second class can deliver power at larger ranges up to 30cm [31, 66, 32], but they require large receiver coils that could not possibly fit on the back of a phone or wearable.

In addition, both classes assume the receiver coil is aligned with the transmitter coil, and do not deal with different receiver orientations with respect to the transmitter. In practice, however, the user cannot benefit from an increase in charging distance if she

Work	Rx Size	Range	Orientation Studied
[31]	Big (22.5cm x 31.5cm)	30cm	Only Aligned
[33]	Big (22.5cm x 31.5cm)	70cm	Only Aligned
[34]	Big (18cm x 16cm)	15cm	Only Aligned
[66]	Big (30cm Diameter, 18cm Height)	28cm	Only Aligned
[44]	Small (1.3cm Diameter)	0-1cm	Only Aligned
[45]	Small (7cm x 8cm)	<1cm	Only Aligned
[60]	Small (4.6cm Diameter)	12mm	Only Aligned
[82]	Small (Fitted o a phone)	10cm	Only Aligned

Table 2.1: **Comparison of Selected Research Work on Wireless Charging:** Existing research work either deals with a receiver coil that is too big to fit onto mobile devices (phones, wearables, etc.), or can only reach a range less than 10cm.

has to hold her device on top of the charging pad and maintain a perfect alignment with the charger. MultiSpot is unique in that it adapts the shape of the magnetic field according to the location and orientation of the receivers by constructively combining the magnetic fields of multiple Tx coils. This allows MultiSpot to reduce the size of the receiver coil to fit on phones and wearables, while supporting larger ranges and flexible receiver orientations.

For completeness, Table 2.1 shows a comparative study of what their proposed system achieves in terms of charging distance, receiver coil size (i.e., whether can be fit onto a mobile device), and study of different receiver orientations. The technologies proposed by them include adjusting the operating frequency [82], adjusting impedance matching networks [96], and designing specific transmit coils [62, 41].

2.1.3 Using Multiple Transmit Coils

Another line of work includes using multiple transmit coils to obtain some flexibility to manipulate the magnitude of the field in a favorable way. Most of such work is fundamentally different from this thesis since they do not shape the magnetic field in a steerable beam and thus do not address the range/orientation limitations. They fall into one of three categories:

- The first class uses multiple transmit coils but at any time only turn on the one that is nearest to or best aligned with the receiver [53, 21];

- The second class simply applies the same voltages or currents to all coils to simulate the effect of having a larger surface area [45];

- The third class use passive coils as repeaters to extend the magnetic fields [34, 80, 93, 94].

These proposals are fundamentally inferior to MultiSpot since they still cannot handle imperfect orientations, moving devices or multiple devices in multiple orientations, all of which are practical realities. MultiSpot actively reshapes and focuses the magnetic flux in terms of steerable beams towards multiple receivers to achieve a provably maximal power delivery. Very recently, another work was accepted for publication, which also uses multiple transmit coils, and examines the possibility of combining their fields at up to 2 receivers [95]. While the work demonstrates the potential of multi-user charging, it presents an optimal solution only for a single receiver, and uses brute force exploration to determine the optimal solution for two receivers. Further, the work presents an implementation only for the single receiver case, and uses simulation for the two-receiver case. In contrast, the work developed in this thesis presents an optimal solution for any number of receivers. Further, the MultiSpot system is implemented and empirically evaluated for up to 6 receivers.

MagMIMO: The system that is most similar to MultiSpot is MagMIMO [55]. In fact, MultiSpot is inspired by MagMIMO's techniques [55]. However, as described earlier in §1, MagMIMO does not work in the presence of more than one receiver, while MultiSpot is designed to work with any number of receivers. We show experimentally (§8) that when two receivers are separated from each other, MagMIMO cannot charge them.

Because having multiple receivers intrinsically changes the system due to the fundamental physics §1, it requires the thesis to establish new theoretical framework that includes more complicated mathematical derivations, as well as more elaborate and extensive circuit designs. Part of thesis is based on the author's previously published paper [84].

2.2 Magnetic Coupling via Other Physics Phenomena

We also note that there have been recent proposals of wireless charging using physical phenomena other than magnetic coupling.

- *Active RF Radiation:* i.e., delivering power to mobile devices via RF radiation at hundreds of MHz to GHz [15, 2]. However, the radiation will at the same time heat up water which composes most of a human body. This is the same principle that allows a microwave oven to cook food [99]. In order to deliver power sufficient to charge a phone, a rough calculation tells us that the minimal amount of radiation is at least 4 times higher than the maximal allowed leakage of a microwave oven.[1] It is also unclear how such technologies can pass FCC regulations. Consequently, wireless power delivery via RF radiation has been largely restricted to lower-power (μW-mW) devices such as sensors [87].

- *Ultra-Sound:* A recent startup [26] has proposed the use of ultra-sound to charge mobile phones. However, there has been no publication of their technologies nor an available product. Furthermore, ultrasound charging is limited to line-of-sight scenarios and will be disrupted if the phone is not directly in front of the charger [71]. It can also negatively affect pets who hear some types of ultrasound [42] and will perceive the sound necessary to power a cell phone at around 120dB (effectively a rock concert in ultra-sound).

- *Laser:* Wireless power delivery via laser has been explored in industrial and military settings [52]. However, despite some claims from recent startups without publication/product support [16], it has not been applied to mobile devices yet. The major barrier is the fact that lasers can cause damage to one's eyesight or to skin at high intensity [48].

[1] To see how delivering power via RF radiation to a phone might be dangerous, let us do a rough calculation. Say that a standard phone requires at least 1W to turn on charging, and it has an area of 5cm$\times$10cm, i.e., the power density is 20mW/cm^2. As a comparison, FDA (Food and Drug Administration) enforces microwave oven leakage to be below 5mW/cm^2 in order to be considered safe [8].

- *Ambient Power Harvesting:* Various forms of ambient power, including ambient RF power [76], sunlight [79] and mechanical power [98] are used to charge different devices. However, because of the very low power density (at most tens of μWs per cm^2 [75]), the application is mostly restrained to lower-power sensors. Of the ones related to consumer mobile devices [43], the energy is only enough to slow down the discharging of a phone's battery.

In summary, these different technologies either only work for devices whose power is orders of magnitude smaller than consumer electronic devices, or has significant safety and regulation concerns. Magnetic coupling is still the standard and most widely-used technology for wirelessly delivering power to mobile devices.

Chapter 3

Problem Formulation

In this chapter, we aim to develop basic circuit equations and formulations that are going to be used throughout the remainder of this thesis.

3.1 From Single-Coil to Multi-Coil

Magnetic coupling and the resulting power transfer can be mathematically described via basic circuit equations [77].

Single Coil System: Consider the system in Fig. 3-1, which shows a single coil transmitter and a single receiver. Let us write the equations that describe this system. As we do so, we will take into account that in magnetic resonance, the inductance and capacitor are chosen so that their impacts cancel each other at the resonant frequency, i.e.,

$$j\omega L + \frac{1}{j\omega C} = 0 \tag{3.1}$$

Thus, we can ignore those terms.

We can describe the system in Fig. 3-1 using two equations. The first equation determines how a current in the transmit coil, I_T, induces a current in the receive coil, I_R, i.e.:

$$Z_R I_R = j\omega M I_T \tag{3.2}$$

where M is the magnetic coupling between the transmit and receive coils, Z_R is the

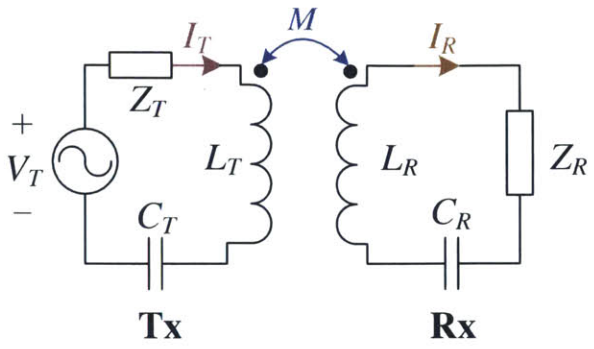

Figure 3-1: **Single-Coil Tx, Single Rx Schematic:** Both the Tx and Rx coils (L_T and L_R) use resonant capacitors (C_T and C_R) to boost efficiency. Z_T and Z_R include all of the remaining impedances in the Tx and Rx circuits.

impedance of the receiver and ω is the resonant frequency.

The above equation would have been sufficient to describe the system if one could directly apply a current to the transmit coil. Unfortunately, in practice, one prefers to use a voltage source instead. Thus, we need a second equation that determines the relationship between the voltage one applies to the transmitter, V_T and the resulting transmitter current, I_T.

For the circuit in Fig. 3-1, we have:

$$V_T = Z_T I_T - j\omega M I_R \tag{3.3}$$

where Z_T represents the impedance in the transmitter. Note in this equation how the current in the receiver induces a voltage back on the transmitter via the same magnetic coupling M. We can further substitute I_R from Eq. (3.2) to obtain:

$$V_T = \left(Z_T + \omega^2 M^2 / Z_R\right) I_T. \tag{3.4}$$

Together Eq. (3.2) and Eq. (3.4) describe the single-coil charging system.

Multi-coil Tx, Single-Rx System: Further, these equations can be expanded to account for multiple transmitters (Fig. 3-2). When multiple transmitters are on, they each have current in their coils. Therefore, each transmitter will induce a voltage on the receiver through magnetic coupling. These voltages will sum at the receiver so

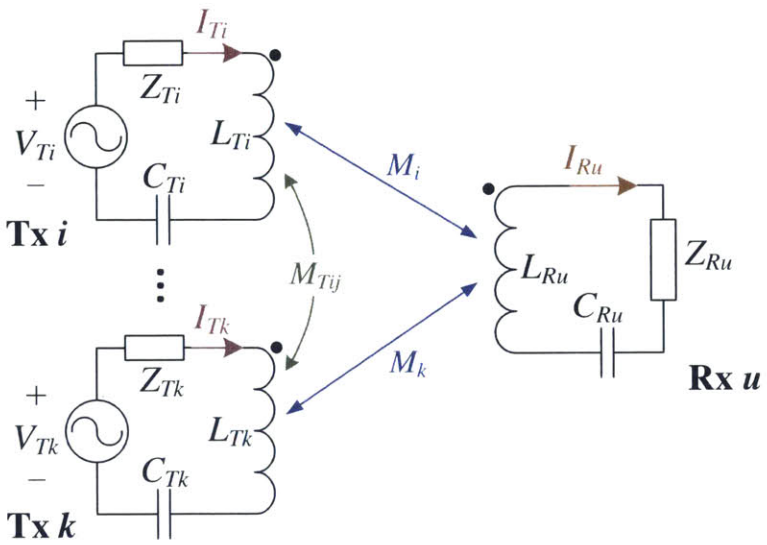

Figure 3-2: **Multi-Coil Tx, Single Rx Schematic**

Eq. (3.2) is rewritten as:

$$Z_R I_R = \underbrace{\sum_i j\omega M_i I_{Ti}}_{\text{from all transmitters}} \tag{3.5}$$

In addition, each transmitter magnetically couples to all other transmitters, so Eq. (3.4) becomes:

$$V_{Ti} = Z_{Ti} I_{Ti} - \underbrace{\sum_{k \neq i} j\omega M_{Tik} I_{Tk}}_{\text{from other transmitters}} - \underbrace{j\omega M_i I_R}_{\text{from the receiver}} \tag{3.6}$$

where, comparing with Equ. (3.4), the new term $\sum_{k \neq i} j\omega M_{Tik} I_{Tk}$ captures the voltages due to coupling from the other transmitters.

Multi-Coil Tx, Multi-Rx System: The above derivations can further be generalized to address the case of multiple transmitter coils and multiple receiver coils, shown in Fig. 3-3. The difference is that now in general every pair of coils has magnetic coupling between them. Specifically, there are three types of couplings: M_{Tik} between transmitter i and k, M_{iu} between transmitter i and receiver u, and M_{Ruv} between receiver u and v.

We can update Eq. (3.2) and Eq. (3.4) to account for the additional coupling

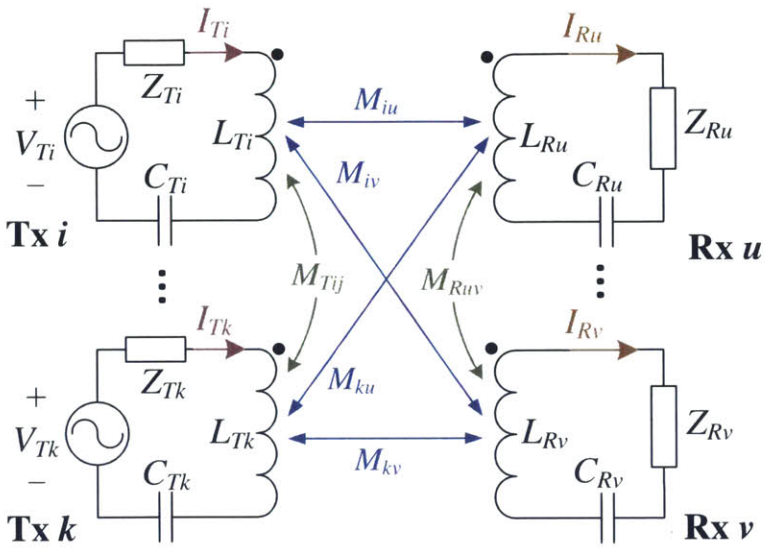

Figure 3-3: **Multi-Coil Tx, Single Rx Schematic**

between transmitter coils, and between receiver coils. Receiver u's circuit equation becomes:

$$Z_{Ru}I_{Ru} + \underbrace{\sum_{v\neq u} j\omega M_{Ruv}I_{Rv}}_{\text{from the other receivers}} = \underbrace{\sum_{i} j\omega M_{iu}I_{Ti}}_{\text{from the transmitters}} \tag{3.7}$$

while the transmitter voltage at coil i is:

$$V_{Ti} = Z_{Ti}I_{Ti} + \underbrace{\sum_{k\neq i} j\omega M_{Tik}I_{Tk}}_{\text{from the other transmitters}} - \underbrace{\sum_{u} j\omega M_{iu}I_{Ru}}_{\text{from the receivers}} \tag{3.8}$$

3.2 The Transmitter & Receiver Equation

For convenience, we rewrite Eq. (3.7) and (3.8) in matrix form:

$$\boldsymbol{Z}_R\vec{\boldsymbol{i}}_R = j\omega\boldsymbol{M}\vec{\boldsymbol{i}}_T \tag{3.9}$$

and

$$\vec{\boldsymbol{v}}_T = \boldsymbol{Z}_T\vec{\boldsymbol{i}}_T - j\omega\boldsymbol{M}^\top\vec{\boldsymbol{i}}_R \tag{3.10}$$

Term	Definition	Explanation
n	Number of Tx coils	
m	Number of Rx coils	
$\vec{\boldsymbol{v}}_T$	$[V_{T1}, V_{T2}, \cdots, V_{Tn}]^\top_{n\times 1}$	Tx voltages
$\vec{\boldsymbol{i}}_T$	$[I_{T1}, I_{T2}, \cdots, I_{Tn}]^\top_{n\times 1}$	Tx currents
$\vec{\boldsymbol{i}}_R$	$[I_{R1}, I_{R2}, \cdots, I_{Rm}]^\top_{n\times 1}$	Rx currents
$\boldsymbol{Z}_R$	$\begin{bmatrix} Z_{R1} & j\omega M_{R12} & \cdots & j\omega M_{R1m} \\ j\omega M_{R21} & Z_{R2} & \cdots & j\omega M_{R2m} \\ \vdots & \vdots & \ddots & \vdots \\ j\omega M_{Rm1} & j\omega M_{Rm2} & \cdots & Z_{Rm} \end{bmatrix}_{m\times m}$	Rx impedance and inter-Rx magnetic couplings
$\boldsymbol{Z}_T$	$\begin{bmatrix} Z_{T1} & j\omega M_{T12} & \cdots & j\omega M_{T1n} \\ j\omega M_{T21} & Z_{T2} & \cdots & j\omega M_{T2n} \\ \vdots & \vdots & \ddots & \vdots \\ j\omega M_{Tn1} & j\omega M_{Tn2} & \cdots & Z_{Tn} \end{bmatrix}_{n\times n}$	Tx impedance and inter-Tx magnetic couplings
$\boldsymbol{M}$	$\begin{bmatrix} M_{11} & M_{21} & \cdots & M_{n1} \\ \vdots & \vdots & \ddots & \vdots \\ M_{1m} & M_{2m} & \cdots & M_{nm} \end{bmatrix}_{m\times n}$	Tx-Rx magnetic couplings

Table 3.1: **Matrix & Vector Denotations**

where the matrix and vector denotations are defined in Table 3.1. By inverting $\boldsymbol{Z}_R$ on Eq. (3.9), and plugging it into Eq. (3.10), we can get the following two equations:

$$\text{Reciever Equation:} \qquad \vec{\boldsymbol{i}}_R = j\omega \boldsymbol{Z}_R^{-1} \boldsymbol{M} \vec{\boldsymbol{i}}_T \tag{3.11}$$

$$\text{Transmitter Equation:} \qquad \vec{\boldsymbol{v}}_T = \left(\boldsymbol{Z}_T + \omega^2 \boldsymbol{M}^\top \boldsymbol{Z}_R^{-1} \boldsymbol{M}\right) \vec{\boldsymbol{i}}_T \tag{3.12}$$

Table 3.1.

Eq. (3.11) and Eq. (3.12) are sufficient to describe the multi-coil system in Fig. 3-3. Specifically, Eq. (3.11) describes what receiver current $\vec{\boldsymbol{i}}_R$ we will get if a transmitter current $\vec{\boldsymbol{i}}_T$ is applied, thus we call it the *Receiver Equation.* Eq. (3.12), on the other hand, shows what voltage $\vec{\boldsymbol{v}}_T$ we need to apply in order to obtain transmitter currents $\vec{\boldsymbol{i}}_T$, so we name it the *Transmit Equation.* These two equations describe the most fundamental relationships in our multi-Tx multi-Rx system, and are the basis of *all* of the following conclusions of MultiSpot.

Chapter 4

MultiSpot

MultiSpot is a new technology for charging multiple devices wirelessly via magnetic resonance. It uses multiple transmit coils, which could be built into a desk mat to deliver a user experience analogous to a mini hotspot –i.e., when the user sits at her desk, all of her electronic gadgets start receiving power automatically.

MultiSpot's design is mainly focused on the transmitter side. The receiver design follows that of standard wireless charging circuits, which can be built into the sleeve of a phone or the strap of a smartwatch. It is able to deliver power simultaneously to a range of devices if they are equipped with a receiver, including but not limited to phones, smartwatches, tablets, ereaders, headphones, wireless mice and keyboards. Furthermore it is able to deliver power to these devices as they exist in their natural environments, with no requirement for the devices to physically touch the MultiSpot transmitter nor any limitation on the orientation of these devices relative to the transmitter or relative to each other.

At first blush, it might seem that one can build a wireless power hotspot by beamforming the magnetic field to one receiver at a time using MagMIMO [55], and iterating between receivers using a TDMA style MAC. Unfortunately MagMIMO intrinsically assumes only one receiver. If multiple receivers are nearby, they will couple with each other and the transmitter coils. As a result, MagMIMO cannot discover the coupling due to each individual receiver (i.e., the magnetic channel to the receiver [55]) and hence cannot compute the beamforming parameters correctly.

In fact MagMIMO would not know whether there is a single or multiple receivers.

One could also try to add out-of-band communication (e.g., via WiFi or Bluetooth) to coordinate receivers, turn some receivers off so that at any point in time there is coupling only from one receiver, synchronize the receivers as they turn on and off, and have receivers detect any motion and inform each other so that they can re-estimate coupling. Such an approach is excessively complex and involves a large amount of overhead. Furthermore it is not even clear how one can extend this idea into a full system.

Below we describe a design that requires neither receiver coordination nor out-of-band communication. It operates entirely on the transmitter allowing it to shape the magnetic field in multiple beams focused on the receivers, in a manner that is analytically proven to maximize power delivery.

4.1 Analogy to Beamforming

In this section, we briefly explain the analogy between the conventional beamforming that is used in communication systems and magnetic beamforming [55].

For the sake of simplicity, we focus only on a single receiver in this subsection. Also, we use the example of a standard MIMO transmitter with two antennas. Say that the transmit signal from the two transmit antennas are x_1 and x_2, from standard MIMO equations [90, 39], the received signal y can be expressed as:

$$y = h_1 x_1 + h_2 x_2 \tag{4.1}$$

where h_1 and h_2 are the wireless channels from the two transmitting antennas to the receiving antenna.

We also know that we can maximize the SNR of y at the receiver by beamforming the transmitted signal, by using a beamforming vector (α_1, α_2), and transmitting $x_1 = \alpha_1 x$ on the first antenna, and $x_2 = \alpha_2 x$ on the second antenna. By Maximal-

Ratio Combining (MRC), the elements of the beamforming vector should satisfy:

$$\alpha_i = c \cdot h_i^* \tag{4.2}$$

where c is a scalar constant, and h_i^* is the complex conjugate of the channel coefficient h_i. Intuitively, the beamforming vectors above ensure that the signal from each antenna is rotated and weighted according to the phase and strength of the channel, such that the signals from all antennas are aligned to maximize the power at the receiver.

Now, consider the wireless power transfer system. Let us assume that there are two transmitter coils and one receiver. In this case, Eq. (3.11) becomes

$$I_{R1} = j\omega \frac{1}{Z_{R1}} \left(M_{11} I_{T1} + M_{21} I_{T2}\right) = m_1 I_{T1} + m_2 I_{T2} \tag{4.3}$$

where $m_i = \frac{j\omega M_{i1}}{Z_{R1}}$. If we analogously define the transmitter currents I_{T1} and I_{T2} as the transmit signals, and correspondingly define the receiver current I_{R1} as the received signal, then Eq. (4.3) has the same format as the MIMO Eq. (4.1). Specifically, m_i is defined as the *Magnetic Channel*, in the analogy to the wireless channel. Thus, similar to traditional MIMO beamforming, we can maximize the current induced in the receiver's coil (i.e., I_{R1}), by scaling the current flowing in the transmitterâĂŹs coils with a magnetic-beamforming vector (β_1, β_2), such that

$$I_{Ti} = \beta_i I_T, \text{ where } \beta_i = c \cdot m_i^* \tag{4.4}$$

We note that maximizing the receiver's current, I_{R1}, naturally translates to magnetic-beamforming the field toward the receiver's coil, in a manner similar to how maximizing the received symbol, y, translates to standard MIMO beamforming. This is because the magnetic field amplitude at the receiver coil is proportional to I_{R1} [99]. The proportionality means that maximizing I_{L1} is identical to maximization of the local magnetic flux magnitude at the receiver coil. [1]

[1]Nonetheless, we note that shaping the non-radiated magnetic field as a beam while analogous

4.2 Optimizing Power Delivery to Receivers

In wireless communication systems, such as MU-MIMO, beamforming effectively combines the signals constructively at the receivers so that the received signal gets maximized. This is achieved by carefully setting the transmitter signal according to the wireless channels. Similar concepts can be applied to wireless power delivery systems. However, to beamform in MultiSpot, we need to answer two questions. What exactly are the "signals" and "channels"? And how do we maximize the power of the received signal? This will be addressed in the following two subsections respectively.

4.2.1 Magnetic Channel

The Receiver Eq. (3.11) provides us a way to analogously define magnetic channels. Specifically, if we analogize currents to signals, the transmitted and received signals will be $\vec{i}_T$ and $\vec{i}_R$. Therefore, the coefficient between them is the magnetic channel, i.e.:

$$\vec{i}_R = \boldsymbol{H}\vec{i}_T, \quad \text{where } \boldsymbol{H} = j\omega \boldsymbol{Z}_R^{-1}\boldsymbol{M} \tag{4.5}$$

Note that the magnetic channel $\boldsymbol{H}$ is different from the channel matrix in MU-MIMO, where it is simply a concatenation of individual channels between every pair of transmitter and receiver. Rather, in MultiSpot, it is the multiplication of two parts: $\boldsymbol{H} = \boldsymbol{H}_{Rx-Rx}\boldsymbol{H}_{Rx-Tx}$ where $\boldsymbol{H}_{Rx-Rx} = \boldsymbol{Z}_R^{-1}$ contains receiver-receiver couplings and $\boldsymbol{H}_{Rx-Tx} = j\omega\boldsymbol{M}$ contains transmitter-receiver couplings. Physically, these two sub-channel matrices describe two processes that occur in multi-TX-coil multi-receiver power transfer system: $\boldsymbol{H}_{Rx-Tx}$ characterizes the induced power on the receivers from transmitters, while $\boldsymbol{H}_{Rx-Rx}$ captures the redistribution of transmitted power among receivers due to receiver-receiver coupling.

---

to traditional beamforming is also quite different from it and cannot be implemented by simply using traditional beamforming. These are two different phenomena: the former operates over the near-field magnetic flux while the latter operates over the far-field propagating waves. Thus, while the analogy is helpful in understanding and developing the design, MultiSpot requires developing a new mathematical formalization that optimizes power transfer.

4.2.2 Maximizing Received Power

The challenge becomes how to set the transmitter signals, (i.e., $\vec{i}_T$), so that the received power is maximized. This question can be formulated as an optimization problem that maximizes the received power P_R, under the constraint of a total input power P.

The received power P_R can be written as the summation of the power delivered to each receiver, i.e.:

$$P_R = \vec{i}_R^* \boldsymbol{R}_R \vec{i}_R, \tag{4.6}$$

where $\vec{i}_R$ is a vector of the receiver currents. The superscript (*) denotes conjugate transpose, and $\boldsymbol{R}_R$ is a diagonal matrix whose entries are the resistances of each receiver.[2]

The input power can be written as the total power dissipated on the transmitter and receivers, i.e., $P = P_R + P_T$. This is because power does not disappear, and hence must either be delivered to the receivers, or be consumed on the transmitters. Thus:

$$P = P_R + P_T = \vec{i}_R^* \boldsymbol{R}_R \vec{i}_R + \vec{i}_T^* \boldsymbol{R}_T \vec{i}_T, \tag{4.7}$$

where $\boldsymbol{R}_R$ and $\boldsymbol{R}_T$ are diagonal matrices of transmitter and receiver resistances.

Now, we can re-write the optimization problem that maximizes power transfer by substituting the received power and the input power by their values from Eq. (4.6) and Eq. (4.7). We also substitute the received currents from Eq. (4.5), $\vec{i}_R = \boldsymbol{H}\vec{i}_T$. Thus, our optimization problem becomes: Find the transmit currents that satisfy:

$$\begin{aligned} \vec{i}_T^{\,\text{bf}} &= \arg\max \left\{ \vec{i}_T^* \boldsymbol{H}^* \boldsymbol{R}_R \boldsymbol{H} \vec{i}_T \right\} \\ \text{conditioned on: } & \vec{i}_T^* \boldsymbol{R}_T \vec{i}_T + \vec{i}_T^* \boldsymbol{H}^* \boldsymbol{R}_R \boldsymbol{H} \vec{i}_T = P, \end{aligned} \tag{4.8}$$

where $\vec{i}_T^{\,\text{bf}}$ denotes the set of currents that beamforms.

In §4.8.1, We prove that the solution to this optimization is (see §4.8.1 for the

[2]If a receiver is not fully resistive, i.e., its impedance Z_{Ru} has an imaginary component, then $R_{Ru} = Real(Z_{Ru})$.

proof):

Theorem 4.2.1. *The following transmitter current vector will maximize the received power:*

$$\vec{i}_T^{bf} = c \cdot maxeig(\boldsymbol{H}^* \boldsymbol{R}_R \boldsymbol{H}) \tag{4.9}$$

where maxeig $(\boldsymbol{H}^* \boldsymbol{R}_R \boldsymbol{H})$ *is the eigenvector of* $\boldsymbol{H}^* \boldsymbol{R}_R \boldsymbol{H}$ *that corresponds to the largest real eigenvalue* λ*, and* c *is a normalization scalar defined in App. 4.8.1. Specifically, the maximal delivered power is equal to* $\frac{\lambda}{\lambda+1} P$.

This theorem guarantees that MultiSpot maximizes the power delivered from the transmitter coils to the receiver coils. This means that for the same hardware and any given relative locations of transmitter and receiver coils, no other algorithm can deliver more power than what is specified by the theorem.

4.2.3 Applying the Beamforming Solution

The solution from Thm. 4.2.1 would be sufficient if one could directly apply the currents to the coil. However, in practice, one has to use a voltage source instead. Therefore, we need to convert these currents to their corresponding voltages so that they are directly applicable to the Tx coils via standard voltage sources.

Fortunately, the Transmitter Eq. (3.12) that relates transmitter currents to voltages was derived in §3.1. Specifically, the set of voltages that we need to apply to the Tx coils is:

$$\vec{\boldsymbol{v}}_T^{\text{bf}} = \left(\boldsymbol{Z}_T + \omega^2 \boldsymbol{M}^\top \boldsymbol{Z}_R^{-1} \boldsymbol{M}\right) \vec{\boldsymbol{i}}_T^{\text{bf}}. \tag{4.10}$$

In summary, maximizing power delivery requires two steps:

1. Calculate the beamforming currents, $\vec{\boldsymbol{i}}_T^{\text{bf}}$.

2. Convert the currents to voltages by $\vec{\boldsymbol{v}}_T^{\text{bf}}$, and apply the voltages to the transmitter coils.

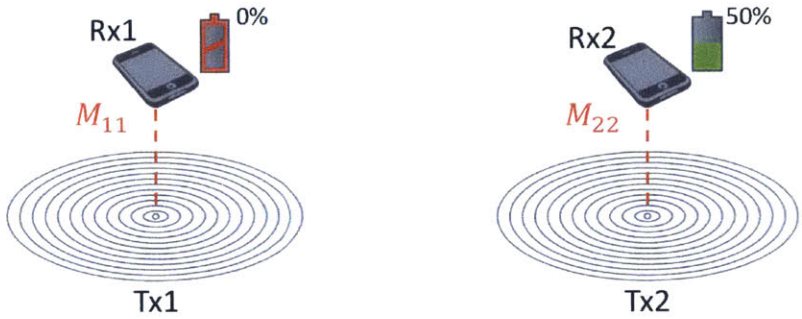

Figure 4-1: **Example of Two Phones with Different Battery Levels:** Two transmitters, with two receivers equally distanced to each transmitter and far away from the other transmitter. Receiver 1 has 0% battery while receiver 2 has 50% battery.

4.3 Beamforming Examples

In this section, we explore two representative examples of the solution given by Thm. 4.2.1.

4.3.1 Two phones with different battery levels

Please consider the scenario with two identical transmitters (i.e., $Z_{T1} = Z_{T2}$), with two receivers equally near to each transmitter while very far away from each other (Fig. 4-1). Effectively, this leads to $M_{12} \approx 0$, $M_{21} \approx 0$, and $M_{11} = M_{22}$, which for simplification we use M to denote. Moreover, let us assume that the receiver is well-tuned such that the equivalent impedances are purely real, i.e., $Z_{T1} = R_{T1}$ and $Z_{T2} = R_{T2}$. However, the two receivers have different battery levels, e.g., Rx1 has a dead battery while Rx2 has a 50% battery.

Taking all of the assumptions in Fig. 4-1 into Equ. (4.9), the optimal solution given by Thm. 4.2.1 that maximizes the total power received is:

$$\boldsymbol{H}^* \boldsymbol{R}_R \boldsymbol{H} = \omega^2 M^2 \begin{bmatrix} \frac{1}{R_{L1}} & 0 \\ 0 & \frac{1}{R_{L2}} \end{bmatrix} \tag{4.11}$$

It has two eigenvalues, $1/R_{L1}$ and $1/R_{L2}$, and the corresponding eigenvectors are $[1\ 0]^\top$ and $[0\ 1]^\top$. By Thm. 4.2.1, the optimal solution is the eigenvector associated

with the largest eigenvalue, i.e., in this case, it is to always charge the one with lower equivalent load resistance. Said differently, in this example, MultiSpot will always charge the receiver with smaller load resistance.

So which receiver has a smaller load resistance? The load resistance itself is a function of charge level. Common personal electronic devices (e.g., iPhone, iPad, etc) use lithium batteries. During the charging process, voltages and currents change with battery percentage. When the battery level is low, the current is big in order to quickly charge the battery, yielding small load resistance; when the battery level is high, current gradually reduces to nearly zero until the phone is fully charged, yielding big load resistance. Therefore, the equivalent resistance grows with the charge level, a phone with smaller battery percentage has a smaller resistance.

Combining this relationship between battery percentage and load resistance with our statement that MultiSpot in the example of Fig. 4-1 always charges the receiver with smaller load resistance, we reach the conclusion that *MultiSpot will always charge the phone with lower battery first.* This implies some underlying fairness about power distributions among receivers, which we will expand on in Sec. 4.6.

4.3.2 Repeater Example

As mentioned earlier, every receiver in our system also works as a transmitter since it repeats and redistributes the power. In some scenarios, a particular receiver can extend the range of the transmitters by relaying the power to another receiver. We call this receiver a "repeater". In the following example, we will show how the solution in Thm. 4.2.1 works in a repeater scenario.

As shown in Fig. 4-2, we have two transmitters. We define one coil is "reachable" from the other one if the coupling between them is not negligible. In this example, one receiver Rx1 is reachable from the transmitters ($M_{11} \neq 0, M_{21} \neq 0$), while the other receiver Rx2 is far away from the transmitters that it gets very weak couplings ($M_{12} \approx 0, M_{22} \approx 0$). However, Rx2 is coupled to Rx1 such that their coupling (M_R) is not negligible. For simplicity we also assume the loads are resistive. Applying

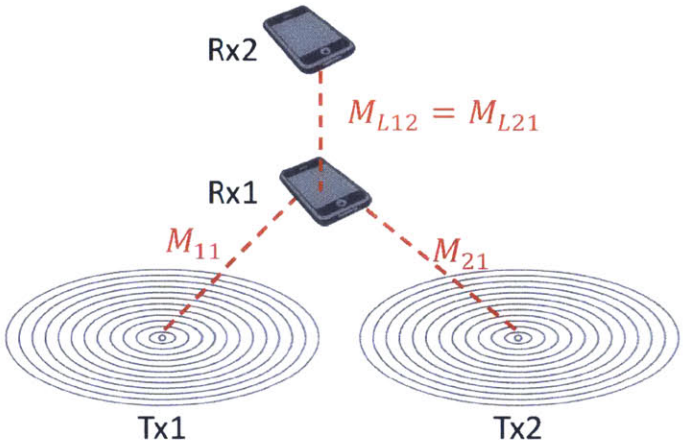

Figure 4-2: **Example of Receiver Repeater:** Rx1 is reachable from the transmitters, while Rx2 is not reachable from the transmitters but reachable from Rx1.

Thm. 4.2.1, we get:

$$\boldsymbol{H}^* \boldsymbol{R}_R \boldsymbol{H} = \frac{\omega^2 R_{R2}}{R_{R1} R_{R2} + \omega^2 M_R^2} \begin{bmatrix} M_{11}^2 & M_{11} M_{21} \\ M_{11} M_{21} & M_{21}^2 \end{bmatrix} \tag{4.12}$$

It only has one non-zero eigenvalue whose eigenvector is $[M_{11}\ M_{12}]^\top$. This means the optimal current is $I_{T1} = cM_{11}, I_{T2} = cM_{21}$. This turns out to be exactly the beamforming solution when only Rx1 is around, i.e., we effectively focus the power to form a beam towards Rx1. Moreover, since we use Rx1 as a relay to deliver power to Rx2, maximizing power on Rx1 also maximizes power on Rx2. Specifically, the current on the Rx2 is

$$I_{R2} = -\frac{j\omega M_R}{R_{R2}} I_{R1} \tag{4.13}$$

which is proportional to the current on Rx1 (I_{R1}). Therefore, we maximize the power delivered to Rx2 by maximizing the power to Rx1 and using it as a repeater.

4.4 Eliminating the Need for Receivers' Communication

In the previous section, we showed how a MultiSpot charger could beamform. However, two steps are needed to beamform, both of which require information that resides on the receivers, and is unavailable at the transmitter in the absense of communication with the receivers.

- In the first step, the beamforming currents, $\vec{i}_T^{\text{bf}}$, are calculated via Thm. 4.2.1, which is strictly dependent on knowing $\boldsymbol{H}^*\boldsymbol{R}_R\boldsymbol{H}$. Recall, however, that the channel contains receiver-receiver couplings, unknown to the transmitter.

- In the second step, the beamforming voltages, $\vec{v}_T^{\text{bf}}$, are computed using Eq. (4.10), which depends on knowing $(\boldsymbol{Z}_T + \omega^2\boldsymbol{M}^\top\boldsymbol{Z}_R^{-1}\boldsymbol{M})$. $\boldsymbol{Z}_T$ contains only transmitter specific parameters (i.e., transmitter to transmitter couplings and impedances) and hence can be estimated a priori in a factory setting (for details, see §4.7.1). However, the matrix $(\omega^2\boldsymbol{M}^\top\boldsymbol{Z}_R^{-1}\boldsymbol{M})$ contains receiver-receiver couplings and receiver impedances. This matrix which we denote $\boldsymbol{Y} = \omega^2\boldsymbol{M}^\top\boldsymbol{Z}_R^{-1}\boldsymbol{M}$ is unknown a priori to the transmitter (and changes with time because the coupling depends on receiver position).

Thus, beamforming requires estimating $\boldsymbol{H}^*\boldsymbol{R}_R\boldsymbol{H}$ and $\boldsymbol{Y}$, both of which involve receiver dependent information. So, how can a MultiSpot transmitter estimate these matrices without explicit information from the receivers?

4.4.1 Estimating $\boldsymbol{Y}$

Let us first consider estimating $\boldsymbol{Y}$. The Transmitter Eq. (3.12) can be rewritten as $\vec{v}_T = (\boldsymbol{Z}_T + \boldsymbol{Y})\,\vec{i}_T$, where the only unknown coefficient is $\boldsymbol{Y}$ because $\boldsymbol{Z}_T$ is measured during pre-calibration. By applying voltages and measuring the resulting currents on the Tx coils, we can estimate the coefficient between them. Since both $\vec{v}_T$ and $\vec{i}_T$ are vectors of length n, we need to repeat the measurement process n times before

applying matrix inversion, where n is the number of Tx coils. More formally, if one applies n different sets of voltages $\vec{v}_T^{(1)}, \cdots, \vec{v}_T^{(n)}$ and measures the corresponding currents $\vec{i}_T^{(1)}, \cdots, \vec{i}_T^{(n)}$, one can estimate $\boldsymbol{Y}$ by:

$$\boldsymbol{Y} = \left[\vec{v}_T^{(1)} \quad \cdots \quad \vec{v}_T^{(n)}\right] \cdot \left[\vec{i}_T^{(1)} \quad \cdots \quad \vec{i}_T^{(n)}\right]^{-1} - \boldsymbol{Z}_T \tag{4.14}$$

4.4.2 Estimating $\boldsymbol{H}^*\boldsymbol{R}_R\boldsymbol{H}$

After obtaining $\boldsymbol{Y}$, we are still left with the problem of estimating $\boldsymbol{H}^*\boldsymbol{R}_R\boldsymbol{H}$. Recall that $\boldsymbol{H} = j\omega\boldsymbol{Z}_R^{-1}\boldsymbol{M}$, which means both transmitter-receiver couplings and receiver-receiver couplings need to be estimated. Unlike the matrix $\boldsymbol{Y}$ however, which can be estimated at the transmitter using measurements of $\vec{v}_t$ and $\vec{i}_T$, there is no way to measure $\boldsymbol{H}$ at the transmitter.

Fortunately, MultiSpot does not need to estimate $\boldsymbol{H}$. Instead, we show that a MultiSpot transmitter can estimate the matrix product $\boldsymbol{H}^*\boldsymbol{R}_R\boldsymbol{H}$ as a whole; and it can do so completely passively. Further, we can relate $\boldsymbol{H}^*\boldsymbol{R}_R\boldsymbol{H}$ to something we have already measured, namely $\boldsymbol{Y}$. Specifically, we prove the following theorem (proof in §4.8.2):

Theorem 4.4.1. *Define Real($\cdot$) as the real part of a matrix, then*

$$\boldsymbol{H}^*\boldsymbol{R}_R\boldsymbol{H} = \mathit{Real}(\boldsymbol{Y}) \tag{4.15}$$

where $\boldsymbol{H} = j\omega\boldsymbol{Z}_R^{-1}\boldsymbol{M}$ *and* $\boldsymbol{Y} = \omega^2\boldsymbol{M}^\top\boldsymbol{Z}_R^{-1}\boldsymbol{M}$.

Since we have already shown how to compute $\boldsymbol{Y}$, the above theorem allows us to compute $\boldsymbol{H}^*\boldsymbol{R}_R\boldsymbol{H}$ by taking its real part.

Therefore, we have developed a method to estimate all needed parameters solely on the transmitter, without any communication or feedback from the receivers.

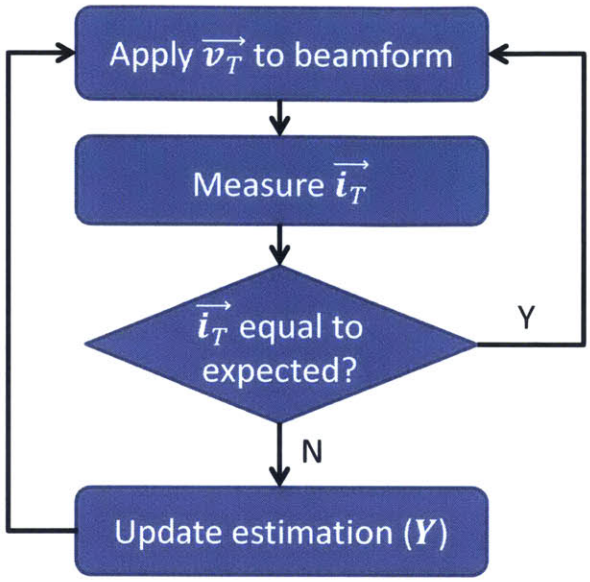

Figure 4-3: **Framework of the Adaptive Beamforming Algorithm**

4.5 Adaptive Beamforming

Next, we would like to ensure that MultiSpot can smoothly adapt to receiver motion and receivers entering and leaving the system. This is particularly important for wearable receivers which tend to be highly dynamic, e.g., a smartwatch on a user's wrist. Furthermore as users introduce an increasing number of devices into the MultiSpot's vicinity, the importance of handling movement and entry-exit scenarios increases rapidly as the likelihood that the user is physically interacting with at least one device at any given time, causing it to move, approaches certainty (especially if one of said devices is a wireless mouse).

When receivers move (or are added/removed), the magnetic couplings change across all devices, leading to new values for $\boldsymbol{H}$ and $\boldsymbol{Y}$. One could address this problem by repeatedly estimating $\boldsymbol{Y}$ and $\boldsymbol{H}^*\boldsymbol{R}_R\boldsymbol{H}$, as explained in §4.4. This, however, would be suboptimal since estimating $\boldsymbol{Y}$ from scratch requires the MultiSpot charger to stop beamforming and apply other voltages in order to obtain enough measurements as required by Eq. (4.17) thus losing valuable system time actually delivering power to devices.

Furthermore, since the transmitter does not know when receivers move, it is left

Algorithm 1 Beamforming to Multiple Receivers

procedure MULTIBEAMFORMING($\boldsymbol{Z}_T$)
  $\widetilde{\boldsymbol{Y}} \leftarrow$ BOOTSTRAP($\boldsymbol{Z}_T$) ▷initialize $\widetilde{\boldsymbol{Y}}$, see Alg. 2
  while true **do**
    $\vec{\boldsymbol{i}}_T^{\text{bf}} = c \cdot \text{maxeig}(\text{Real}(\widetilde{\boldsymbol{Y}}))$
    ▷compute beamforming currents
    Apply $\vec{\boldsymbol{v}}_T^{\text{bf}} = \left(\boldsymbol{Z}_T + \widetilde{\boldsymbol{Y}}\right) \vec{\boldsymbol{i}}_T^{\text{bf}}$ ▷beamform
    Measure $\vec{\boldsymbol{i}}_T$ on the transmitter
    $\Delta\vec{\boldsymbol{i}}_T \leftarrow \vec{\boldsymbol{i}}_T - \vec{\boldsymbol{i}}_T^{\text{bf}}$
    if $\Delta\vec{\boldsymbol{i}}_T \neq \vec{\boldsymbol{0}}$ **then** ▷if the channel changes
      $\widetilde{\boldsymbol{Y}} \leftarrow \widetilde{\boldsymbol{Y}} + \frac{\Delta\vec{\boldsymbol{v}}_T \Delta\vec{\boldsymbol{v}}_T^{\top}}{\Delta\vec{\boldsymbol{v}}_T^{\top}\vec{\boldsymbol{i}}_T}$, where $\Delta\vec{\boldsymbol{v}}_T = (\boldsymbol{Z}_T + \widetilde{\boldsymbol{Y}})\Delta\vec{\boldsymbol{i}}_T$ ▷ update $\widetilde{\boldsymbol{Y}}$
    end if
  end while
end procedure

with a difficult choice: Either it can repeat the estimation infrequently, which would be inefficient in scenarios with lots of motion, or it can repeat the estimation, often leading to frequent and unnecessary interruptions in beamforming when the receivers are static.

In this section, we propose an adaptive algorithm, which we call *adaptive beamforming*, that addresses the conflict: It uninterruptedly beamforms whenever the receivers remain static, and seamlessly and quickly adapts when any receiver moves, enters or exists the vicinity.

The key idea is that instead of estimating $\boldsymbol{Y}$ from scratch, which would interrupt beamforming, the adaptive algorithm iteratively computes the new $\boldsymbol{Y}$. In each iteration, the algorithm computes an incremental update to $\boldsymbol{Y}$ that satisfies the following two constraints: 1) If no receiver moves, the update is zero; and 2) If any receiver moves, the update rule is guaranteed to move $\boldsymbol{Y}$ toward its true value and converge to the true value within a small number of steps.

Alg. 1 outlines MultiSpot's adaptive beamforming. For clarity, we use $\widetilde{\boldsymbol{Y}}$ to denote the algorithm's estimate of the true $\boldsymbol{Y}$ matrix. To start the algorithm we need to initialize the values of $\widetilde{\boldsymbol{Y}}$, by a process called bootstrap, which will be explained in §4.7.2. In each iteration, the algorithm calculates the beamforming currents and converts them to beamforming voltages, which it applies to the transmitter coils.

Next (Line 7), the algorithm measures the currents on the transmit coils. If $\widetilde{\boldsymbol{Y}}$ is accurate, the measured currents should be equal to the currents that beamform ($\vec{\boldsymbol{i}}_T^{\text{bf}}$). Otherwise the algorithm uses the mismatch between the measured and expected currents and the resulting mismatch in voltages to update its estimate of $\widetilde{\boldsymbol{Y}}$ (Line 9).

It should be clear from the update rule in Line 9 that if nothing changes (e.g., no receiver moves), no update will occur and the beamforming is unmodified. Further, the theorem below guarantees that when a change occurs, the algorithm quickly converges to the optimal beamforming solution.

Theorem 4.5.1. *If $\widetilde{\boldsymbol{Y}} \neq \boldsymbol{Y}$, then Alg. 1 is guaranteed to update $\widetilde{\boldsymbol{Y}}$ to $\boldsymbol{Y}$ in less than n iterations, where n is the number of transmitters.*

Thm. 4.5.1 is formally proven in §4.8.3. Thm. 4.5.1 not only proves convergence but it puts an upper bound on the time to convergence. The convergence time is bounded only by the number of transmit coils, and is independent of the number of receivers. In our implementation where the transmitter uses a standard microcontroller, each iteration in Alg. 1 can be finished in less than 1ms. When there is any movement, the algorithm takes about 5ms to converge to the new set of channels. This speed is more than sufficient for our application.

There are three more points we would like to raise regarding Thm. 4.5.1:

- Thm. 4.5.1 only proves an upper bound on the number of iterations that are needed to converge. However, many scenarios require fewer iterations. For example, if only one receiver comes into range of MultiSpot while no other receivers move, then Alg. 1 only needs one iteration to converge. More generally, the number of iterations needed to converge is bounded by the number of receivers that move, as described by the following theorem (proof in §4.8.4):

  Theorem 4.5.2. *If r receiver moves so that $\widetilde{\boldsymbol{Y}} \neq \boldsymbol{Y}$, then Alg. 1 is guaranteed to update $\widetilde{\boldsymbol{Y}}$ to $\boldsymbol{Y}$ in less than $2r$ iterations.*

  Furthermore, this speed can be proven to be the *fastest*. It is formally stated in the following theorem and is proven in §4.8.6.

Theorem 4.5.3. *If $\boldsymbol{Y} \neq \widetilde{\boldsymbol{Y}}$, Alg. 1 takes the smallest number of steps to update $\widetilde{\boldsymbol{Y}}$ to be $\boldsymbol{Y}$ by applying the fewest sets of different voltages to the Tx.*

- A MultiSpot charger does not need to know the number of receivers to run Alg. 1. The charger has enough information to infer the number of receivers, which is equal to the rank of $\boldsymbol{Y}$.

- Thm. 4.5.1 as well as Alg. 1 assumes the load impedances do not change during the convergence period. However, in some cases this might not hold. In the next chapter we will discuss how we can extend the algorithm to deal with varying receiver impedances.

4.6 Power Distribution Among Receivers

The previous section presents an algorithm that adaptively delivers maximal power to the receivers. But how does the solution distribute this power among the various receivers? In order to gain insight into power distribution, we discuss three representative cases.

- In the first scenario, we consider identical receivers from the perspective of wireless charging – i.e., receivers with the same battery level, distance, and orientation with respect to the transmitter, and hence the same magnetic coupling. In this case, all receivers are allocated equal amounts of power. This is because the system is symmetric with respect to the receivers and hence an even power distribution yields the optimal solution. For a formal proof, please refer to §4.8.5.

- In the second scenario, we consider receivers that have the same battery level (i.e., the same demands for charging), but different magnetic couplings. Physically, this can be caused by some receivers being placed closer to the transmitter than others, with more favorable orientations, or simply having a larger coil. Either way, the receivers with stronger magnetic coupling will receive more power.

This property is similar in spirit to resource allocation in typical networking systems. For example, TCP flows with shorter RTTs and WiFi clients with higher SNRs receive higher data rates.

- In the final case, we consider what happens as some receivers approach a fully charged battery while others are still in need for charging. We argue that in this case the MultiSpot charger naturally reduces the power allocated to the more charged receivers, diverting that power to those receivers who are still in need for wireless power. Specifically, consider two receivers with the same magnetic coupling, one of which is fully charged while the other has a low battery level.

  When the battery is charged, the device needs very little power so it does not accept current. In this case the receiver circuit can be approximated by an open circuit, i.e., $I_R \approx 0$ for that receiver [19]. As a result, the receiver does not reflect power toward the transmitter. Therefore, the MultiSpot transmitter will not sense this receiver or beamform to it. In general, the progression from accepting current when the receiver has low battery levels to not accepting current when it is fully charged is gradual. Therefore, the algorithm gradually allocates less power to devices that are more charged.

To validate this intuition, we test each of the above situations experimentally in §8.

4.7 Precalibration and Bootstrap

4.7.1 Pre-Calibration

The goal of pre-calibration is to estimate $\boldsymbol{Z}_T$. Since $\boldsymbol{Z}_T$ only contains transmitter-specific information that is fixed after the transmitter is fabricated, it can be done immediately after manufacturing the transmitter coils where their relative positions are hardcoded.

During pre-calibration, there is no receiver around, so the Transmitter Eq. (3.12)

is reduced to

$$\vec{v}_T = \boldsymbol{Z}_T \vec{i}_T \tag{4.16}$$

Now, in order to estimate $\boldsymbol{Z}_T$, we need to apply n different sets of $\vec{v}_T$ and measure the corresponding $\vec{i}_T$. $\boldsymbol{Z}_T$ can be consequently obtained by matrix inversion, i.e., similar to how we estimate $\boldsymbol{Y}$ in Sec. §4.4:

$$\boldsymbol{Z}_T = \begin{bmatrix} \vec{v}_T^{(1)} & \cdots & \vec{v}_T^{(n)} \end{bmatrix} \cdot \begin{bmatrix} \vec{i}_T^{(1)} & \cdots & \vec{i}_T^{(n)} \end{bmatrix}^{-1} \tag{4.17}$$

4.7.2 Bootstrap

§4.5 shows how we can iteratively track the receiver and steer the beam: we infer the magnetic channel and the coefficient matrix passively by measuring the currents in the transmitter coils, and use this learned information to update the beam. This process of passively estimating the channel and updating the beam will iterate repeatedly, so that the system can track a moving receiver.

However, we still need some mechanism to bootstrap this iterating algorithm. Specifically, the question is, how can the system detect when an Rx comes into range so that it can then track the Rx?

When there is no receiver around, the system is in detection mode. While in this mode, the circuit tries to search for possible Rx devices by a technique we call "diagonalizing the current" which we will expand on later in this section. Once an Rx comes in, it will impose changes to the currents, which could be captured by our algorithm. These changes can be then used to infer the magnetic channels in the same way as in §4.5, and the whole system bootstraps and starts to beamform.

1) Trying to detect possible receiver devices when no Rx is around When there is no Rx around, the circuit cannot be totally idle since an Rx can come in at any time and needs to be detected immediately for optimal user experience. Thus, we wake up the transmitter coils in turn to detect possible receiver devices. When an Rx comes into range, at least the nearest transmitter should be able to detect this Rx when awakened. Doing this minimizes power dissipation while no Rx is around

and maintains high sensitivity to a possible Rx.

The straightforward way to implement this round-robin detection would be to add electrically-controlled switches to the coils and open-circuit them successively. However, this might interrupt the coils, risk damaging a high-Q, high-power, resonating circuit, and complicate the circuit design. Instead, we zero out the current in any given Tx coil by carefully applying a particular set of voltages. The intuition is, if we drive a Tx coil with the voltage that exactly opposes the total induced voltage from all of the other coils, we can zero-out the current in this coil.

We call this process "diagonalizing the current" because of the following formulation in matrix form: Say that we repeatedly issue n different sets of voltages, we get

$$\left[\vec{\boldsymbol{v}}_T^{(1)} \quad \cdots \quad \vec{\boldsymbol{v}}_T^{(n)}\right] = \boldsymbol{Z}_T \left[\vec{\boldsymbol{i}}_T^{(1)} \quad \cdots \quad \vec{\boldsymbol{i}}_T^{(n)}\right] \tag{4.18}$$

Note that we have the freedom to choose what the voltage matrix is. If we set

$$\left[\vec{\boldsymbol{v}}_T^{(1)} \quad \cdots \quad \vec{\boldsymbol{v}}_T^{(n)}\right] = \boldsymbol{Z}_T \tag{4.19}$$

we effectively diagonalize the current matrix $\left[\vec{\boldsymbol{i}}_T^{(1)} \quad \cdots \quad \vec{\boldsymbol{i}}_T^{(n)}\right]$ so that each time only one coil has current and all of the other coils have zero currents. [3]

2) Bootstrap once an Rx is detected Without loss of generality, assume an Rx comes in. In this case, we can use the method as in Alg. 1 to detect its occurrence and further estimate the channel. Specifically, we compare measured $\vec{\boldsymbol{i}}_T$ with the expected one, any mismatch between them indicates an Rx is coming in. We can then use the same form as used in Alg. 1 to estimate the channel, i.e.,

$$\boldsymbol{Y} = \frac{\Delta\vec{\boldsymbol{v}}_T \Delta\vec{\boldsymbol{v}}_T^\top}{\Delta\vec{\boldsymbol{v}}_T^\top \vec{\boldsymbol{i}}_T} \tag{4.20}$$

Alg. 2 shows the pseudo-code of the bootstrap process.

[3] In a practical system, we would like to control the amount of power going into the system. In this case, we set $\vec{\boldsymbol{v}}_T^{(i)}$ to be proportional to the i-th column of $\boldsymbol{Z}_T$, where the scaling factor depends on the power budget.

Algorithm 2 Bootstrap

procedure BOOTSTRAP($\boldsymbol{Z}_T$)
  $i \leftarrow 1$ ▷i is the iteration counter
  while true **do**
    Apply $\vec{\boldsymbol{v}} \propto (i \mod N)$-th column of $\boldsymbol{Z}_T$ ▷ Diagonalize the current
    Measure $\vec{\boldsymbol{i}}_T$ on the transmitter
    $\Delta\vec{\boldsymbol{v}}_T \leftarrow \vec{\boldsymbol{v}} - \boldsymbol{Z}_T\vec{\boldsymbol{i}}_T$
    if $\Delta\vec{\boldsymbol{i}}_T \neq \vec{\boldsymbol{0}}$ **then** ▷if rx is detected
      $\widetilde{\boldsymbol{Y}} \leftarrow \frac{\Delta\vec{\boldsymbol{v}}_T\Delta\vec{\boldsymbol{v}}_T^\top}{\Delta\vec{\boldsymbol{v}}_T^\top\vec{\boldsymbol{i}}_T}$ ▷ estimate $\widetilde{\boldsymbol{Y}}$
    end if
    $i \leftarrow i + 1$
  end while
  return $\widetilde{\boldsymbol{Y}}$
end procedure

4.8 Proofs

4.8.1 Proof of Theorem 4.2.1

Proof: We start with converting the optimization problem to another equivalent one. Specifically, We define

$$\vec{\boldsymbol{x}} = \sqrt{\boldsymbol{R}_T}\vec{\boldsymbol{i}}_T \tag{4.21}$$

where $\sqrt{\boldsymbol{R}_T}$ is a diagonal matrix whose diagonal entries are square root of those of $\boldsymbol{R}_T$. Similarly, $\sqrt{\boldsymbol{R}_R}$ can be defined. Now the problem becomes that we want to find

$$\vec{\boldsymbol{i}}_T^{\,\text{bf}} = \sqrt{\boldsymbol{R}_T^{-1}}\vec{\boldsymbol{x}}_T^{\,\text{bf}} \tag{4.22}$$

where $\vec{\boldsymbol{x}}_T^{\,\text{bf}}$ is the solution to the following:

$$\vec{\boldsymbol{x}}_T^{\,\text{bf}} = \arg\max_{\vec{\boldsymbol{x}}} \left\{\vec{\boldsymbol{x}}^* \boldsymbol{A}\vec{\boldsymbol{x}}\right\}, \quad \text{where } \boldsymbol{A} \triangleq \sqrt{\boldsymbol{R}_T^{-1}}\boldsymbol{H}^*\boldsymbol{R}_R\boldsymbol{H}\sqrt{\boldsymbol{R}_T^{-1}}$$

The constraint correspondingly becomes

$$\vec{\boldsymbol{x}}^*\vec{\boldsymbol{x}} + \vec{\boldsymbol{x}}^*\boldsymbol{A}\vec{\boldsymbol{x}} = P \tag{4.23}$$

Now, since $\boldsymbol{A}$ is a positive semi-definite Hermitian matrix (recall both $\boldsymbol{R}_R$ and $\boldsymbol{R}_T$ are

real positive diagonal matrices), it can be eigen-decomposed to $\boldsymbol{A} = \boldsymbol{Q}\boldsymbol{\Lambda}\boldsymbol{Q}^*$, where $\boldsymbol{Q}$ is a unitary matrix and $\boldsymbol{\Lambda}$ is a diagonal matrix of the eigenvalues of $\boldsymbol{A}$. Furthermore, all eigenvalues, $\lambda_1, \cdots, \lambda_n$, are real and non-negative. If we define $\vec{\boldsymbol{x}}' = \boldsymbol{Q}^*\vec{\boldsymbol{x}}$, then the objective function $\vec{\boldsymbol{x}}^*\boldsymbol{A}\vec{\boldsymbol{x}}$ can be written as

$$\vec{\boldsymbol{x}}^*\boldsymbol{A}\vec{\boldsymbol{x}} = \left(\vec{\boldsymbol{x}}'\right)^*\boldsymbol{\Lambda}\vec{\boldsymbol{x}}' = \sum_i \lambda_i |x_i'|^2 \tag{4.24}$$

Similarly, the constraint becomes:

$$\vec{\boldsymbol{x}}^*\vec{\boldsymbol{x}} + \vec{\boldsymbol{x}}^*\boldsymbol{A}\vec{\boldsymbol{x}} = \left(\vec{\boldsymbol{x}}'\right)^*\vec{\boldsymbol{x}}' + \left(\vec{\boldsymbol{x}}'\right)^*\boldsymbol{\Lambda}\vec{\boldsymbol{x}}' = \sum_i (\lambda_i + 1)|x_i'|^2 \tag{4.25}$$

Therefore, we have converted our optimization problem to:

$$\begin{array}{ll} \max & \sum_i \lambda_i |x_i'|^2 \\ \text{s.t.} & \sum_i (\lambda_i + 1)|x_i'|^2 = P \end{array}$$

Since all λ_i's are real non-negative, the optimal solution $\vec{\boldsymbol{x}}'$ is zero in every entry except the one that λ_i is maximal. More formally, say that $\lambda_k = \arg\max\{\lambda_1, \cdots, \lambda_n\}$, then $\vec{\boldsymbol{x}}'$ is zero on entries except the k-th one. In this case, the maximal value that is achieved is $\frac{\lambda_k}{\lambda_k+1}P$. Recall that $\vec{\boldsymbol{x}}' = \boldsymbol{Q}^*\vec{\boldsymbol{x}}$, or equivalently, $\vec{\boldsymbol{x}} = \boldsymbol{Q}\vec{\boldsymbol{x}}'$. Therefore, the optimal solution $\vec{\boldsymbol{x}}_T^{\text{bf}}$ is proportional to k-th column of $\boldsymbol{Q}$ (i.e., the k-th eigenvector of $\boldsymbol{A}$). Substituting back $\vec{\boldsymbol{x}} = \sqrt{\boldsymbol{R}_T}\vec{\boldsymbol{i}}_T$, we get the optimal $\vec{\boldsymbol{i}}_T^{\text{bf}}$:

$$\vec{\boldsymbol{i}}_T^{\text{bf}} = c \cdot \sqrt{\boldsymbol{R}_T^{-1}} \cdot \text{maxeig}\left(\sqrt{\boldsymbol{R}_T^{-1}}\boldsymbol{H}^*\boldsymbol{R}_R\boldsymbol{H}\sqrt{\boldsymbol{R}_T^{-1}}\right)$$

In this thesis, to simplify the equations, we assume the transmitter coils are identical, i.e., $R_{T1} = \cdots = R_{Tn} = R_T$. In this case, $\boldsymbol{R}_T$ is proportional to an identity matrix, thus when multiplied with another matrix, will not change it eigenvectors. Therefore, in this case, the solution is

$$\vec{\boldsymbol{i}}_T^{\text{bf}} = c \cdot \text{maxeig}(\boldsymbol{H}^*\boldsymbol{R}_R\boldsymbol{H}) \tag{4.26}$$

c is a scalar that captures R_T and other terms. It can be solved by substituting

$\vec{i}_T$ by $\vec{i}_T^{\text{bf}}$ to the constraint $\vec{i}_T^* \boldsymbol{R}_T \vec{i}_T + \vec{i}_T^* \boldsymbol{H}^* \boldsymbol{R}_R \boldsymbol{H} \vec{i}_T = P$. Note that this does not substantially change any of the conclusions in this thesis; plugging back $\boldsymbol{R}_T$ into them is straightforward. □

4.8.2 Proof of Theorem 4.4.1

Let's first expand $\boldsymbol{H}^* \boldsymbol{R}_R \boldsymbol{H}$ and $\boldsymbol{Y}$:

$$\boldsymbol{H}^* \boldsymbol{R}_R \boldsymbol{H} = \omega^2 \boldsymbol{M}^\top \left(\boldsymbol{Z}_R^{-1}\right)^* \boldsymbol{R}_R \boldsymbol{Z}_R^{-1} \boldsymbol{M} \tag{4.27}$$

and

$$\boldsymbol{Y} = \omega^2 \boldsymbol{M}^\top \boldsymbol{Z}_R^{-1} \boldsymbol{M} \tag{4.28}$$

Recall that $\boldsymbol{M}$ is a real matrix, therefore in order to prove $\boldsymbol{H}^* \boldsymbol{R}_R \boldsymbol{H} = \text{Real}(\boldsymbol{Y})$, what we need to prove is

$$\left(\boldsymbol{Z}_R^{-1}\right)^* \boldsymbol{R}_R \boldsymbol{Z}_R^{-1} = \text{Real}\left(\boldsymbol{Z}_R^{-1}\right)$$

which is proved as follows:

Proof: By definition, $\boldsymbol{R}_R$ is the real part of $\boldsymbol{Z}_R$. Therefore, we can denote

$$\boldsymbol{Z}_R = \boldsymbol{R}_R + j\boldsymbol{A}, \quad \boldsymbol{Z}_R^{-1} = \boldsymbol{B} + j\boldsymbol{C} \tag{4.29}$$

where $\boldsymbol{R}_R, \boldsymbol{A}, \boldsymbol{B}, \boldsymbol{C}$ are all real matrices. Therefore,

$$\boldsymbol{Z}_R \boldsymbol{Z}_R^{-1} = (\boldsymbol{R}_R \boldsymbol{B} - \boldsymbol{A}\boldsymbol{C}) + j(\boldsymbol{R}_R \boldsymbol{C} + \boldsymbol{A}\boldsymbol{B}) = \boldsymbol{I} \tag{4.30}$$

$$\boldsymbol{Z}_R^{-1} \boldsymbol{Z}_R = (\boldsymbol{B}\boldsymbol{R}_R - \boldsymbol{C}\boldsymbol{A}) + j(\boldsymbol{C}\boldsymbol{R}_R + \boldsymbol{B}\boldsymbol{A}) = \boldsymbol{I} \tag{4.31}$$

which leads to

$$\begin{aligned} \boldsymbol{R}_R\boldsymbol{B} - \boldsymbol{A}\boldsymbol{C} &= \boldsymbol{I} && (4.32)\\ \boldsymbol{R}_R\boldsymbol{C} + \boldsymbol{A}\boldsymbol{B} &= \boldsymbol{O} && (4.33)\\ \boldsymbol{B}\boldsymbol{R}_R - \boldsymbol{C}\boldsymbol{A} &= \boldsymbol{I} && (4.34)\\ \boldsymbol{C}\boldsymbol{R}_R + \boldsymbol{B}\boldsymbol{A} &= \boldsymbol{O} && (4.35) \end{aligned}$$

Since $\left(\boldsymbol{Z}_R^{-1}\right)^* = \boldsymbol{B} - j\boldsymbol{C}$ (note $\boldsymbol{B}$ and $\boldsymbol{C}$ are both real symmetric matrices),

$$\left(\boldsymbol{Z}_R^{-1}\right)^* \boldsymbol{R}_R \boldsymbol{Z}_R^{-1} = (\boldsymbol{B}\boldsymbol{R}_R\boldsymbol{B} + \boldsymbol{C}\boldsymbol{R}_R\boldsymbol{C}) + j(\boldsymbol{B}\boldsymbol{R}_R\boldsymbol{C} - \boldsymbol{C}\boldsymbol{R}_R\boldsymbol{B}) \tag{4.36}$$

The real part can be reduced by a series of substitution:

$$\begin{aligned} & \boldsymbol{B}\boldsymbol{R}_R\boldsymbol{B} + \boldsymbol{C}\boldsymbol{R}_R\boldsymbol{C} \overset{\text{Eq. (4.32)}}{\Longrightarrow} \boldsymbol{B}(\boldsymbol{I} + \boldsymbol{A}\boldsymbol{C}) + \boldsymbol{C}\boldsymbol{R}_R\boldsymbol{C} \\ = \; & \boldsymbol{B} + (\boldsymbol{B}\boldsymbol{A} + \boldsymbol{C}\boldsymbol{R}_R)\boldsymbol{C} \overset{\text{Eq. (4.35)}}{\Longrightarrow} \boldsymbol{B} \end{aligned} \tag{4.37}$$

as well as the imaginary part:

$$\begin{aligned} & \boldsymbol{B}\boldsymbol{R}_R\boldsymbol{C} - \boldsymbol{C}\boldsymbol{R}_R\boldsymbol{B} \overset{\text{Eq. (4.33)}}{\Longrightarrow} \boldsymbol{B}(-\boldsymbol{A}\boldsymbol{B}) - \boldsymbol{C}\boldsymbol{R}_R\boldsymbol{B} \\ = \; & -(\boldsymbol{B}\boldsymbol{A} + \boldsymbol{C}\boldsymbol{R}_R)\boldsymbol{B} \overset{\text{Eq. (4.35)}}{\Longrightarrow} \boldsymbol{O} \end{aligned} \tag{4.38}$$

Therefore,

$$\left(\boldsymbol{Z}_R^{-1}\right)^* \boldsymbol{R}_R \boldsymbol{Z}_R^{-1} = \boldsymbol{B} = \text{Real}\left(\boldsymbol{Z}_R^{-1}\right) \tag{4.39}$$

Thm. 4.4.1 can be then proved by simply plugging this relationship back to $\boldsymbol{H}^*\boldsymbol{R}_R\boldsymbol{H}$ and $\boldsymbol{Y}$ respectively. □

4.8.3 Proof of Theorem 4.5.1

We prove the theorem by showing that the rank of $\boldsymbol{Y} - \widetilde{\boldsymbol{Y}}$ gets reduced in every iteration, by the following lemma:

Lemma 4.8.1. *For any complex symmetric matrix $\boldsymbol{A}$ (i.e., $\boldsymbol{A} = \boldsymbol{A}^\top$), any vector $\vec{\boldsymbol{\eta}}$ such that $\vec{\boldsymbol{\eta}}^\top \boldsymbol{A}\vec{\boldsymbol{\eta}} \neq 0$, define $\vec{\boldsymbol{\xi}} = \boldsymbol{A}\vec{\boldsymbol{\eta}}$, then rank $\left(\boldsymbol{A} - \frac{\vec{\boldsymbol{\xi}}\vec{\boldsymbol{\xi}}^\top}{\vec{\boldsymbol{\xi}}^\top\vec{\boldsymbol{\eta}}}\right) \leq$ rank$(\boldsymbol{A}) - 1$.*

Proof: Since $\boldsymbol{A}$ is a complex symmetric matrix, there exists an Autonne-Takagi factorization [86] such that

$$\boldsymbol{A} = \boldsymbol{Q}\boldsymbol{\Lambda}\boldsymbol{Q}^{\top}, \text{ where } \boldsymbol{\Lambda} = \begin{bmatrix} \boldsymbol{\Lambda}_0 & \boldsymbol{O} \\ \boldsymbol{O} & \boldsymbol{O} \end{bmatrix}$$

where $\boldsymbol{Q}$ is a $n \times n$ unitary matrix, and $\boldsymbol{\Lambda}_0$ is a $r \times r$ diagonal matrix, where r is the rank of $\boldsymbol{A}$. Now substitute this as well as $\vec{\boldsymbol{\xi}} = \boldsymbol{A}\vec{\boldsymbol{\eta}}$, we get:

$$\boldsymbol{A} - \frac{\vec{\boldsymbol{\xi}}\vec{\boldsymbol{\xi}}^{\top}}{\vec{\boldsymbol{\xi}}^{\top}\vec{\boldsymbol{\eta}}} = \boldsymbol{Q}\left(\boldsymbol{\Lambda} - \frac{\boldsymbol{\Lambda}\boldsymbol{Q}^{\top}\vec{\boldsymbol{\eta}}\vec{\boldsymbol{\eta}}^{\top}\boldsymbol{Q}\boldsymbol{\Lambda}}{\vec{\boldsymbol{\eta}}^{\top}\boldsymbol{Q}\boldsymbol{\Lambda}\boldsymbol{Q}^{\top}\vec{\boldsymbol{\eta}}}\right)\boldsymbol{Q}^{\top} \tag{4.40}$$

Define $\vec{\boldsymbol{\zeta}} = \boldsymbol{Q}^{\top}\vec{\boldsymbol{\eta}}$, and substitute it into Eq. (4.40), we get

$$\boldsymbol{A} - \frac{\vec{\boldsymbol{\xi}}\vec{\boldsymbol{\xi}}^{\top}}{\vec{\boldsymbol{\xi}}^{\top}\vec{\boldsymbol{\eta}}} = \boldsymbol{Q}\begin{bmatrix} \boldsymbol{\Lambda}_0 - \frac{\boldsymbol{\Lambda}_0\vec{\boldsymbol{\zeta}}_0\vec{\boldsymbol{\zeta}}_0^{\top}\boldsymbol{\Lambda}_0}{\vec{\boldsymbol{\zeta}}_0^{\top}\boldsymbol{\Lambda}_0\vec{\boldsymbol{\zeta}}_0} & \vec{\boldsymbol{0}} \\ \vec{\boldsymbol{0}}^{\top} & \boldsymbol{O} \end{bmatrix}\boldsymbol{Q}^{\top} \tag{4.41}$$

Since $\boldsymbol{Q}$ is unitary, we have

$$\operatorname{rank}\left(\boldsymbol{A} - \frac{\vec{\boldsymbol{\xi}}\vec{\boldsymbol{\xi}}^{\top}}{\vec{\boldsymbol{\xi}}^{\top}\vec{\boldsymbol{\eta}}}\right) = \operatorname{rank}\left(\boldsymbol{\Lambda}_0 - \frac{\boldsymbol{\Lambda}_0\vec{\boldsymbol{\zeta}}_0\vec{\boldsymbol{\zeta}}_0^{\top}\boldsymbol{\Lambda}_0}{\vec{\boldsymbol{\zeta}}_0^{\top}\boldsymbol{\Lambda}_0\vec{\boldsymbol{\zeta}}_0}\right) \triangleq \operatorname{rank}(\boldsymbol{B}) \tag{4.42}$$

where for convenience, we define matrix $\boldsymbol{B} = \boldsymbol{\Lambda}_0 - \frac{\boldsymbol{\Lambda}_0\vec{\boldsymbol{\zeta}}_0\vec{\boldsymbol{\zeta}}_0^{\top}\boldsymbol{\Lambda}_0}{\vec{\boldsymbol{\zeta}}_0^{\top}\boldsymbol{\Lambda}_0\vec{\boldsymbol{\zeta}}_0}$. If we define $\vec{\boldsymbol{\zeta}}_0$ to be the first r entries of $\vec{\boldsymbol{\zeta}}$, we observe that:

$$\boldsymbol{B}\vec{\boldsymbol{\zeta}}_0 = \boldsymbol{\Lambda}_0\vec{\boldsymbol{\zeta}}_0 - \frac{\boldsymbol{\Lambda}_0\vec{\boldsymbol{\zeta}}_0\vec{\boldsymbol{\zeta}}_0^{\top}\boldsymbol{\Lambda}_0}{\vec{\boldsymbol{\zeta}}_0^{\top}\boldsymbol{\Lambda}_0\vec{\boldsymbol{\zeta}}_0}\vec{\boldsymbol{\zeta}}_0 = \boldsymbol{\Lambda}_0\vec{\boldsymbol{\zeta}}_0 - \boldsymbol{\Lambda}_0\vec{\boldsymbol{\zeta}}_0 = \vec{\boldsymbol{0}} \tag{4.43}$$

i.e., $\boldsymbol{B}$ is not full rank, such that $\operatorname{rank}(\boldsymbol{B}) \leq \operatorname{rank}(\boldsymbol{A}) - 1$. Therefore,

$$\operatorname{rank}\left(\boldsymbol{A} - \frac{\vec{\boldsymbol{\xi}}\vec{\boldsymbol{\xi}}^{\top}}{\vec{\boldsymbol{\xi}}^{\top}\vec{\boldsymbol{\eta}}}\right) \leq \operatorname{rank}(\boldsymbol{A}) - 1 \tag{4.44}$$

□

Since $\boldsymbol{Y}$ is a complex symmetric matrix, we can set $\boldsymbol{A} = \boldsymbol{Y} - \tilde{\boldsymbol{Y}}$, $\vec{\boldsymbol{\eta}} = \vec{\boldsymbol{i}}_T$, thus

$\vec{\xi} = (\boldsymbol{Y} - \tilde{\boldsymbol{Y}})\vec{i}_T = \Delta\vec{v}_T$. Therefore, applying the lemma, we get:

$$\text{rank}\left(\boldsymbol{Y} - \tilde{\boldsymbol{Y}} - \frac{\Delta\vec{v}_T \Delta\vec{v}_T^{\top}}{\Delta\vec{v}_T^{\top}\vec{i}_T}\right) \leq \text{rank}(\boldsymbol{Y} - \tilde{\boldsymbol{Y}}) - 1 \tag{4.45}$$

This means that the rank of $\boldsymbol{Y} - \tilde{\boldsymbol{Y}}$ gets reduced by at least 1 in each iteration. Since the initial rank cannot be larger than n, which is the size of the matrix, then the number of iterations that is needed cannot exceed n.

4.8.4 Proof of Thm. 4.5.2

To prove the theorem, we first prove the following lemma:

Lemma 4.8.2. *When a single receiver comes into range and existing receivers do not move, Alg. 1 needs only one iteration to converge.*

Proof: According to Lemma 4.8.1, we only need to prove that the rank of the matrix $\boldsymbol{Y} - \tilde{\boldsymbol{Y}}$ is equal to 1. When a new receiver comes into range, the matrices $\boldsymbol{M}$ and $\boldsymbol{Z}_R$ changes to $\boldsymbol{M}'$ and $\boldsymbol{Z}'_R$ in the following way:

$$\boldsymbol{M}' = \begin{bmatrix} \boldsymbol{M} \\ \vec{\boldsymbol{m}}^{\top} \end{bmatrix}, \quad \boldsymbol{Z}'_R = \begin{bmatrix} \boldsymbol{Z}_R & \vec{\boldsymbol{m}}_R \\ \vec{\boldsymbol{m}}_R^{\top} & z_R \end{bmatrix} \tag{4.46}$$

where $\vec{\boldsymbol{m}}$ contains the couplings between the transmitters to this receiver, $\vec{\boldsymbol{m}}_R$ contains the couplings from the other receivers to this one, and z_R is the impedance of this receivers. Therefore,

$$\begin{aligned} \boldsymbol{Y} &= \omega^2 \boldsymbol{M}'^{\top} \left(\boldsymbol{Z}'_R\right)^{-1} \boldsymbol{M}' && (4.47) \\ &= \omega^2 [\boldsymbol{M}^{\top} \quad \vec{\boldsymbol{m}}] \begin{bmatrix} \boldsymbol{Z}_R^{-1} + \frac{\boldsymbol{Z}_R^{-1}\vec{\boldsymbol{m}}_R\vec{\boldsymbol{m}}_R^{\top}\boldsymbol{Z}_R^{-1}}{z_R} & -\frac{\boldsymbol{Z}_R^{-1}\vec{\boldsymbol{m}}_R}{z_R} \\ -\frac{\vec{\boldsymbol{m}}_R^{\top}\boldsymbol{Z}_R^{-1}}{z_R} & \frac{1}{z_R} \end{bmatrix} \begin{bmatrix} \boldsymbol{M} \\ \vec{\boldsymbol{m}}^{\top} \end{bmatrix} && (4.48) \\ &= \tilde{\boldsymbol{Y}} + \frac{\omega^2}{z_R} \left(\boldsymbol{M}^{\top}\boldsymbol{Z}_R^{-1}\vec{\boldsymbol{m}}_R - \vec{\boldsymbol{m}}\right)\left(\boldsymbol{M}^{\top}\boldsymbol{Z}_R^{-1}\vec{\boldsymbol{m}}_R - \vec{\boldsymbol{m}}\right)^{\top} && (4.49) \end{aligned}$$

Consequently, if we define

$$\vec{\eta} = \boldsymbol{M}^{\top}\boldsymbol{Z}_R^{-1}\vec{\boldsymbol{m}}_R - \vec{\boldsymbol{m}} \tag{4.50}$$

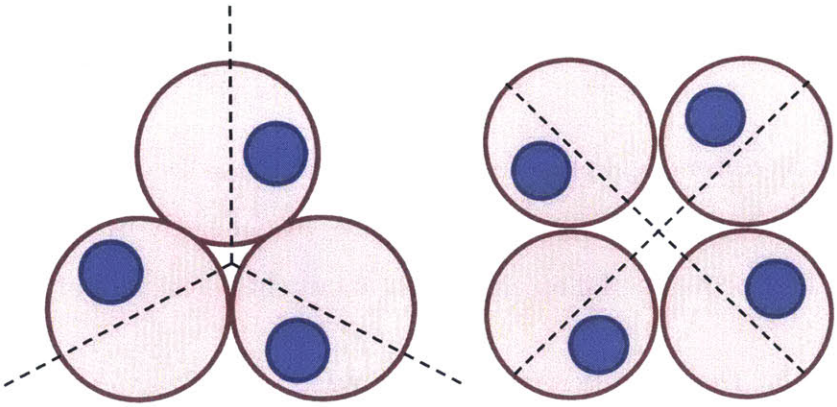

(a) 3 Tx, 3 Rx (b) 4 Tx, 4 Rx

Figure 4-4: **Examples of Symmetric Cases:** The figure shows top-down view of the Tx/Rx layout, where the red circles are Tx coils and blue circuits are Rx coils. In each case, the layout is rotation-symmetric with respect to the center point.

then

$$\boldsymbol{Y} - \tilde{\boldsymbol{Y}} = \frac{1}{z_R}\vec{\eta}\vec{\eta}^\top \tag{4.51}$$

Therefore, $\boldsymbol{Y} - \tilde{\boldsymbol{Y}}$ has rank equal to 1. □

Now, the event that an existing receiver leaves can be treated as the reciprocal event of a new receiver coming, so it also yields a $\boldsymbol{Y} - \tilde{\boldsymbol{Y}}$ matrix of rank 1. The event that one receiver moves is equivalent to a sequence of two events: (1) that specific receiver leaves, then (2) comes back into range with new channels. Since each of these two events is a rank-1 update, so they add up to at most rank two. Similarly, the event that r receivers move can be simulated by a series of r events, with each event involving only one receiver moving. Therefore, the total rank will be at most $2r$.

4.8.5 Proof of Equal Power Allocation in the Symmetric Case

Let us consider the case when the transmitters and receivers are symmetric with respect to a central point. Fig. 4-4 are examples of such cases. Assuming the receivers are identical, we want to prove that under such scenarios, the amount of power delivered to each receiver is the same.

Specifically, in this case, if we look at the couplings from the Tx coils to each Rx, they are the same with some shifts. Said differently, the coupling matrix $\boldsymbol{M}$ can be

written as

$$\boldsymbol{M} = [\boldsymbol{P}_0\vec{\boldsymbol{m}}\ \boldsymbol{P}_1\vec{\boldsymbol{m}}\ \cdots\ \boldsymbol{P}_{n-1}\vec{\boldsymbol{m}}]^\top \tag{4.52}$$

where $\vec{\boldsymbol{m}}$ is the vector of couplings from the first Rx to the Tx coils, and $\boldsymbol{P}_0, \boldsymbol{P}_1, \cdots, \boldsymbol{P}_{n-1}$ are the n shift matrices. $\boldsymbol{P}_i\vec{\boldsymbol{m}}$ effectively shifts $\vec{\boldsymbol{m}}$ circularly by an offset of i.

We will first prove the following lemma about the eigenspace of $\boldsymbol{M}$:

Lemma 4.8.3. *The eigen-decomposition of $\boldsymbol{M}$ is*

$$\boldsymbol{M}^\top = \mathcal{F}^{-1}\boldsymbol{\Lambda}\mathcal{F} \tag{4.53}$$

where $\mathcal{F}$ is the Fourier matrix, $\boldsymbol{\Lambda} = diag(\lambda_1, \lambda_2, \cdots, \lambda_n)$, and vector $[\lambda_1, \cdots, \lambda_n]$ is the Fourier domain of $\vec{\boldsymbol{m}}$.

Proof: Let us consider applying Fourier Transform to the i-th column of $\boldsymbol{M}^\top$, i.e., $\mathcal{F}(\boldsymbol{P}_i\vec{\boldsymbol{m}})$. The primal domain is a shifted version of $\vec{\boldsymbol{m}}$, thus the Fourier domain will be a phase shifted version of $\mathcal{F}\vec{\boldsymbol{m}}$, i.e., $[\lambda_1, \cdots, \lambda_n]$, which can be written in the following way:

$$\mathcal{F}(\boldsymbol{P}_i\vec{\boldsymbol{m}}) = \begin{bmatrix} \lambda_1 & & \\ & \ddots & \\ & & \lambda_n \end{bmatrix} \begin{bmatrix} e^{-j\frac{0\cdot i}{n}} \\ e^{-j\frac{1\cdot i}{n}} \\ \vdots \\ e^{-j\frac{(n-1)\cdot i}{n}} \end{bmatrix} = \boldsymbol{\Lambda}\mathcal{F}_i \tag{4.54}$$

where $\mathcal{F}_i$ is the i-th column of $\mathcal{F}$. Therefore,

$$\mathcal{F}\boldsymbol{M}^\top = \mathcal{F}[\boldsymbol{P}_0\vec{\boldsymbol{m}}\ \boldsymbol{P}_1\vec{\boldsymbol{m}}\ \cdots\ \boldsymbol{P}_{n-1}\vec{\boldsymbol{m}}] = \boldsymbol{\Lambda}[\mathcal{F}_0\ \mathcal{F}_1\ \cdots\ \mathcal{F}_{n-1}] = \boldsymbol{\Lambda}\mathcal{F} \tag{4.55}$$

or equivalently, $\boldsymbol{M}^\top = \mathcal{F}^{-1}\boldsymbol{\Lambda}\mathcal{F}$. □

For simplicity, let us assume $\boldsymbol{Z}_R = \boldsymbol{R}_R = R\mathbf{I}$, where $\mathbf{I}$ is the identity matrix. Now, applying Thm. 4.2.1,

$$\boldsymbol{H}^*\boldsymbol{R}_R\boldsymbol{H} = \frac{\omega^2}{R}\boldsymbol{M}^\top\boldsymbol{M} = \frac{\omega^2}{R}\mathcal{F}^{-1}\boldsymbol{\Lambda}^2\mathcal{F} \tag{4.56}$$

Therefore, each eigenvector of $\boldsymbol{H}^*\boldsymbol{R}_R\boldsymbol{H}$ is a column from Fourier Transform. Without loss of generality, let us say that it is the k-th column. Now the received current is

$$\vec{\boldsymbol{i}}_R = \boldsymbol{H}\vec{\boldsymbol{i}}_T = c \cdot \frac{j\omega}{R}\mathcal{F}^{-1}\boldsymbol{\Lambda}\mathcal{F}\mathcal{F}_k \tag{4.57}$$

Because of the orthogonality of the columns of the Fourier matrix, $\mathcal{F}^{-1}\boldsymbol{\Lambda}\mathcal{F}\mathcal{F}_k = \lambda_k\overline{\mathcal{F}_k}$, where $\overline{\mathcal{F}_k}$ is the k-th column of the inverse Fourier matrix, whose entries all have magnitudes equal to 1. Therefore, all entries in $\vec{\boldsymbol{i}}_R$ have the same magnitude, i.e., all receivers receive the same power.

4.8.6 Proof of Theorem 4.5.3

As shown in Lemma 4.8.1, if the rank of $\boldsymbol{Y} - \widetilde{\boldsymbol{Y}}$ is r, the algorithm will take exactly r steps (i.e., r different sets of voltages) to converge. Since we know

$$\Delta\vec{\boldsymbol{v}}_T = (\boldsymbol{Y} - \widetilde{\boldsymbol{Y}})\vec{\boldsymbol{i}}_T \tag{4.58}$$

By the fundamental theorem of linear algebra [67], the least number of different $\Delta\vec{\boldsymbol{v}}_T$ needed to uniquely solve the coefficient $\boldsymbol{Y} - \widetilde{\boldsymbol{Y}}$ is the rank of the coefficient, i.e., r. Therefore, Alg. 1 takes the least number of steps.

Chapter 5

Dealing with Power Circuit Limitations

5.1 What is the Problem?

In the previous chapter, we developed an algorithm that can maximize the power delivery to the receivers. It is based on the assumption that the power circuit on the receiver side can absorb however much power the transmitter delivers. However in reality there are many cases when this approximation is no longer true, and we are limited by the receiver's ability of the receiver to receive power. For example:

- *Receivers with very different power requirements:* Today's mobile devices require very different power levels in order to charge. On one hand, wearable devices require a fraction of a watt while a laptop require between 20W to 80W. There is an order of magnitude difference in the amount of power needed for different devices. Therefore, when they co-exist in the charging range the transmitter needs to recognize and acknowledge their huge difference in the expectation of power. Said differently, if the Tx treats them equally and tries to maximize the power delivery to both of them, it will end up trying to deliver an overwhelming amount of power to a device that requires much less power.

- *Near-Far problem:* as pointed out by §4.6, without explicit control, the amount of power delivered to each device is intrinsically tied to the couplings of the transmitter. This is natural and often acceptable, but in some cases can cause problems. Specifically, if one device is very near to the base and the other very far, the algorithm in §4 can easily overdraw the near receiver by exceeding its ratings but at the same time still cannot deliver enough power to the far one. The correct approach, however, should be optimizing on improving power delivery to the far receiver but at the same time making sure the near receiver is not overdrawn and when necessary even reduce the strength of magnetic field at the near receiver.

Both of these cases represent important limitations on the transmitter system architecture imposed by the practical limitations of the receivers' power circuits. These are limitations we have not yet addressed in the preceding chapters.

Thus it is not always advantageous to blindly maximize the amount of power the transmitter delivers. In both cases a naive transmitter may fall into the trap of trying to deliver too much power to the receiver. This is suboptimal and can even be dangerous. Every standard mobile device has its own charging circuit that controls how much power it needs at different stages of a charging cycle [47]. Trying to deliver more power than this desired amount will have at best a marginal increase in the actual power going into the device's battery, if there is any increase at all. At the same time, any power converter that converts the wirelessly delivered power to charge the mobile device can only have a limited range of operation with respect to voltage and current. So as the Tx tries to deliver more power, at some point it's going to exceed such a limitation, and it will either temporarily force the receiver out of its normal operation, or even permanently destroys its power circuit.

An alternative approach is to design transmitter with the ability to fine-tune the amount of power to each receiver to fit its specific requirement, instead of blindly maximizing the power delivery capability. In some cases, this might even mean reducing the magnetic field at some receivers is better than maximizing it. The transmitter controls this power delivery by either strengthening or weakening the magnetic field

around the receiver thus manipulating the induced voltage on the receiver. At the same time, the transmitter should know what the preferred and acceptable input voltages are for each receiver, such that the transmitter makes sure it does not exceed any of the receiver's desired parameters.

From a practical standpoint, this approach also requires communication between the transmitter and the receiver. The receiver locally decides the amount of power it needs, which it sends to the transmitter. The receiver also monitors how much actual power it receives as well as its own impedance and provides this feedback to the transmitter. In other words, this approach achieves the aforementioned benefit at the cost of increasing the expense and complexity of the receiver circuit. With the population of low-cost low-power communication modules such as BLE (Bluetooth Low Energy), in many cases this added complexity is likely worth the tradeoff even in a mass-produced product. Evidently, existing industrial standards of wireless charging have already embedded Bluetooth in their receiver module [25, 10]. However there are cases when we cannot have additional modules, in which case we can simply run the basic algorithm defined in §4.

This chapter also deals with other problems that are raised due to limitations of power circuits. One example is the varying receiver impedance. The equivalent receiver impedance depends on the input impedance of the power converters, which unfortunately changes dramatically with the input voltage [91]. For example, an ideal voltage regulator has the input impedance increasing quadratically with the input voltage [74]. In §5.4, we show how we can make the algorithm adapt to changing load impedances.

5.2 Fine-Control of Delivered Power

In this section, we will focus on the problem of how to set transmit voltages/currents to finely control the received power. Specifically, an ideal algorithm should have the following properties:

- *Power Control:* given specified amount of power $P_{u1}, P_{u2}, \cdots, P_{um}$, the Tx will deliver the exact amount P_i to receiver i.

- *Optimal Delivery:* at the same time, we minimize the loss of the transmitter, thus maximizing the coil-to-coil efficiency.

In this chapter, we assume the Tx knows all couplings and Rx impedances, and we assume fixed Rx impedance. We will address these two problems later in this chapter.

5.2.1 How Does the Algorithm Work?

So how does Tx control individual power delivery to Rx? Recall the Receiver Equation:

$$\vec{i}_R = \boldsymbol{H}\vec{i}_T = j\omega \boldsymbol{Z}_R^{-1}\boldsymbol{M}\vec{i}_T \tag{5.1}$$

which shows the relationship between transmit current and received current. So intuitively, if we inverse this equation, we will be able to know in order to yield the set of receiver currents $\vec{i}_R$, what transmit currents are needed. This is formally explained by the following lemma, which is proved in §5.5.1:

Lemma 5.2.1. *The solution to the following optimization problem:*

$$\min_{\vec{i}_T} \ \{P_T\}, \ \textit{where } P_T = \vec{i}_T^{*}\boldsymbol{R}_T\vec{i}_T \tag{5.2}$$

$$\textit{s.t.} \ \ \vec{i}_R = \boldsymbol{H}\vec{i}_T \tag{5.3}$$

i.e., minimizing transmit power loss conditioned on the received currents are equal to $\vec{i}_R$*, is*

$$\vec{i}_T = \boldsymbol{H}^{\dagger}\vec{i}_R \tag{5.4}$$

where $\cdot^{\dagger}$ *is the pseudo-inverse operation. Specifically, the condition is reached if and only if rank*$(\boldsymbol{H}) < n$ *where* n *is the number of transmitters. The achieved efficiency is*

$$\eta = \frac{\vec{i}_R^{*}(\boldsymbol{H}\boldsymbol{R}_T\boldsymbol{H}^{*})^{\dagger}\vec{i}_R}{\vec{i}_R^{*}\boldsymbol{R}_R\vec{i}_R} \tag{5.5}$$

Note the following:

- The condition of the transmitter having full degree of freedom to control the receiver is that the number of transmitters cannot be smaller than the number of receivers. [1] This conclusion is very similar to the degree-of-freedom concept in MIMO [90].

- When the conditions are met, the Tx theoretically has the ability to provide any amount of power to the receiver. Of course this is not true in practice, and the reason is because the achieved efficiency η can be very small thus in order to deliver such power we have to afford a huge loss on the Tx side. We will expand on this topic in §5.2.2.

Now we know how to control the receiver currents to be exactly $\vec{i}_R$. However our goal is to control the *power* delivered, not the currents. More specifically, we do not wish to specify the phase of each receiver current, since controlling amplitudes of currents is enough to control the power. Of all of the possible combinations of relative phases among receivers, we want to pick the combination that achieves the lowest Tx loss. Therefore, we revise the optimization problem in Lemma 5.2.1 to be the following:

$$\min_{\vec{i}_T} \ \{P_T\}, \text{ where } P_T = \vec{i}_T^* \boldsymbol{R}_T \vec{i}_T \tag{5.6}$$

$$\text{s.t. } \forall u, |I_{Ru}|^2 R_{Ru} = P_{Ru} \tag{5.7}$$

The following lemma shows what are the phases that achieves the optimization:

[1] $\text{rank}(\boldsymbol{H})$ is equal to the number of receivers except for very rare singular cases. This is very similar to the common approach in MIMO where the rank of channel matrix is treated as equal to the number of either transmitters or receivers, whichever is smaller [90].

Algorithm 3 Calculate Tx Voltages Needed to Finely Control Rx Power

procedure CALCTXCONTROLVOLTAGE($\boldsymbol{Z}_R$, $\boldsymbol{M}$, $P_{R1}, \cdots, P_{Rm}$)
  $\boldsymbol{H} \leftarrow j\omega \boldsymbol{Z}_R^{-1} \boldsymbol{M}$
  $\forall i,\ \vec{\boldsymbol{a}}_i \leftarrow i$-th column of $\boldsymbol{H}^\dagger$ multiplied by $\frac{\sqrt{P_{Ri}}}{R_{Ri}}$
  $\theta_1 \leftarrow 0$ ▷ We only care about relative phases so fix θ_1
  $\forall i \neq 1,\ \theta_i \leftarrow \text{rand}(0, 2\pi)$
  $\forall i,\ \vec{\boldsymbol{\xi}}_i \leftarrow e^{j\theta} \vec{\boldsymbol{a}}_i$
  repeat
    for $i = 2$ to m **do** ▷m is number of receivers
      $\theta_i \leftarrow \angle \left\{ \sum_{k \neq i} \vec{\boldsymbol{\xi}}_k \vec{\boldsymbol{a}}_i^* \right\} + \pi$ ▷ Update according to Lemma 5.2.2
      $\vec{\boldsymbol{\xi}}_i \leftarrow e^{j\theta} \vec{\boldsymbol{a}}_i$
    end for
  until Changes in θ_i's are small
  $\forall u, I_{Ru} \leftarrow e^{j\theta_u} \sqrt{P_{Ru}/R_{R_u}}$
  $\vec{\boldsymbol{i}}_T \leftarrow \boldsymbol{H}^\dagger \vec{\boldsymbol{i}}_R$ ▷Lemma 5.2.1
  $\vec{\boldsymbol{v}}_T \leftarrow (\boldsymbol{Z}_T + \omega^2 \boldsymbol{M}^\top \boldsymbol{Z}_R^{-1} \boldsymbol{M}) \vec{\boldsymbol{i}}_T$
  return $\vec{\boldsymbol{v}}_T$
end procedure

Lemma 5.2.2. *Define*

$$\boldsymbol{A} \triangleq \boldsymbol{H}^\dagger \begin{bmatrix} \frac{\sqrt{P_{R1}}}{R_{R1}} & & \\ & \ddots & \\ & & \frac{\sqrt{P_{Rm}}}{R_{Rm}} \end{bmatrix} \tag{5.8}$$

and define $\vec{\boldsymbol{a}}_i$ is the i-th column vector of $\boldsymbol{A}$. A set of receiver current phases $\theta_1, \theta_2, \cdots, \theta_m$ that minimizes Tx losses if and only if

$$\forall i, \quad \angle \left\{ \sum_{k \neq i} \vec{\boldsymbol{\xi}}_k^* \vec{\boldsymbol{\xi}}_i \right\} = \pi \tag{5.9}$$

where $\angle\{\cdot\}$ is the angle of the complex value, and $\vec{\boldsymbol{\xi}}_i$ is defined as

$$\vec{\boldsymbol{\xi}}_i \triangleq e^{j\theta_i} \vec{\boldsymbol{a}}_i \tag{5.10}$$

The lemma is proven in §5.5.2. Although there is no closed-form solution to what

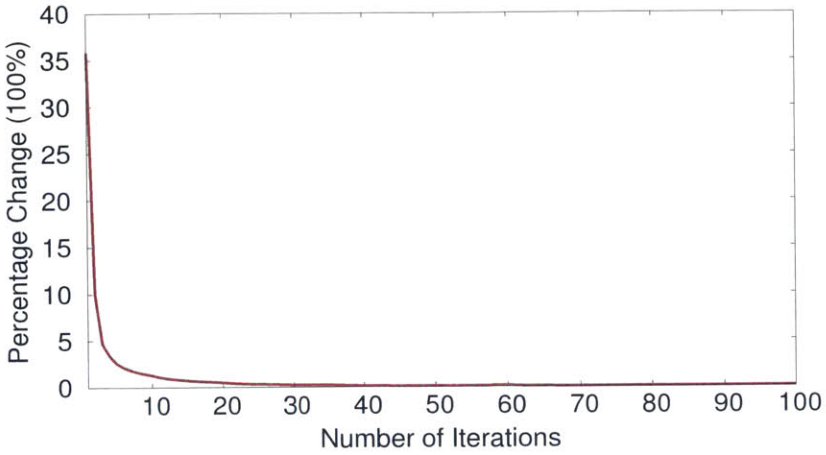

Figure 5-1: **Convergence of Alg. 3:** We show the percentage change vs. number of iterations averaged by simulated data of 6 Txs and 6 Rxs. With 20 iterations the percentage change is already below 1%.

the phases of the receivers should be, we can still compute these angles very efficiently using a technique called alternating minimization [56], based on the properties given by Lemma 5.2.2. Alg. 3 shows the pseudocode to compute what optimal Tx voltages $\vec{\boldsymbol{v}}_T$ is given any set of Rx power $P_{R1}, \cdots, P_{Rm}$. The following theorem guarantees the convergence of this algorithm, which is proven in §5.5.2.

Theorem 5.2.3. *Alg. 3 is guaranteed to converge to the solution of the optimization problem specified by Eq.* (5.6).

Thm. 5.2.3 guarantees convergence but does not specify the speed of convergence. The convergence speed depends on the number of transmitters and receivers. In practice, with number of transmitters and receivers not greater than 6, 10-20 iterations is sufficient for Alg. 3 to converge, as shown by Fig. 5-1.

5.2.2 How Much Control Does The Tx Have?

When the number of receivers does not exceed the number of transmitters, theoretically the Tx has the ability drive any set of receivers power. However, in some cases the voltage/current required by the Tx is too big to be practical. Specifically, it is bounded by the condition number of the matrix $\boldsymbol{H}$. The higher that the condition number is (i.e., the singular case), the more likely we need high transmitter cur-

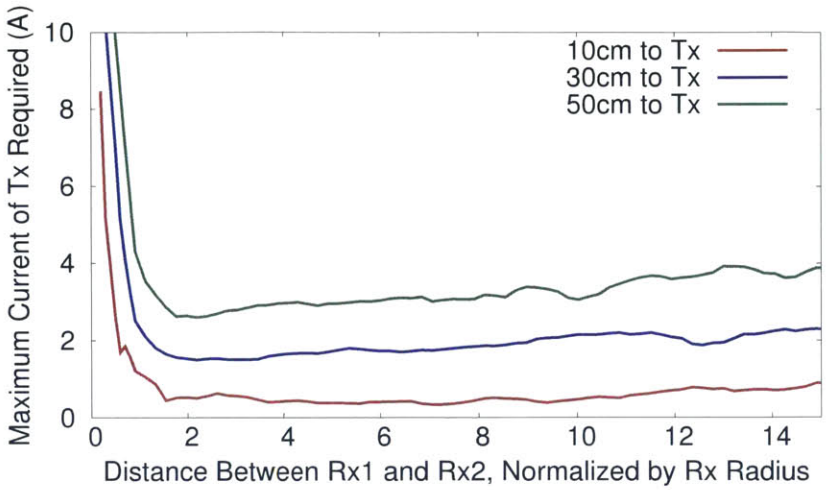

Figure 5-2: **Maximal Current Required by the Tx in order to Deliver 1W & 25W to Two Receivers Respectively:** There is a cliff around the diameter of the receiver. When two receivers are nearer than this distance, practically we cannot control the amount of power delivered to them separately.

rents/voltages to achieve a set of Rx currents, thus having low efficiency. Practically the power circuit on Tx only works when its voltage and current are within some range. Therefore, when the required voltage/current reach the point of exceeding the rating, Tx would be able to deliver the power that is demanded.

The question we want to ask is, in practical scenarios, when could $\boldsymbol{H}$ be singular, and how much control does the Tx have? To answer this, we simulate different scenarios to test the Tx's ability to deliver specified amounts of power to receivers. Specifically, we pick the two most challenging scenarios to present here: 1) two receivers with very different power requirements; 2) the near-far scenario.

Receivers Needing Significantly Different Power: In this case, since the two receivers have very similar couplings to the Tx, $\boldsymbol{H}$ can easily go singular. Tx loses its capability to separately set the power of the two receivers. To investigate how near the two receivers need to be for this problem to occur, we run a simulation where Tx is asked to deliver 1W to Rx1 and 25W to Rx2. This simulates the case when The result is shown in Fig. 5-2. We have two conclusion from this simulation:

- There is a clear cut-off distance, which is roughly 1.5 times the radius of the receiver, and below which Tx is not able to control power separately to each re-

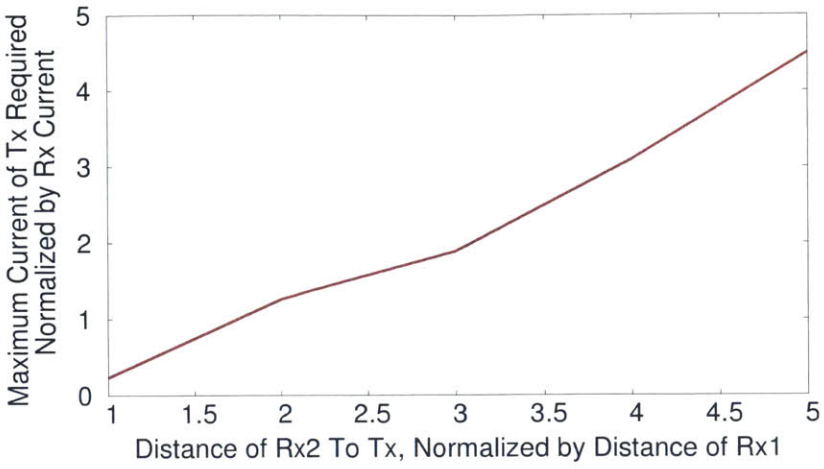

Figure 5-3: **Maximal Current Required by the Tx when One Receiver Is Near and Another Is Far** The required current on the Tx goes up almost linearly as Rx2 goes further away.

ceiver. The fact that this distance is a function of Rx radius is not a coincidence – this can be understood as the "beamwidth" from the Tx. Since the Tx tries to increase the density of the magnetic flux through the Rx coil, the effective beamwidth is closely related to the size of the Rx coil. If two receivers happen to be in the same beam, i.e., their distance is smaller than the beamwidth, Tx would be able to deliver significantly different amounts of power to each of them.

- Outside of this cut-off distance, Tx has the ability to reliably deliver significantly different and pre-specified amounts of power to each receiver.

Near-Far Scenario: In the near-far scenario, one receiver is near to the base while the other can be very far. In the simulation, we ask the Tx to deliver the same amount of power to each receiver. We fix Rx1 and increase the distance of Rx2 until it's far enough that the coupling is too weak to deliver the required amount of power. Fig. 5-3 shows the simulation result. The required current on the Tx goes up almost linearly as Rx2 goes further away. In the whole range, the Tx current remains in a reasonable range (less than 5 times the received current), and does not have a cliff that is too high to be practical. Therefore, the conclusion is that with the solution proposed in §5.2, Tx is able to handle the near-far problem reliably.

5.3 Estimating Magnetic Couplings

Alg. 3 requires us to know $\boldsymbol{H}$. Therefore, the communicationless channel estimation method used by 4.4 no longer works because it estimates $\boldsymbol{H}^*\boldsymbol{R}_R\boldsymbol{H}$ as a whole and does not have any knowledge of each of the entries of $\boldsymbol{H}$. So, how can we estimate $\boldsymbol{H}$?

Recall that Alg. 3 assumes there are communications between the Rx and Tx, which we have already used to request receive power. We can also make use of this communication channel to help in estimating the couplings. Specifically, the Rx can perform some local measurements, and communicate it back to the Tx, which collects the information from all Rxs and updates the channel. Ideally, in order for the Tx to gather as much information as possible, we would like the Rx to be able to measure the magnitude and phase of its own current/voltages. In §5.3.1 we will show how to estimate channels with such information.

However, it is practically very challenging to synchronize different receivers and transmitters so that the phase any of them measures locally is consistent with each other. Therefore, we would want to remove the requirement for the receiver to measure its own phase of the voltage or current in a way that is consistent with other receivers' measurements. In §5.3.2 we will show how we can extend the algorithm in §5.3.1 to do so. The final algorithm only requires the Rx to communicate back its received power and impedance.

5.3.1 Estimating with Amplitude & Phase Feedback from Rx

In order to estimate $\boldsymbol{H} = j\omega\boldsymbol{Z}_R^{-1}\boldsymbol{M}$, we will estimate $\boldsymbol{M}$ and $\boldsymbol{Z}_R$ separately.

Estimating $\boldsymbol{M}$: How to estimate $\boldsymbol{M}$ is similar to how we estimate $\boldsymbol{Y}$ in the previous chapter. Specifically, we want to develop a relationship between two known parameters where $\boldsymbol{M}$ is the coefficient matrix between them. This can be done via the following series of substitution: first, we rewrite the transmitter Eq. (3.12):

$$\vec{\boldsymbol{v}}_T = \left(\boldsymbol{Z}_T + \omega^2\boldsymbol{M}^\top\boldsymbol{Z}_R^{-1}\boldsymbol{M}\right)\vec{\boldsymbol{i}}_T = \boldsymbol{Z}_T\vec{\boldsymbol{i}}_T - j\omega\boldsymbol{M}^\top\left(j\omega\boldsymbol{Z}_R^{-1}\boldsymbol{M}\vec{\boldsymbol{i}}_T\right) \tag{5.11}$$

Algorithm 4 Control Rx Power with Phase Feedback

procedure RxPowerControlPhaseFeedback($\boldsymbol{Z}_T$)
  $\{\widetilde{\boldsymbol{M}}, \widetilde{\boldsymbol{Z}_R}\} \leftarrow$ Bootstrap'($\boldsymbol{Z}_T$) ▷Bootstrap can be adopted from Alg. 2
  while true **do**
    Rx requests power $P_{R1}, P_{R2}, \cdots, P_{Rm}$
    $\vec{\boldsymbol{v}}_T^{\,c} \leftarrow$ CalcTxControlVoltage($\widetilde{\boldsymbol{Z}_R}, \widetilde{\boldsymbol{M}}, P_{R1}, \cdots, P_{Rm}$) ▷Alg. 3
    Apply $\vec{\boldsymbol{v}}_T^{\,c}$ ▷Try to deliver $P_{R1}, \cdots, P_{Rm}$ to receivers
    Measure $\vec{\boldsymbol{i}}_T$ on the transmitter
    Get $\vec{\boldsymbol{i}}_R$ communicated from Rx
    if $\{\vec{\boldsymbol{i}}_R \neq j\omega \boldsymbol{Z}_R^{-1} \boldsymbol{M} \vec{\boldsymbol{i}}_T\}$ **then** ▷if the channel changes
      $\widetilde{\boldsymbol{M}} \leftarrow \widetilde{\boldsymbol{M}} + \frac{\vec{\boldsymbol{i}}_R \vec{\boldsymbol{u}}^\top}{\Delta \vec{\boldsymbol{u}}^\top \vec{\boldsymbol{u}}}$, where $\Delta \vec{\boldsymbol{u}} = \frac{j}{\omega}\left(\vec{\boldsymbol{v}}_T^{\,c} - \boldsymbol{Z}_T \vec{\boldsymbol{i}}_T\right) - \widetilde{\boldsymbol{M}}^\top \vec{\boldsymbol{i}}_R$
      ▷ update $\widetilde{\boldsymbol{M}}$
      $\widetilde{\boldsymbol{Z}_R} \leftarrow \widetilde{\boldsymbol{Z}_R} + \frac{\Delta \vec{\boldsymbol{x}} \Delta \vec{\boldsymbol{y}}^\top}{\Delta \vec{\boldsymbol{y}}^\top \vec{\boldsymbol{y}}}$ where $\Delta \vec{\boldsymbol{y}} = \omega^2 \widetilde{\boldsymbol{M}} \vec{\boldsymbol{i}}_T - \widetilde{\boldsymbol{Z}_R} \left(\boldsymbol{M}^\top\right)^\dagger \left(\vec{\boldsymbol{v}}_T - \boldsymbol{Z}_T \vec{\boldsymbol{i}}_T\right)$
      ▷ update $\widetilde{\boldsymbol{Z}_R}$
    end if
  end while
end procedure

second, we plug in the receiver Eq. (3.11) $\vec{\boldsymbol{i}}_R = j\omega \boldsymbol{Z}_R^{-1} \boldsymbol{M} \vec{\boldsymbol{i}}_T$ to get

$$\vec{\boldsymbol{v}}'_T = \boldsymbol{M}^\top \vec{\boldsymbol{i}}_R, \text{ where } \vec{\boldsymbol{v}}'_T \triangleq \frac{j}{\omega}\left(\vec{\boldsymbol{v}}_T - \boldsymbol{Z}_T \vec{\boldsymbol{i}}_T\right) \tag{5.12}$$

Therefore, $\boldsymbol{M}$ is the coefficient between $\vec{\boldsymbol{i}}_R$ that we can know from Rx feedback, and $\vec{\boldsymbol{v}}'_T$ that we can measure and calculate on the Tx. Now we have just reduced the problem of estimating $\boldsymbol{M}$ to be something that takes the same mathematical form as estimating $\boldsymbol{Y}$ in §4.4. To see why, let's compare Eq. (5.12) to the Tx Eq. (3.12) that we used to estimate $\boldsymbol{Y}$:

$$\frac{j}{\omega}\left(\vec{\boldsymbol{v}}_T - \boldsymbol{Z}_T \vec{\boldsymbol{i}}_T\right) = \boldsymbol{M}^\top \vec{\boldsymbol{i}}_R \quad \text{Eq. (5.12)}$$

$$\vec{\boldsymbol{v}}_T - \boldsymbol{Z}_T \vec{\boldsymbol{i}}_T = \boldsymbol{Y} \vec{\boldsymbol{i}}_T \quad \text{Eq. (3.12)}$$

The only differences are that Eq. (5.12) has an additional constant factor $\frac{j}{\omega}$ on the left, and it has $\vec{\boldsymbol{i}}_R$ instead of $\vec{\boldsymbol{i}}_T$ on the right. Consequently, the same algorithm (Alg. 1) that is used in §4.4 can be adopted to estimating $\boldsymbol{M}$. Alg. 4 shows how we estimate $\boldsymbol{M}$.

Estimating $\boldsymbol{Z}_R$: We can use the same principle to estimate $\boldsymbol{Z}_R$. Specifically, the transmitter Eq. (3.12) can be rewritten to:

$$\vec{\boldsymbol{y}} = \boldsymbol{Z}_R\vec{\boldsymbol{x}}, \text{ where } \vec{\boldsymbol{x}} = \left(\boldsymbol{M}^\top\right)^\dagger \left(\vec{\boldsymbol{v}}_T - \boldsymbol{Z}_T\vec{\boldsymbol{i}}_T\right), \vec{\boldsymbol{y}} = \omega^2\boldsymbol{M}\vec{\boldsymbol{i}}_T \tag{5.13}$$

Here both $\vec{\boldsymbol{x}}$ and $\vec{\boldsymbol{y}}$ are known, so we can estimate $\boldsymbol{Z}_R$ in the same way as $\boldsymbol{M}$.

Alg. 4 shows how we can estimate $\boldsymbol{M}$, $\boldsymbol{Z}_R$ thus $\boldsymbol{H}$, and consequently control the Rx power. It has the same convergence property as Alg. 1, summarized by the following theorem (proven in §5.5.3):

Theorem 5.3.1. *If $\widetilde{\boldsymbol{M}} \neq \boldsymbol{M}$ or $\widetilde{\boldsymbol{Z}_R} \neq \boldsymbol{Z}_R$, then Alg. 4 is guaranteed to update $\widetilde{\boldsymbol{H}}$ to $\boldsymbol{H}$ in less than n iterations, where n is the number of transmitters.*

5.3.2 Eliminating the Need for Phase Feedback from Rx

Now the question becomes how we can estimate $\boldsymbol{M}$ and $\boldsymbol{Z}_R$ even without knowing the phase of $\vec{\boldsymbol{i}}_R$. More specifically, how can we change line 10 and line 14 in Alg. 4 so that it does not require knowing the phase of $\vec{\boldsymbol{i}}_R$?

To answer this, let us first spend a bit more time in understanding the heuristic meaning of line 10 and line 14 in Alg 4. It is characterized by the following lemma, which is proven in §5.5.4:

Lemma 5.3.2. *Define*

$$\Delta\widetilde{\boldsymbol{M}} = \frac{\Delta\vec{\boldsymbol{u}}\Delta\vec{\boldsymbol{u}}^\top}{\Delta\vec{\boldsymbol{u}}^\top\vec{\boldsymbol{i}}_R}, \text{ where } \Delta\vec{\boldsymbol{u}} = \frac{j}{\omega}\left(\vec{\boldsymbol{v}}_T^c - \boldsymbol{Z}_T\vec{\boldsymbol{i}}_T\right) - \widetilde{\boldsymbol{M}^\top}\vec{\boldsymbol{i}}_R \tag{5.14}$$

i.e., $\Delta\widetilde{\boldsymbol{M}}$ is the update that is applied in line 10 of Alg. 4. Then $\Delta\widetilde{\boldsymbol{M}}$ is the solution to the following optimization problem:

$$\min_{\Delta\widetilde{\boldsymbol{M}}}\{\|\Delta\widetilde{\boldsymbol{M}}\|^2\}, \text{ s.t. } \frac{j}{\omega}\left(\vec{\boldsymbol{v}}_T^c - \boldsymbol{Z}_T\vec{\boldsymbol{i}}_T\right) = (\widetilde{\boldsymbol{M}} + \Delta\widetilde{\boldsymbol{M}})^\top\vec{\boldsymbol{i}}_R \tag{5.15}$$

where $\|\cdot\|$ for a matrix stands for Frobenius norm, i.e., entrywise summation of the squares of the absolute values.

Algorithm 5 Control Rx Power without Phase Feedback

procedure RxPowerControlPhaseNoFeedback($\boldsymbol{Z}_T$)
  $\{\widetilde{\boldsymbol{M}}, \widetilde{\boldsymbol{Z}_R}\} \leftarrow$ Bootstrap'($\boldsymbol{Z}_T$) ▷Bootstrap can be adopted from Alg. 2
  while true **do**
    Rx requests power $P_{R1}, P_{R2}, \cdots, P_{Rm}$
    $\vec{\boldsymbol{v}}_T^{\,c} \leftarrow$ CalcTxControlVoltage($\widetilde{\boldsymbol{Z}_R}, \widetilde{\boldsymbol{M}}, P_{R1}, \cdots, P_{Rm}$) ▷Alg. 3
    Apply $\vec{\boldsymbol{v}}_T^{\,c}$ ▷Try to deliver $P_{R1}, \cdots, P_{Rm}$ to receivers
    Measure $\vec{\boldsymbol{i}}_T$ on the transmitter
    Get $\vec{\boldsymbol{i}}_R$ communicated from Rx
    if $\{\vec{\boldsymbol{i}}_R \neq j\omega \boldsymbol{Z}_R^{-1} \boldsymbol{M} \vec{\boldsymbol{i}}_T\}$ **then** ▷if the channel changes
      $\Delta\vec{\boldsymbol{u}} \leftarrow \frac{j}{\omega}\left(\vec{\boldsymbol{v}}_T^{\,c} - \boldsymbol{Z}_T \vec{\boldsymbol{i}}_T\right) - \widetilde{\boldsymbol{M}}^\top \vec{\boldsymbol{i}}_R$
      $\Delta\widetilde{\boldsymbol{M}} \leftarrow$ SolveA($\Delta\vec{\boldsymbol{u}}, \{\frac{\sqrt{P_{R1}}}{R_{R1}}, \cdots, \frac{\sqrt{P_{Rm}}}{R_{Rm}}\}$)
      ▷ calculate the update to $\widetilde{\boldsymbol{M}}$, using the procedure defined in line 20
      $\widetilde{\boldsymbol{M}} \leftarrow \widetilde{\boldsymbol{M}} + \Delta\widetilde{\boldsymbol{M}}$
      $\widetilde{\boldsymbol{Z}_R} \leftarrow \widetilde{\boldsymbol{Z}_R} + \frac{\Delta\vec{\boldsymbol{y}}\Delta\vec{\boldsymbol{y}}^\top}{\Delta\vec{\boldsymbol{y}}^\top\vec{\boldsymbol{x}}}$ where $\Delta\vec{\boldsymbol{y}} = \omega^2\widetilde{\boldsymbol{M}}\vec{\boldsymbol{i}}_T - \widetilde{\boldsymbol{Z}_R}\left(\boldsymbol{M}^\top\right)^\dagger\left(\vec{\boldsymbol{v}}_T - \boldsymbol{Z}_T\vec{\boldsymbol{i}}_T\right)$
      ▷ update $\widetilde{\boldsymbol{Z}_R}$
    end if
  end while
end procedure

procedure SolveA($\vec{\boldsymbol{y}}$, $\{a_1, \cdots, a_m\}$)
  ▷Solving $\min\{\|\boldsymbol{A}\|^2\}$, s.t. $\boldsymbol{A}\vec{\boldsymbol{x}} = \vec{\boldsymbol{y}}$
  ▷where $\vec{\boldsymbol{y}}$ is known,
  ▷but we only know the entrywise amplitude of $\vec{\boldsymbol{x}}$: $\{a_1, \cdots, a_m\}$
  $\forall i, y_i \leftarrow i$-th entry of $\vec{\boldsymbol{y}}$
  $\forall i, x_i \leftarrow e^{j\theta_i} a_i$
  repeat
    for $i = 2$ to m **do** ▷m is the length of vector $\vec{\boldsymbol{x}}$ and $\vec{\boldsymbol{y}}$
      $\theta_i \leftarrow \angle\left\{\sum_{k\neq i} x_k \overline{y_i}\right\} + \pi$
      $x_i \leftarrow e^{j\theta_i} a_i$
    end for
  until Changes in θ_i's are small
  $\vec{\boldsymbol{x}} \leftarrow [x_1, \cdots, x_m]^\top$
  $\boldsymbol{A} \leftarrow \frac{\vec{\boldsymbol{y}}\vec{\boldsymbol{x}}^*}{\vec{\boldsymbol{x}}^*\vec{\boldsymbol{y}}}$
  return $\boldsymbol{A}$
end procedure

Said informally, in Alg. 4 we try to find the *smallest* possible incremental update $\Delta\widetilde{\boldsymbol{M}}$ to $\widetilde{\boldsymbol{M}}$ such that the measured currents would match the updated value, i.e., $\widetilde{\boldsymbol{M}} + \Delta\widetilde{\boldsymbol{M}}$. The way we test if the estimation matches the measurement is via testing

if substituting $\boldsymbol{M}$ to the estimation $\widetilde{\boldsymbol{M}} + \Delta\widetilde{\boldsymbol{M}}$ will make Eq. 5.12 holds or not. Intuitively, since the algorithm iterates rapidly, between each iterations the channel would not change so much, so a heuristic strategy of picking the smallest change that is consistent with measurements is likely to work. Even if the channel happens to change dramatically such that the smallest update is no longer correct, it has the proven property (Thm. 5.3.1) that when accumulated along different iterations, this estimation will ultimately be updated to the correct value.

When we do not have the phase information from the Rx, we can adopt this approach to cope with the lack of this information. In this case, the optimization problem in Equ. (5.14) can be changed to:

$$\begin{aligned} & \min_{\Delta\widetilde{\boldsymbol{M}}} \{\|\Delta\widetilde{\boldsymbol{M}}\|^2\} \\ \text{s.t.} \quad & \exists\{\theta_1, \cdots, \theta_m\},\ \frac{j}{\omega}\left(\vec{\boldsymbol{v}}_T^c - \boldsymbol{Z}_T\vec{\boldsymbol{i}}_T\right) = (\widetilde{\boldsymbol{M}} + \Delta\widetilde{\boldsymbol{M}})^\top \vec{\boldsymbol{i}}_R \\ \text{where} \quad & \vec{\boldsymbol{i}}_R = \left[e^{j\theta_1}\sqrt{\frac{P_{R1}}{R_{R1}}},\ \cdots,\ e^{j\theta_m}\sqrt{\frac{P_{Rm}}{R_{Rm}}}\right]^\top \end{aligned} \tag{5.16}$$

In other words, we still look for the smallest change to make the estimations consistent with the measurements. However, in this case, we only need the amplitude of the currents to match. We use a two-step process to solve this problem: 1) we try to find the angles of $\vec{\boldsymbol{i}}_R$ via an algorithm very similar to the alternating minimization process employed in Alg. 3; 2) we update $\boldsymbol{M}$ and $\boldsymbol{Z}_R$ once we recover the angles, in the same way shown in Alg. 5. Algorithm 5 shows the pseudo-code which contains the details of how we perform the updating process. Its correctness is proven in §5.5.5.

5.4 Dealing with Varying Load Impedance

In the previous sections, we have assumed that the load impedance is stable. However, the load impedance might change due to two reasons:

- The resistance of the mobile device might change. For the same mobile device, its resistance is a function of the battery percentage. Typically, the resistance

is low when the battery percentage is low so that it can charge quickly, and the resistance goes up as the battery percentage increases.

- The equivalent impedance of the power converter in the receiver circuit changes with the input voltage. The specific relationship depends on the architecture of the power converter. For example, the input impedance of a DC/DC voltage regulator changes quadratically with the input voltage.

Therefore, the load impedance Z_R is determined by the input voltage V_R and the battery percentage η, i.e.,

$$Z_R = f(V_R, \eta) \tag{5.17}$$

It is worth noting that f is fixed given a particular receiver circuit and a particular mobile device. Said differently, f can be measured when the receiver is fabricated, and can then be communicated back to the transmitter so that MultiSpot can use it in the algorithm to capture varying load impedance.

Specifically, we need to change the algorithm (Alg. 5) to capture the variance of load impedance in two places:

- *Calculating what transmitter voltages to apply (Line. 5 in Alg. 5)*: We need to calculate what $\boldsymbol{Z}_R$ would be if we want the receiver power to be $P_{R1}, \cdots, P_{Rm}$. Specifically, for receiver u, we decide what its impedance would be if the received power is P_{Ru}, in the following way: First, we need the receiver to communicate back its current battery percentage η_u. Second, we calculate a lookup table between receiver input voltage V_{Ru} and power P_{Ru} as $P_{Ru} = |V_{Ru}|^2 / f(V_{Ru}, \eta_u)$. From this lookup table, we can then solve V_R for a given P_{Ru} and η_u. Finally, once V_{Ru} is solved, Z_{Ru} can be calculated as $f(V_{Ru}, \eta_u)$. After we solve Z_{Ru} for every u, we can recalculate $\boldsymbol{Z}_R$ and put it as the input to procedure CALCTXCONTROLVOLTAGE in Line. 5.

- *Estimating magnetic couplings: (Line. 9 to Line. 16 in Alg. 5)*: We need the receivers to measure their impedances locally and communicate them back. Before executing Line. 9, we replace the diagonals of $\boldsymbol{Z}_R$ and $\widetilde{\boldsymbol{Z}_R}$ with these

impedances measured on receivers, and then execute Line. 9 to Line. 16 as they are in Alg. 5.

In summary, to capture varying load impedances, we can simply augment the system we already have. Specifically, the transmitter needs to augment Alg. 5 before Line. 5 and Line. 9 as explained above. And the receiver needs to do the following in addition:

- Measure function f defined by Eq. (5.17) in a factory setting and communicate f to the transmitter when the receiver comes into the range.
- Measure its impedance repeatedly and communicate it back to the transmitter.

The pseudo-code of the final algorithm is shown in App. A.

5.5 Proofs

5.5.1 Proof of Lemma 5.2.1

If we define

$$\vec{\boldsymbol{x}} = \sqrt{\boldsymbol{R}_T}\vec{\boldsymbol{i}}_T \tag{5.18}$$

$$\boldsymbol{C} = \boldsymbol{H}\sqrt{\boldsymbol{R}_T^{-1}} \tag{5.19}$$

$$\vec{\boldsymbol{y}} = \vec{\boldsymbol{i}}_R \tag{5.20}$$

Then the optimization problem becomes

$$\min_{\vec{\boldsymbol{x}},\,\text{s.t.}\,\vec{\boldsymbol{y}}=\boldsymbol{C}\vec{\boldsymbol{x}}} \left\{\|\vec{\boldsymbol{x}}\|^2\right\} \tag{5.21}$$

This is a standard min-square optimization problem where the solution is given by pseudo-inverse [72]. Specifically, as long as $\text{rank}(\boldsymbol{C})$ is smaller than the length of $\vec{\boldsymbol{y}}$, the optimal solution is $\vec{\boldsymbol{x}} = \boldsymbol{C}^\dagger\vec{\boldsymbol{y}}$. Therefore, the optimal $\vec{\boldsymbol{i}}_T$ is

$$\vec{\boldsymbol{i}}_T = \sqrt{\boldsymbol{R}_T^{-1}}\left(\boldsymbol{H}\sqrt{\boldsymbol{R}_T^{-1}}\right)^\dagger \vec{\boldsymbol{i}}_R = \boldsymbol{H}^\dagger\vec{\boldsymbol{i}}_R \tag{5.22}$$

5.5.2 Proof of Lemma 5.2.2 and Theorem 5.2.3

Firstly, the optimization problem of finding $\{\theta_1, \theta_2, \cdots, \theta_m\}$ can be rewritten as

$$\min_{\theta_1,\cdots,\theta_m} \left\{ \left\| \sum_i e^{j\theta_i} \vec{\boldsymbol{a}}_i \right\|^2 \right\} \tag{5.23}$$

Now for convenience let's define

$$\vec{\boldsymbol{y}} = \sum_i e^{j\theta_i} \vec{\boldsymbol{a}}_i = \sum_i \vec{\boldsymbol{\xi}}_i, \text{ where } \vec{\boldsymbol{\xi}}_i = e^{j\theta_i} \vec{\boldsymbol{a}}_i \tag{5.24}$$

Therefore,

$$\begin{aligned} \|\vec{\boldsymbol{y}}\|^2 &= \left(\sum_i \vec{\boldsymbol{\xi}}_i^* \right) \left(\sum_i \vec{\boldsymbol{\xi}}_i \right) && (5.25) \\ &= \sum_i \|\vec{\boldsymbol{a}}_i\|^2 + 2 \sum_{k \neq i} \text{real} \left\{ \vec{\boldsymbol{\xi}}_i^* \vec{\boldsymbol{\xi}}_k \right\} && (5.26) \end{aligned}$$

If we do the derivatives, we get

$$\frac{\partial \|\vec{\boldsymbol{y}}\|^2}{\partial \theta_i} = \frac{\partial}{\partial \theta_i} \sum_{k \neq i} \text{real} \left\{ \vec{\boldsymbol{\xi}}_i^* \vec{\boldsymbol{\xi}}_k \right\} = -2 \cdot \text{imag} \left\{ \sum_{k \neq i} \vec{\boldsymbol{\xi}}_k^* \vec{\boldsymbol{\xi}}_i \right\} \tag{5.27}$$

And the second order derivative is

$$\frac{\partial^2 \|\vec{\boldsymbol{y}}\|^2}{\partial \theta_i^2} = \frac{\partial}{\partial \theta_i} \left\{ -2 \cdot \text{imag} \left\{ \sum_{k \neq i} \vec{\boldsymbol{\xi}}_k^* \vec{\boldsymbol{\xi}}_i \right\} \right\} = -2 \cdot \text{real} \left\{ \sum_{k \neq i} \vec{\boldsymbol{\xi}}_k^* \vec{\boldsymbol{\xi}}_i \right\} \tag{5.28}$$

A necessary condition of θ_i being the minima is a zero first-order derivative and positive second-order derivative, i.e.,

$$-2 \cdot \text{imag} \left\{ \sum_{k \neq i} \vec{\boldsymbol{\xi}}_k^* \vec{\boldsymbol{\xi}}_i \right\} = 0, \quad -2 \cdot \text{real} \left\{ \sum_{k \neq i} \vec{\boldsymbol{\xi}}_k^* \vec{\boldsymbol{\xi}}_i \right\} > 0 \tag{5.29}$$

or equivalently,

$$\angle \left\{ \sum_{k \neq i} \vec{\boldsymbol{\xi}}_k^* \vec{\boldsymbol{\xi}}_i \right\} = \pi \tag{5.30}$$

Now the sufficient condition is to prove the Hessian matrix of second-order derivatives are positive definite [38]. Note that

$$\frac{\partial^2 \|\vec{\boldsymbol{y}}\|^2}{\partial\theta_i \partial\theta_k} = 2 \cdot \text{real}\left\{\vec{\boldsymbol{\xi}}_k^* \vec{\boldsymbol{\xi}}_i\right\} \tag{5.31}$$

$$\frac{\partial^2 \|\vec{\boldsymbol{y}}\|^2}{\partial\theta_i^2} = -2 \cdot \text{real}\left\{\sum_{k\neq i} \vec{\boldsymbol{\xi}}_k^* \vec{\boldsymbol{\xi}}_i\right\} = 2 \cdot \text{real}\left\{\left(\vec{\boldsymbol{\xi}}_i^* - \vec{\boldsymbol{y}}\right) \vec{\boldsymbol{\xi}}_i\right\} \tag{5.32}$$

And because we fixed θ_1 to be 0 since we only care about the relative phases, the Hessian matrix is a $(m-1) \times (m-1)$ matrix, denoted by $\boldsymbol{B}$. It can be written as

$$\boldsymbol{B} = \text{real}\left\{\begin{bmatrix} \vec{\boldsymbol{\xi}}_2 \\ \vdots \\ \vec{\boldsymbol{\xi}}_m \end{bmatrix} \begin{bmatrix} \vec{\boldsymbol{\xi}}_2 & \cdots & \vec{\boldsymbol{\xi}}_m \end{bmatrix} - \begin{bmatrix} \vec{\boldsymbol{y}}^* \vec{\boldsymbol{\xi}}_2 & & \\ & \ddots & \\ & & \vec{\boldsymbol{y}}^* \vec{\boldsymbol{\xi}}_m \end{bmatrix}\right\} \tag{5.33}$$

Now we want to prove $\boldsymbol{B}$ is positive definite, i.e., for any $\vec{\boldsymbol{x}}$ of length $(m-1)$, $\vec{\boldsymbol{x}}^\top \boldsymbol{B} \vec{\boldsymbol{x}} > 0$:

$$\frac{1}{2}\vec{\boldsymbol{x}}^\top \boldsymbol{B} \vec{\boldsymbol{x}} = \text{real}\left\{\left(\sum_{i\geq 2} \vec{\boldsymbol{\xi}}_i x_i\right)^* \left(\sum_{i\geq 2} \vec{\boldsymbol{\xi}}_i x_i\right) - \sum_{i\geq 2} \left(\sum_{k} \vec{\boldsymbol{\xi}}_k\right)^* \vec{\boldsymbol{\xi}}_i x_i^2\right\} \tag{5.34}$$

$$= -\text{real}\left\{\sum_{i\geq 2} \left(\sum_{k\neq i} \vec{\boldsymbol{\xi}}_k^* \vec{\boldsymbol{\xi}}_i\right) x_i^2\right\} \tag{5.35}$$

Note that from Equ. (5.29), $\text{real}\left\{\sum_{k\neq i} \vec{\boldsymbol{\xi}}_k^* \vec{\boldsymbol{\xi}}_i\right\} > 0$. Therefore, $\vec{\boldsymbol{x}}^\top \boldsymbol{B} \vec{\boldsymbol{x}} > 0$. □

5.5.3 Proof of Theorem 5.3.1

It can be directly proved by applying Lemma 4.8.1. Specifically, to prove the update of $\widetilde{\boldsymbol{M}}$ is correct, set the following parameters in Lemma 4.8.1 to be:

$$\boldsymbol{A} = \boldsymbol{M} - \widetilde{\boldsymbol{M}}, \vec{\boldsymbol{\eta}} = \vec{\boldsymbol{i}}_R, \vec{\boldsymbol{\xi}} = \Delta\vec{\boldsymbol{u}} \tag{5.36}$$

where $\Delta\vec{\boldsymbol{u}}$ is defined as in line 10 in Alg. 4, and then apply the lemma. Similarly, the parameters need to be set to the following to prove $\boldsymbol{Z}_R$:

$$\boldsymbol{A} = \boldsymbol{Z}_R - \widetilde{\boldsymbol{Z}_R}, \vec{\boldsymbol{\eta}} = \vec{\boldsymbol{x}}, \vec{\boldsymbol{\xi}} = \Delta\vec{\boldsymbol{y}} \tag{5.37}$$

where $\Delta\vec{\boldsymbol{y}}$ and $\vec{\boldsymbol{x}}$ are defined as in line 14 in Alg. 4.

5.5.4 Proof of Lemma 5.3.2

Can be proven via the following lemma:

Lemma 5.5.1. *The solution to the following optimization problem:*

$$\min_{\boldsymbol{A}} \left\{ \|\boldsymbol{A}\|^2 \right\}, \ s.t. \ \boldsymbol{A}\vec{\boldsymbol{x}} = \vec{\boldsymbol{y}} \tag{5.38}$$

where $\|\cdot\|$ *standards for Frobenius norm, is*

$$\boldsymbol{A} = \frac{\vec{\boldsymbol{y}}\vec{\boldsymbol{x}}^*}{\vec{\boldsymbol{x}}^*\vec{\boldsymbol{x}}} \tag{5.39}$$

Proof: Can be directly proven by the property of pseudoinverse [72], the solution to the optimization problem in Eq. 5.41 is

$$\boldsymbol{A} = \vec{\boldsymbol{y}}\vec{\boldsymbol{x}}^\dagger = \vec{\boldsymbol{y}}\frac{\vec{\boldsymbol{x}}^*}{\vec{\boldsymbol{x}}^*\vec{\boldsymbol{x}}} \tag{5.40}$$

5.5.5 Proof of the Correctness of Alg. 5

We need to prove that the procedure given in line 20 solves the following optimization problem: Given $\vec{\boldsymbol{y}}$, and a set of real positive values $\{a_1, \cdots, a_m\}$, find:

$$\min_{\boldsymbol{A}} \left\{ \|\boldsymbol{A}\|^2 \right\}, \text{ s.t. } \exists\{\theta_1, \cdots, \theta_m\}, \boldsymbol{A}\vec{\boldsymbol{x}} = \vec{\boldsymbol{y}}, \vec{\boldsymbol{x}} = \begin{bmatrix} e^{j\theta_1}a_1 & \cdots & e^{j\theta_m}a_m \end{bmatrix}^\top \tag{5.41}$$

Proof: from Lemma 5.5.1 we know that for any given set of $\{\theta_1, \cdots, \theta_m\}$, we can solve $\boldsymbol{A}$ with pseudo-inversion. If we substitute the solution into the objection function, it's minimized to:

$$\|\boldsymbol{A}\|^2_{\min} = \frac{\left|\sum_i \overline{y_i} a_i e^{j\theta_i}\right|^2}{\sum_i a_i^2} \tag{5.42}$$

Let's use f to denote this value. Next, we can treat f as a function of θ_i's, and try to find the set of θ_i's which minimizes f. Therefore, this set of θ_i's and its corresponding $\boldsymbol{A}$ will be the solution to the original problem defined by Eq. (5.41). Formally, this new optimization problem is (the denominator of f is omitted since it is constant):

$$\min_{\theta_1,\cdots,\theta_m} \left|\sum_i e^{j\theta} \overline{y_i} a_i\right|^2 \tag{5.43}$$

if we compare this problem to Eq. (5.23) in proving Lemma 5.2.2, we will notice that it is equivalent if we assign $\vec{\boldsymbol{a}}_i$ to be scalars $\overline{y_i} a_i$. Therefore, after proper variable substitution, the same algorithm proven in Lemma 5.2.2 and Thm. 5.2.3 will still work.

Chapter 6

Coil Design

As in most systems that manipulate electromagnetic fields, the design of the antennas, which in our specific case are the coils, is fundamental to the performance of the resulting system. Analysis and fine-tuning of what the optimal antenna should look like is a problem complicated enough to be its own field [36], so the goal of this chapter is not to thoroughly study how in general the coils should be optimized, but rather focus on how to pick the right size/shape of the coil for the specific use case that the thesis is aiming for.

The shape and form factor of the coils on both the Tx and the Rx side are restricted in the following way:

- The transmitter is designed to be mat-like such that one can put it on top or underneath the office table. Because of this, the design of a single coil as well as the layout of multiple coils is restricted to two-dimensional. Therefore, the mat can be very thin but at the same time can have enough surface area to support the range for which we are aiming.

- The receiver coil needs to be small enough to be attached to mobile devices. For mobile phones this means its surface area needs to be smaller than or equal to the area of a phone; for smartwatches this means the size of the coil is the size of band (i.e., we embed the coil in the watch band).

The rest of the chapter is organized in the following way: §6.1 and §6.2 explores

the basic shape and size of the transmitter coils we want. §6.3 explores how to lay out multiple Tx coils, i.e., given a specific area, how to pick the desired number of coils, relative locations of the coils, how many turns of each coil, etc. §6.4 explains how to pick the right Rx coil design.

6.1 The Shape of the Transmitter Coil

6.1.1 Circular or Rectagular?

The first question we need to answer is what is the most basic shape of the current loop. In making this decision, the relevant design factor is the strength of magnetic field that the coil is able to generate with a unit current, versus the amount of copper (thus resistance) the coil has. We want to maximize the strength of magnetic field while minimizing the resistance. Assuming a given material and a fixed cross-section of the wire, the first principle is the following:

$$\begin{aligned} \text{Strength of magnetic field} &\propto \text{Area} \\ \text{Resistance} &\propto \text{Circumference} \end{aligned}$$

These relationships are approximate since they do not consider parasitics and other complications. However they work well as a rule-of-thumb in designing the coils. As we know, a circle has the largest area given any circumference, so naturally it aligns well with our goal of maximizing the strength of the magnetic field given any resistance. Therefore, we use a circular shape as the basic shape of a transmitter coil.

6.1.2 Single loop, multi-turn, or spiral?

As we just said, the best way to create a big surface area (i.e., roughly proportional to the total amount of magnetic flux generated) with a fixed amount of copper is to use a single loop. However, in reality we often do not want the transmitter to occupy too much area due to the realistic form factor that we can afford, so we overlap different

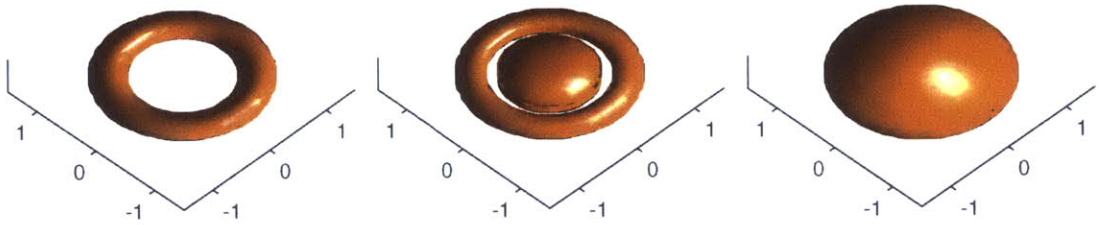

(a) Single Loop (b) Two Loops (c) Four Loops

Figure 6-1: **Visualization of the Magnetic Field of Different Coil Shapes** (a) When there is only a single loop (centered at 0 with radius 1), the magnetic field shapes like a donut where the field at the center is weak; (b) When there are two loops (radius 1/2 and 1), the magnetic field in the center starts to add up; (c) When there are four loops (radius 1/4, 1/2, 3/4 and 1), the magnetic field is much more smoothly and evenly distributed.

loops so their effective areas are additive but the occupied area is bounded by the biggest loop. Typically there are two ways to do this, under the constraint that we want our coil to be two-dimensional: (1) *multi-turn*, where we keep the radius of each loop the same, and simply repeat the same loop multiple times, and (2) *spiral*, where we progressively change the radius of each loop such that they form a spiral shape.

Different designs exhibit different pros and cons. To determine which design is better, we consider two different metrics:

- The total amount of magnetic flux generated: in other words, what the effective area is conditioned on the same amount of copper. Simple math can give us that single-coil $>$ multi-turn $>$ spiral.

- The evenness of the magnetic field: both single and multi-turn coils have a donut-like magnetic field (Fig. 6-1a). Generally, the magnetic field in the center of the coil is weaker than that at the edge. This is true because there is much higher current density at the edge around where the circle is than in the center. Consequently, spiral shapes help to alleviate this problem by distributing the current much more evenly across the surface. In doing so, we have a more balanced magnetic field across the space. The effect is shown by Fig. 6-1.

In MultiSpot, we chose the spiral design because it distributes the magnetic field much more evenly. This is necessary for MultiSpot, since MultiSpot operates by

combing the magnetic fields from different coils at each location in the space. In doing so, having the strength of the magnetic field at approximately the same order of magnitude maximizes MultiSpot's ability to combine fields either constructively or destructively. Otherwise, the stronger fields would always dominate the weaker fields.

6.2 The Size of the Transmitter Coil

As we said in the previous section, the first principle in deciding the size of the transmitter coil is that the "strength" of the magnetic field is roughly proportional to the area of the coil. This works as a reasonable approximation in some cases, however, it is not true that a bigger coil would always yield a stronger magnetic field at any location; instead, we need to look at the range and use case for which we are designing MultiSpot.

6.2.1 An Illustrative Example

As a demonstration of how the size of the transmitter coil affects the magnetic field, let us start with a simple problem: say that we have a small receiver at distance d directly above the center of the transmitter coil, thus we want to maximize the magnetic field at that location. Say that the radius of the transmitter coil is R, the magnetic strength generated by a unit current at distance d perpendicularly above the center of the coil is the following [78]:

$$\frac{B}{I} = \frac{\mu_0}{4\pi} \cdot \frac{2\pi R^2}{(d^2 + R^2)^{\frac{3}{2}}} \tag{6.1}$$

This leads to

$$\frac{B}{I} = \frac{\mu_0}{4\pi} \cdot \frac{2\pi}{\left(\left(\frac{d}{R^{\frac{2}{3}}}\right)^2 + R^{\frac{2}{3}}\right)^{\frac{3}{2}}} \tag{6.2}$$

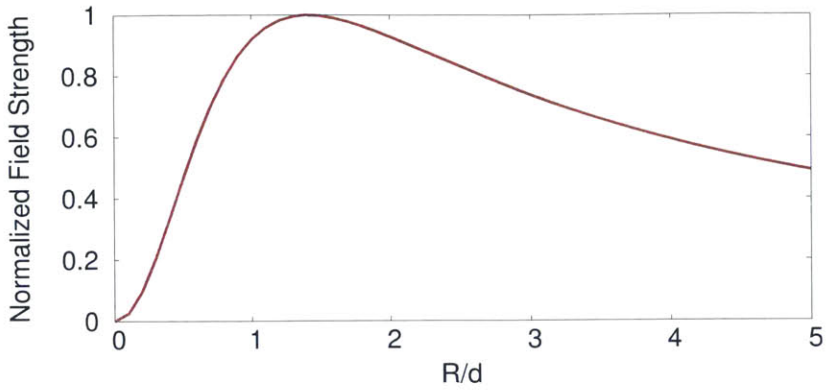

Figure 6-2: **Magnetic Field Strength at Distance d above the Center of the Tx Coil** The x-axis is transmitter coil radius R normalized by d. The curve has a peak at $R/d = \sqrt{2}$.

Simple derivation from this equation [1] tells us that the best radius for the transmitter coil is

$$R = \sqrt{2}d \tag{6.3}$$

Fig. 6-2 shows the magnetic field at the location that is distance d directly above the center of the coil as a function of transmitter coil radius R. As expected, it spikes at $R = \sqrt{2}d$, instead of monotonically increasing.

One point worth noting is that Eq. (6.1) also illustrates under what conditions the approximation that the magnetic field increases with transmitter coil size remains true. Specifically, when the receiver is *reasonably far away* from the transmitter, the strength of the magnetic field at the receiver is roughly proportional to the area of the transmitter coil. Particularly, if the distance d is much larger than the transmitter coil radius R, Equ. (6.1) can be approximated by:

$$\frac{B}{I} \approx \frac{\mu_0}{4\pi} \cdot \frac{2\pi R^2}{d^3} \tag{6.4}$$

i.e., magnetic field is proportional to the area ($2\pi R^2$) and inversely proportional to the cube of distance d.

[1] If we define $x = R^{\frac{2}{3}}$, then equivalently we want to minimize $f(x) = \frac{d^2}{x^2} + x$. Taking the derivative of f gives $f'(x) = -\frac{2d^2}{x^3} + 1$. Therefore, f is minimized when $x = \sqrt[3]{2d^2}$, i.e., $R = \sqrt{2}d$.

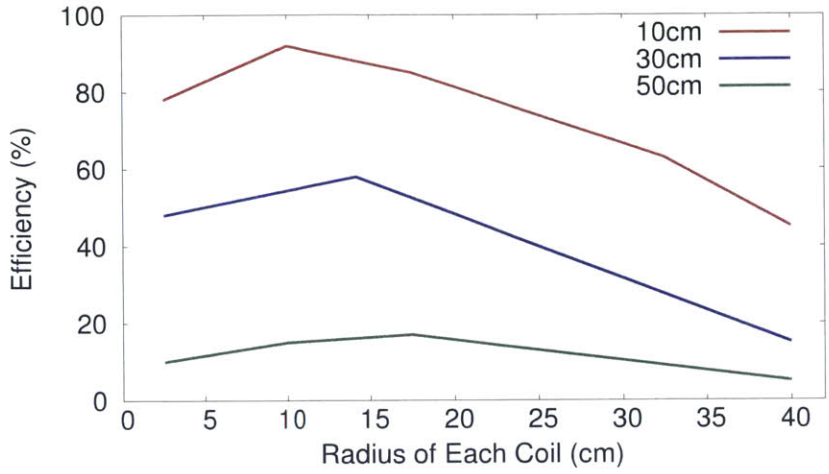

Figure 6-3: **Efficiency vs. Radius of Each Tx Coil** We vary the radius of each transmitter coil, and the distance of the receiver to the transmitter. At each distance, the efficiency first increases then decreases when each transmitter coil becomes bigger; the sweet spot of transmitter size increases with the receiver distance.

6.2.2 Simulation of the Effect of Different Tx Sizes

When we consider different possible receiver locations and orientations, as well as the fact that we are using multiple transmitter coils, the math of deciding the size of a single coil starts to be intractable and there would not be an analytical solution for the best transmitter size. Instead, we use simulation to see what is the effect of the size of the transmitter coil.

Fig. 6-3 shows the simulation result. In this simulation, we use 4 transmitter coils, and vary the size of them. The radius of a single coil is shown as the x-axis. We measure the efficiency to deliver power to a single receiver, while varying the distance of the receiver to the transmitter. At each distance, we average over different locations and orientations of the receiver.

The simulation shows the following:

- As coil size increases, the efficiency increases at first and then decreases. There is a "sweet spot" where the efficiency is maximized. This complies with the observation in Fig. 6-2 when there is a single coil.

- The "sweet spot" increases as the receiver distance increases. Said differently, a bigger coil is beneficial when the receiver is further away. However, it might

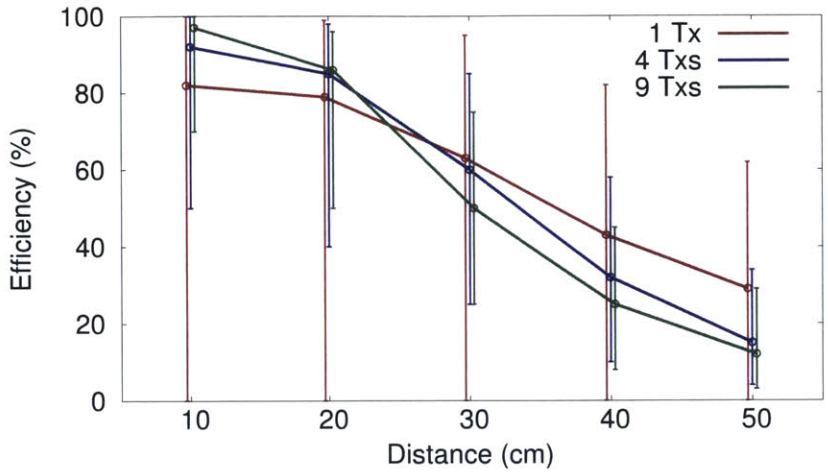

Figure 6-4: **Efficiency vs. Number of Tx Coils** We vary the number of transmitters while keeping the same total area and amount of copper, and record the efficiency while the receiver is at different distances from the transmitters. The error bars represents the best/worst efficiency. The result shows 1) more transmitter coils result in less deviation; 2) more transmitter coils perform better at close range and worse at long range.

hurt the performance if the receiver is nearby.

- In terms of order of magnitude, *the effective radius of the transmitter is at the same order as the range we want to reach.* This is the rule-of-thumb in choosing the size of the transmitter. Particularly in the simulation, the sweet spot is when the radius of a single coil is about 0.15m. Since there are 2×2 coils, the effective radius of the transmitter in total is around 0.3m, which is at the same order of the distances we consider, i.e., 0-0.5m.

6.3 Layout of Multiple Transmitter Coils

6.3.1 Number of Transmitter Coils

The first problem we aim to solve in this section is: how many transmitter coils do we want? The intuition is: we want more transmitter coils so that we have better flexibility in combing the magnetic fields; we want less transmitter coils because more transmitter coils means less area for each coil, given that the total area is fixed.

We explore this problem via simulation. Specifically, in the simulation, we fixed

two constraints: 1) the total area 2) the amount of copper (i.e., the total length of wires). We vary the number of transmitters. Specifically, we layout the transmitters in a $n \times n$ array and we vary the value of n. We then measure the efficiency of the transmitter delivering power to a single receiver at different distances.

Fig. 6-4 shows the simulation result. We have two observations:

- *More transmitter coils yield less deviation, i.e., better flexibility.* Specifically, as shown in Fig. 6-4, the standard deviation gets smaller as the number of coils increase. When there is only one coil, there are many location and orientation combinations in which the receiver receives almost zero power (e.g., receiver directly above the center of the coil with perpendicular orientation). As the number of transmitter coils increases, we gain a better ability to combine magnetic field at different orientations such that the deviation at the same distance decreases.

- *As the number of transmitter coils increases, average efficiency at near distance increases while average efficiency at far distance decreases.* This is due to the size of each coil. As said in §6.2, smaller coils perform better at nearer distance while bigger coils perform better at further distance. As the number of transmitter coils increases, the size of each coil decreases. Therefore, the performance at near distance improves while the performance at far distance degrades.

6.3.2 Overlapping Between Transmitter Coils

An interesting factor to consider is whether we want different coils to overlap or not. In this section, we will delve into why having some overlapping between coils might be helpful, and what amount of overlap would be the best.

Why overlapping coils might be helpful? The amount of overlap between two coils will change the mutual inductance of them. Particularly, the magnetic flux in the area where they overlap will have opposing directions to the magnetic flux in the area where they do not overlap. Therefore, they will cancel each other when calculating

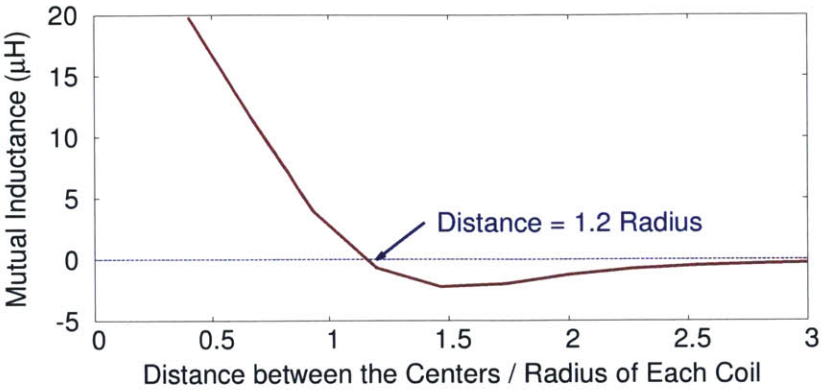

Figure 6-5: **Mutual Inductance vs Overlaps between Two Coils** When the distance between the centers of the two coils is equal to 1.2 times their radius, their mutual inductance cancels to zero.

the mutual inductance of the two coils. Moreover, there will be a point where they exactly cancel to zero mutual inductance.

In a practical system, having a big mutual inductance will make it harder to implement beamforming, in the way that it often requires high voltages on the transmitter coils. To see why, consider the case of two transmitter coils, and say that their mutual inductance is M, and impedances are both Z. If we want the transmit current to be I_1 and I_2, then the voltages required are:

$$V_1 = I_1 Z + j\omega M I_2 \tag{6.5}$$

$$V_2 = I_2 Z + j\omega M I_1 \tag{6.6}$$

Specifically, assuming the coils are well-tuned, Z is relatively small. Therefore, the value of V_1 and V_2 are dominated by $j\omega M I_2$ and $j\omega M I_1$. Consequently, the value of M directly decides how much voltage we need to apply to the coils. For example, a typical value of M is 5μH when two coils are just next to each other, and Z is 1Ω. Say we want both I_1 and I_2 to be 1A. Now $I_1 Z$ is equal to 1V, but $j\omega M I_2$ is roughly 30V at 1MHz. If we overlap the coils to make $M = 0\mu$H, then we only need 1V to achieve the same current.

What is the best amount of overlap? Now the question is how big the overlap should be. Specifically, we want to pick the amount of overlap such that the resulting

mutual inductance is zero. To do that, we run a simulation of the mutual inductance of two coils while varying their distance. Each coil is spiral with 15 evenly distributed loops. Fig. 6-5 shows how mutual inductance changes with the amount of overlap. The sweet spot is when the distance between the two centers is equal to 1.2 times their radius, the mutual inductance cancels to zero. When the two coils are further apart, their mutual inductances are negative and the absolute value decreases; when the two coils come nearer, their mutual inductances are positive and finally converge to the self-inductance.

6.4 Design of the Rx Coil

The size of the receiver coil: The size of the receiver coil is majorly restricted by the specific mobile device that the receiver is designed for. Since the receiver coil is often much smaller than the transmitter coil, we can think that the magnetic flux going through the receiver adds up constructively, i.e., increasing the size will not decrease the net flux going through the coil due to cancelation. Therefore, we design the receiver coil to be as close as possible to the size of the mobile device.

The shape of the receiver coil: Unlike on the transmitter side, where we want to use spiral coil to make the generated magnetic field as even as possible, on the receiver side the primary concern is the amount of magnetic flux that it can pick up. Therefore, we want to maximize the size of each turn in the coil, resulting in the optimum being a multi-turn coil design.

Chapter 7

Implementation

We built a prototype of MultiSpot to charge electronics in an office scenario. All circuits are implemented as Printed Circuit Boards (PCBs) with off-the-shelf components. Specifically, the transmitter is composed of 6 copper coils and is mounted to the bottom of an office desk. Each transmit coil covers an area of 0.05m^2, which collectively cover an area of 0.38m^2. The transmitter can be attached to a regular office desk with metallic, plastic and wood contents. The only restriction of the system is that the desk surface must not be conductive.[1] Each phone receiver contains a single copper coil, of area 0.005m^2, that is embedded into a sleeve that attaches to the back of the device. As for the smartwatch, we embed the coil into the band of the watch. We have built receivers for various cellphones, a Samsung smartwatch, a Fitbit, an iPad 2, a Logitech wireless keyboard, and a wireless touchpad.

In our implementation, the transmitter and receivers resonate at 1MHz, as in [55], which is within the frequency range of common wireless charging systems [17, 25, 10]. In addition, the setup is compatible with FCC regulations including part 15 and part 18.

We will explain the circuit implementations of the setup in the following sections. In App. B we include the circuit schematics of the setup.

[1]Conductive materials as large as the desk surface might negatively affect MultiSpot's performance. This is a standard assumption required by magnetic wireless power delivery and can be found in research papers [55] and commercial systems [1].

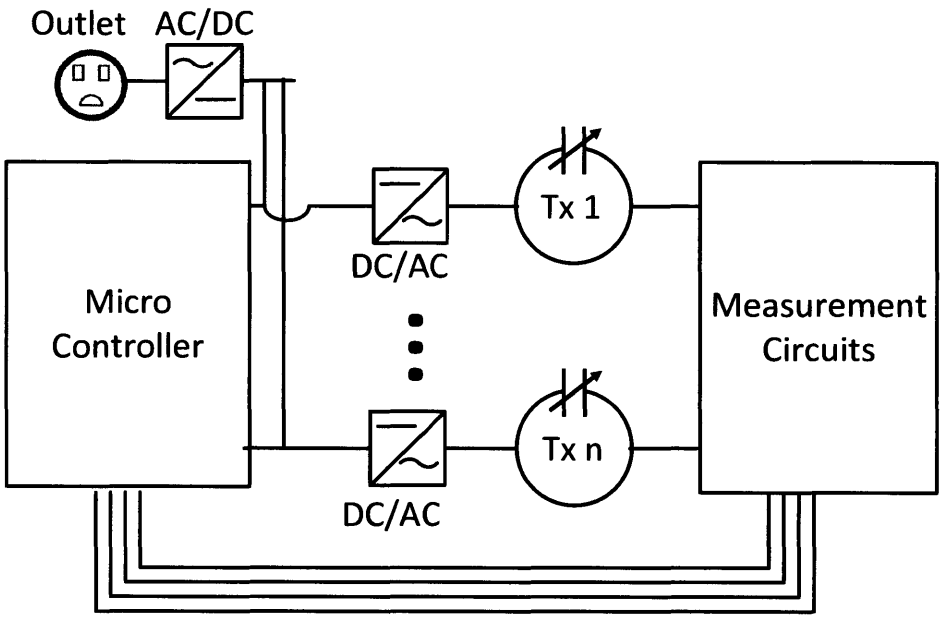

Figure 7-1: **Tx Diagram**

7.1 Transmitter Implementation

The transmitter's architecture is shown in Fig. 7-1. MultiSpot drives 6 transmit coils to beamform a magnetic field towards the receivers. The output voltage and current of each coil are measured by the measurement circuit in real time. Specifically, the measurement circuit measures the amplitude and phase of each signal and outputs them to the microcontroller. The microcontroller platform, Zynq 7Z010 [18], takes as input these amplitudes and phases and runs MultiSpot's algorithm. Every time Alg. 1 receives new measurements, it updates its estimates accordingly, and calculates the new voltages needed to beamform. It then sends the new set of voltages to the controller circuits which apply them to the transmit coils. This converter allows the controller circuit to flexibly control both the amplitudes and phases of the voltages applied to the transmit coils.

We will expand in detail on how we implement each of the Tx's key components: the transmit coils, the power converters and the measurement circuits in the following sections.

7.1.1 High-Q Transmit Coils

The primary goal when we implement the transmitter coils is to improve the Q-factor of the resonant circuit. In an L-C resonant circuit (i.e., $j\omega L = \frac{1}{j\omega C}$), Q is defined as

$$Q = \frac{\omega L}{R} = \frac{1}{\omega CR} \tag{7.1}$$

where R is the equivalent serial resistance of the circuit, which includes all parasitic resistances of the inductor, capacitor and other parts. The higher Q is, the sharper the frequency response is at the resonant frequency, and the circuit is able to deliver a higher power transfer efficiency. Specifically, theoretical upper bound of the power delivery efficiency is given by [59]:

$$\eta_{\max} = \frac{k^2 Q_T Q_R}{\left(1 + \sqrt{1 + k^2 Q_T Q_R}\right)^2} \tag{7.2}$$

where Q_T and Q_R are the Q factors of the transmitter and receiver resonant circuit, k is the coupling factor determined by the relative location/orientation between the transmitter and the receiver. When building the setup, we only have control over Q_T and Q_R. Since the receiver has much more constrained requirements with regards to form factor and cost, it is practically often easier to try to reduce the Q-factor on the transmit side.

We employ the following approaches to build a high-Q transmit circuit:

- *Pitch of the Spiral Coil:* we face a tradeoff when choosing the pitch of the spiral coil (i.e., the distance between each concentric loop in the coil): smaller pitch means higher inductance and potentially stronger magnetic field; however, with the same surface area, smaller pitch means more copper thus more parasitic resistance. Not only this, smaller pitch forces two parallel currents to be closer to each other, yielding superlinearly increasing resistances due to skin effect [78] and proximity effect [49]. Both effects are widely recognized as the major source of parasitic resistance in spiral coils operating in the MHz range [85].

- *Choice of materials:* First, we choose copper because of its good conductivity and affordable price. Second, we choose 1/8-inch general purpose copper so that it has enough cross-section to allow current flow. Third, as an effort to reduce the weight of the setup, we use hollow copper tubes since most of the current is concentrated in the outer ring of the cross section.

- *Choice of Resonating Capacitors:* It is also important to choose the right resonant capacitor that has ultra-low ESR (equivalent series resistance) so that it does not introduce significant parasitic resistance, and possess low temperature efficiency so that the temperature of the capacitor will not rise unacceptably high. In the end we chose AVX Hi-Q ceramic capacitors (3.6KV 5%) [6] to approximately satisfy all of these constraints.

- *Tuning of the coils:* For each transmitter coil we made for MultiSpot, because of slight imperfections in the manufacturing process, they were non-identical with subtle differences in the length and pitch of each coil. Therefore, there might be a slight difference in their resonant frequency. To compensate for this, we always manually tune their resonant frequency back to the desired one by carefully laying connecting wires to the coil to cancel out any outstanding inductance or capacitance.

In our implemented system, the Q factor of the transmit resonant circuits is in the range of a few hundred (>200).

7.1.2 Tx Power Converter

There are two major considerations that guide the design of the Tx power converter:

Real-Time Configurable Output Phase/Magnitude: MultiSpot requires the ability to set the voltages of the coils, i.e., the output voltages of the Tx power converters, to any phase and any amplitude (within a predefined range). Because of this, we consider a Class D Full Bridge Power Converter architecture [58], as shown in Fig. 7-2.

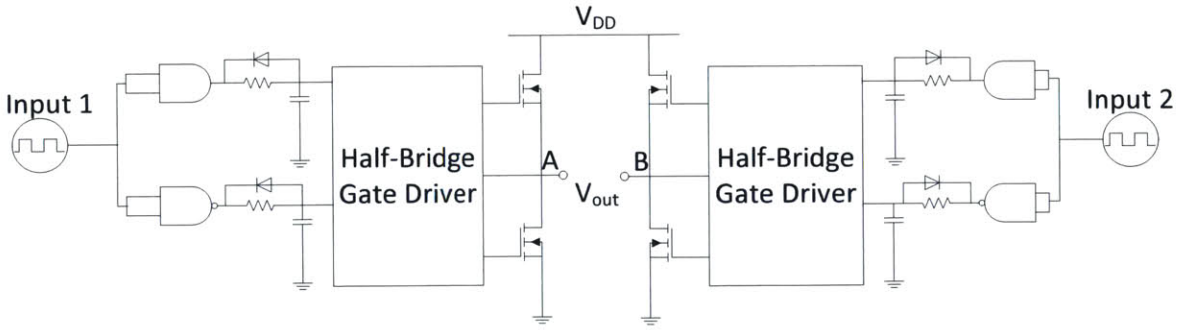

(a) Basic Schematic

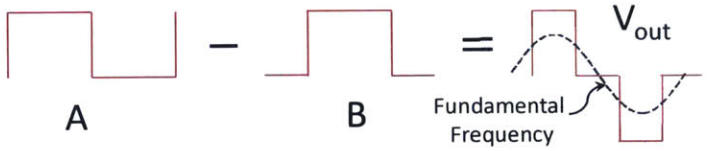

(b) Demonstration of How to Control V_{out}

Figure 7-2: **Class D Full Bridge Converter on Tx**

Fig. 7-2b demonstrates how this Full-Bridge structure can freely set the phase and amplitude of the output. Specifically, V_{out} is a differential voltage between output A of the left Half-Bridge and output B of the right Half-Bridge. Driven by digital square waves, both Half-Bridges output square waves between 0V and V_{DD}, whose delay is controlled by the input wave signal. By controlling the relative delay between A and B, we can control the amplitude of their difference: if A and B have the same delay, $V_{\text{out}} = 0$; if A and B have 180° delay, V_{out} will have the maximal amplitude in the fundamental frequency. Since V_{out} drives a high-Q resonant circuit which itself is a good bandpass current filter, we do not need to specifically filter out V_{out}. Any delay in between yields an amplitude in between, like the one shown in Fig. 7-2b. Similarly, by controlling the absolute delay of A and B, we can control the phase of the output voltage.

Mathematically, if we want V_{out} to have an amplitude of V and phase of θ, we need to set the delay ϕ_A, ϕ_B of A and B to be

$$\phi_A = \theta - \frac{1}{2}\arcsin\left(\frac{\pi}{4}\cdot\frac{\sqrt{2}V}{V_D D}\right) \tag{7.3}$$

$$\phi_B = \theta + \frac{1}{2}\arcsin\left(\frac{\pi}{4}\cdot\frac{\sqrt{2}V}{V_D D}\right) \tag{7.4}$$

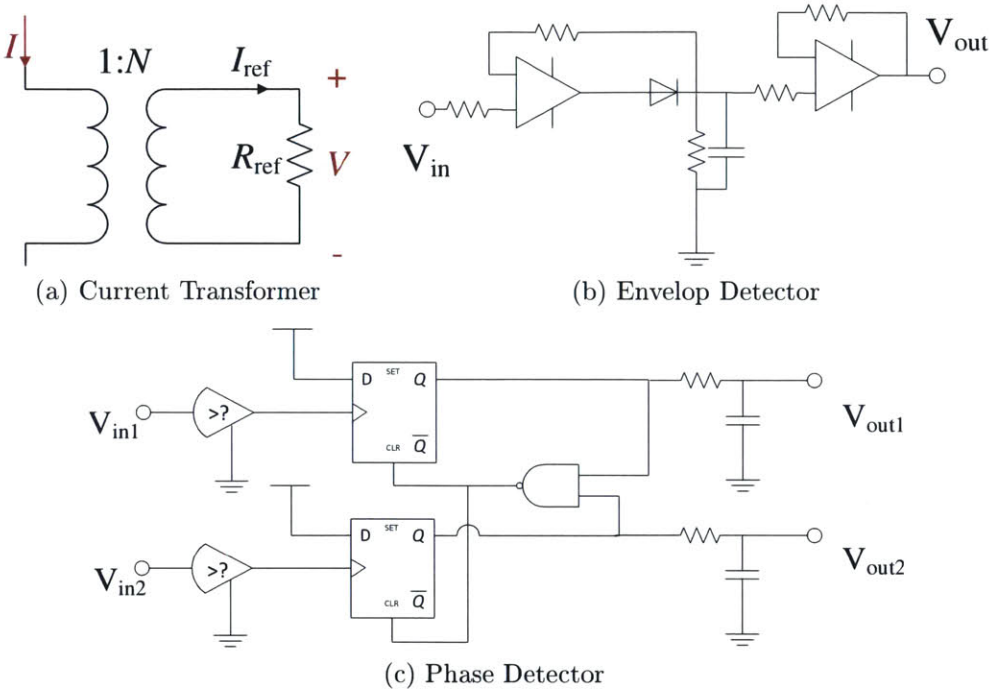

(a) Current Transformer

(b) Envelop Detector

(c) Phase Detector

Figure 7-3: **Key Schematics of the Measurement Circuits**: (a) Current transformer that relates current I to voltage V, which is much easier to measure; (b) Envelope detector to measure the amplitude of an ac signal; (c) Phase Detector to measure the relative phase between two input ac signals.

Low Loss at MHz Operating Frequency: Our operating frequency is 1MHz, delivering tens of watts at 1MHz requires careful design of the circuit. We choose enhancement mode monolithic half-bridge GaN transistors from EPC [27], due to their small switch losses at moderate to high frequencies.

Another challenge to the power converter circuit is the pressure from the High-Q downstream circuit. Specifically, any non-smooth change in the resonant circuit might translate to a voltage or current surge to the transistors. We address this problem by careful PCB layout and adding proper damping components.

7.1.3 Tx Measurement Circuit

The requirement of the Tx measurement circuit is to accurately measure the voltage over the resonant circuit and the current going through.

1) How to measure current? The typical approach is to transfer the current signal

to voltage signal, which is much easier to measure. The most straightforward way is to add a resistor (R_{ref}) in series and measure the voltage V over the resistor – then the current is equal to $\frac{V}{R_{\text{ref}}}$. However, as explained in §7.1.1, we want to minimize the series resistance in the resonant circuit to optimize the Q-factor. Therefore, adding additional resistances is not the preferred way.

In MultiSpot, we use a transformer to translate currents to voltages (Fig. 7-3a). It has two benefits:

- It allows us to measure I accurately by measuring voltage V on the secondary coil. After applying the transformer equations [51], we can calculate I as

$$I = N\frac{V}{R_{\text{ref}}} \tag{7.5}$$

- The added parasitics are negligible if we carefully selectthe values of N and R_{ref}. First, since we only have one winding on the primary side, the self-inductance of the primary coil can be ignored. Second, the imposed resistance from the secondary coil is only R_{ref}/N^2. In our implementation, we choose N to be a big number ($N = 100$) and $R_{\text{ref}} = 5\Omega$, the added parasitics is only $0.5\text{m}\Omega$.

2) How to measure both the amplitude and phase of an ac signal? There are many ways to measure the amplitude and phase of an ac signal, e.g., using quadrature mixers [14], RF gain/phase detector [13], or a combination of an envelope detector (Fig. 7-3b) to measure the amplitude, and a phase/frequency detector (Fig. 7-3c) to measure the phase. We choose the last option for our MultiSpot implementation.

7.2 Receiver Implementation

The receiver circuit is shown in Fig. 7-4. It has an impedance matching network designed to maximize the power that gets delivered to the device. This is followed by an ac/dc rectifier which converts the ac signal into a dc voltage. This dc voltage passes through a dc-dc voltage regulator that converts the input voltage to a constant 5V that can be accepted by the USB standard [20]. This allows the power to

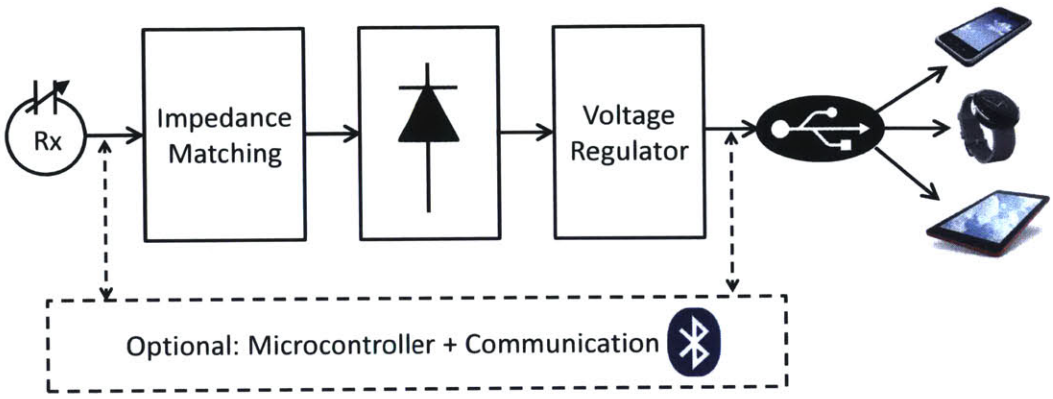

Figure 7-4: **Tx Diagram**

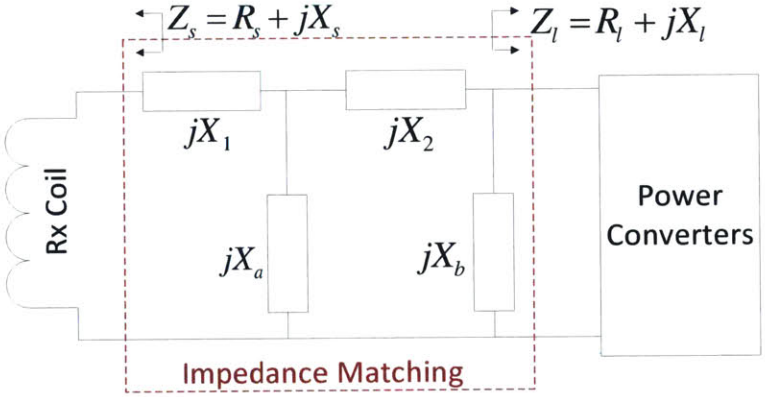

Figure 7-5: **Schematics of Rx Static Impedance Matching Network** We use a combination of L and Pi network

be distributed across a USB port so that the receiver can support a large variety of unmodified devices that can be charged via USB, including most phones, tablets and wearables. Finally, depending on the available space and budget, the Rx can optionally include a Bluetooth outband communication channel supported by corresponding microcontroller. In our implementation, we use Nordic Semiconductor's nRF51822 [23] chip for the Bluetooth Low Energy protocol. As explained by §5, it facilitates MultiSpot's ability to finely control the amount of power delivered to each receiver. If the outband communication module is not included, the Tx will run the basic algorithm specified in §4.

7.2.1 Impedance Matching

Impedance matching on the receiver is a challenging problem. This is because the equivalent impedances change on both sides: on the Rx coil side, the equivalent impedance changes with the couplings between Tx and Rx; on the converter & load side, the power converter's input impedance changes dramatically with input voltages to power converters.

This leaves us with two categories of approaches. The first category is to soft-tune the impedance matching or other relevant circuits to make sure the impedances stay well-tuned regardless of the changing impedances on both side. These approaches often require a fair bit of circuit complication, for example, adding active components like a switch capacitor network for adaptive tuning [92, 57], or replicating the power converter in carefully designed ways to cancel out its changing impedances [50, 37].

The second category of approaches is to use a static impedance matching network and try to pick its parameters so that it is less prone to changing impedances [40]. It is much cheaper than the former approach but cannot guarantee to match the impedances perfectly.

In MultiSpot, we pick the second approach, since we favor a clean and simple design on the receiver side so that it can be miniaturized to mobile devices with a small form factor. The impedance matching network we use is a combination of Π-network and an L-network, to save us additional degrees of freedom to pick the component values (Fig. 7-5). In the schematics, X_a, X_b, X_1 and X_2 can be either inductive or capacitive. Specifically, for any given source and load impedances $Z_s = R_s + jX_s$ and $Z_l = R_l + jX_l$, and when fixing parameter X_a and X_b, we can calculate X_1 and X_2

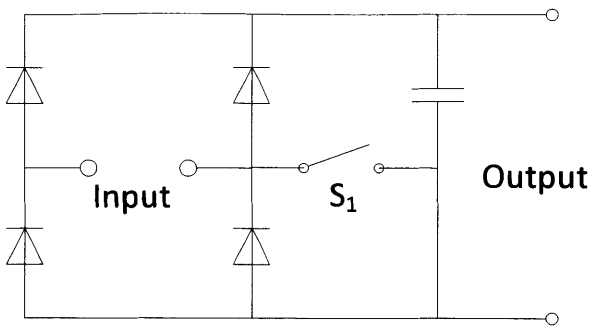

Figure 7-6: **Schematics of Rx ac/dc rectifier:** We use a hybrid of a voltage doubler and a full bridge rectifier.

as follows:

$$R' \triangleq \frac{R_l^2 + X_l^2}{R_l} \tag{7.6}$$

$$Q \triangleq \frac{R_l^2 + X_l^2}{R_l X_b} + \frac{X_b}{R_l} \tag{7.7}$$

$$X_1 = \pm\sqrt{\frac{(1+Q^2)\,R_s X_a^2}{R'} - R_s^2} - X_a - X_s \tag{7.8}$$

$$X_2 = -\frac{R_s^2 X_a + (X_1 + X_s)X_a(X_1 + X_s + X_a)}{R_s^2 + (X_1 + X_s + X_a)^2} - \frac{Q}{1+Q^2}R' \tag{7.9}$$

And then we run a matlab script to search different sets of values of X_a and X_b, and pick the one that works well with the desired large range of Z_s and Z_l.

7.2.2 Rx Power Converter

The power converter on the Rx has two modules in series: 1) an ac/dc rectifier that rectifies input ac voltages on the Rx coils to a dc voltage; 2) a voltage regulator that regulates the dc voltage. The challenge of the design of the Rx power converter is that it needs to work with a relatively large input voltage while keeping mostly constant output voltage and preferably it is rated for high power.

a) ac/dc rectifier We use a hybrid of a voltage doubler and a full bridge rectifier (Fig. 7-6). The idea is as follows: when the input voltage is relatively low, we double the output voltage; otherwise we simply use a full bridge rectifier. By connecting the output voltage to a Schmitt trigger that controls the switch S_1, one can switch

between the voltage doubling mode and the normal mode.

b) dc/dc regulator We use standard switch-mode buck converter to convert a dc voltage in a large range to a 5V output rail.

With the combination of the rectifier and regulator, our power converters on the Rx side works with an input range of 3V-40V and output power up to 10W. We also add protective Zener diodes at the input to protect against possible high voltage surge due to delays in the Tx's ability to control the voltage.

Chapter 8

Evaluation

8.1 Evaluation Environment

8.1.1 Metrics

We define *distance* as the distance between the nearest point on the receiver coil and the nearest transmitter coil. For example, if a receiver is in the same plane as the transmitter but outside the area that the transmitter coils cover, then the distance is from the edge of the receiver to the edge of the nearest transmitter coil.

We define *charging time ratio* as the ratio between the time taken to wirelessly charge a phone from a dead to a full battery, and the time it takes a wall plug to charge from a dead to a full battery. For multiple phones, the charging time ratio reported is the largest time ratio of all involved phones, i.e., it is the charging time of the phone that takes the longest to charge.

We define *orientation* as the angle between the plane of the receiver coil and the plane of the transmitter coils.

8.1.2 Baselines

We compare the following systems:

- Commercially available multi-device wireless chargers: Duracell Powermat [4],

Energizer Qi [5] and LUXA2 [12]. Each of them requires a proprietary receiving case, which we attach to the phone during the experiments.

- State-of-the-art Prototype. Specifically, we chose the WiTricity WiT-5000 prototype [17] that charges multiple devices. Since the prototype is not publicly available, we extract the data from their technical sheet [17].

- *Idealized* Selective Coil: This baseline uses the same six Tx coils as MultiSpot, but given a set of receivers, it identifies the best Tx coil for each receiver, and divides the input power equally between the set of best Tx coils. For example, given two receivers, it identifies the best Tx coil for the first receiver, and the best Tx coil for the second receiver, and divides the power between those two Tx coils.

  We note that this baseline requires an oracle to decide which Tx coil would deliver the maximum power to each receiver. Specifically, one cannot identify the Tx coil that has the best magnetic coupling to a receiver in the presence of other receivers. Hence, to implement this system, for each receiver, we physically remove the other receivers and measure the receiver coupling to the transmitter. While this is hard to do in a real-world setup, the baseline provides insights about how well one can do by distributing the input power between the best performing Tx coils.

- Single Large Coil: A single transmitter coil that covers the same area as MultiSpot covers using six coils.

- Our MultiSpot prototype as described in this thesis.

- MagMIMO [55] using the same Tx coils as MultiSpot.

We note that the input powers of Duracell Powermat [4], Energizer Qi [5], LUXA2 [12], and WiTricity WiT-500 [17] are 15W, 18W, 22W, and 24W, respectively. Since these baselines have different input powers, we set the input power of MultiSpot, selective coil, and MagMIMO to the mean of those values, i.e., 20W.

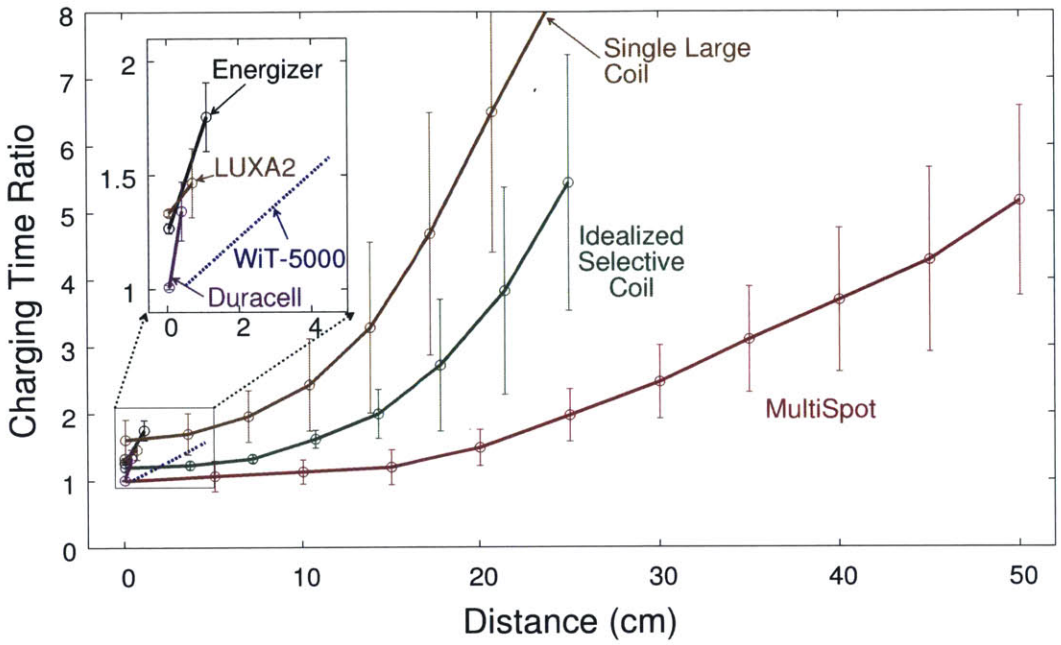

Figure 8-1: **Charging Time Ratio vs. Distance from Charger.** Each run uses two phones at equal distance, but in different locations. (Note: on the vertical axis, lower charging time ratio is better)

8.1.3 Setup

All experiments are performed in an office environment. The charger is placed on a standard office desk. Unless specified otherwise, the charged devices (e.g., phones) are held using configurable arms which allows us to test different charging distances and orientations.

8.2 Charging Time vs. Distance

We evaluate MultiSpot's ability to charge multiple phones at various distances from the transmitter. We run each experiment with two phones because the commercial baselines are constrained to charging two receivers.

8.2.1 Two Phones with Equal Distance

We first run experiments with two phones having the same distance to the transmitter, but at different locations and with different orientations. At each distance, multiple

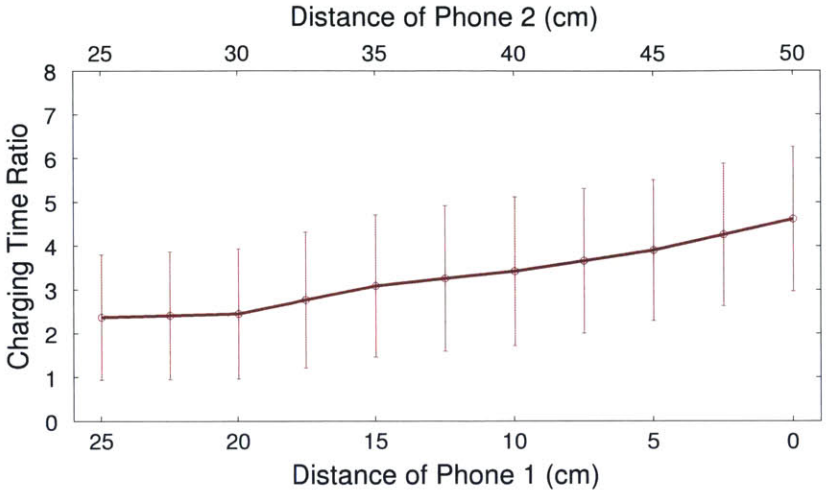

Figure 8-2: **Charging Time Ratio vs. Distance from Charger.** Two phones have different distances to the Tx. From left to right, phone 1's distance increases while phone 2's distance decreases.

experiments are run with different receiver positions and orientations.

Fig. 8-1 shows the charging time ratio of MultiSpot and the baselines as a function of the distance from the charger. At near distances (0-10cm), MultiSpot's charging time is comparable to a wired charger. It starts to increase as the receiver moves from mid-range to long-range. MultiSpot reaches a maximum charging distance of 50cm. Comparing with the baselines, MultiSpot has much larger range, and shorter charging time at the same range. The commercial baselines (Energizer, LUXA2, Duracell) and development prototype (WiT-5000) are constrained to less than 5cm. Even when compared to the idealized selective-coil and single large coil, MultiSpot reaches a much larger range. And even within the same range, MultiSpot's charging time is on average 3x smaller than that of the idealized selective coil.

8.2.2 Two Phones with Different Distances

Having two phones with equal distance to the base does not represent all possible cases. As mentioned earlier, special care needs to be taken in cases where one phone is very near to the case thus having a strong coupling, while the other phone is farther away from the base thus having a much weaker coupling (the near-far problem). In this experiment, we aim to test MultiSpot's ability to deal with such problems.

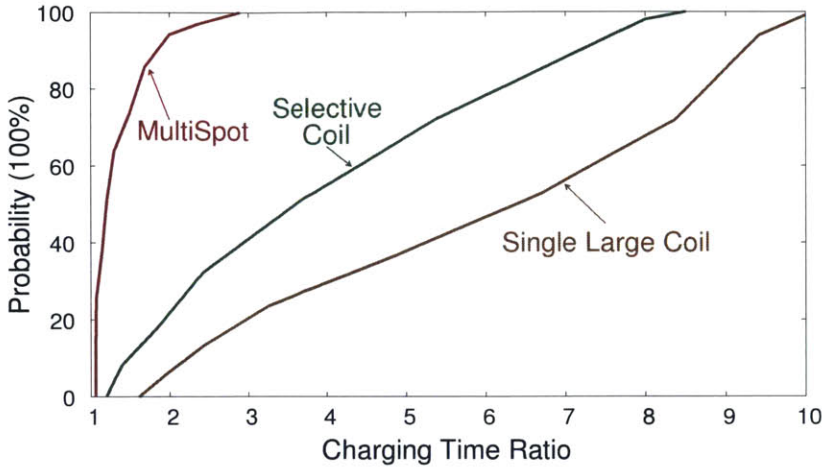

Figure 8-3: **CDF of Charging Time Ratio**

Specifically, we run the experiment with two receivers, where we keep the mean of the distances between them and the transmitter at 25cm, and vary the difference of their distances. For example, a difference of 10cm means the two receivers are at distances of 20cm and 30cm respectively. Fig. 8-2 shows the result. As expected, with the difference of distances increasing, the near-far problem gets increasingly severe and charging time increases. However, it only increases very slightly. When one phone is at 0cm and the other phone at 50cm, the charging time ratio is only 2x slower than the case when two phones are at the same distance. Therefore, MultiSpot deals with the near-far problem gracefully.

8.2.3 Two phones at Random Locations

In this experiment, we totally remove the constrains of where the two phones are in the previous experiment, and evaluate the system's performance with any set of random receiver locations. Specifically, we put the receivers in randomly sampled positions where the distances to the transmitters is not larger than 50cm, each with a random orientation, and draw the CDF (Cumulative Distribution Function) of the charging time ratio (Fig. 8-3). This experiment shows in the average case how MultiSpot performs and how it compares to other systems. The 50^{th} percentile of MultiSpot's charging time ratio is 2, which means half of the time, the phone takes

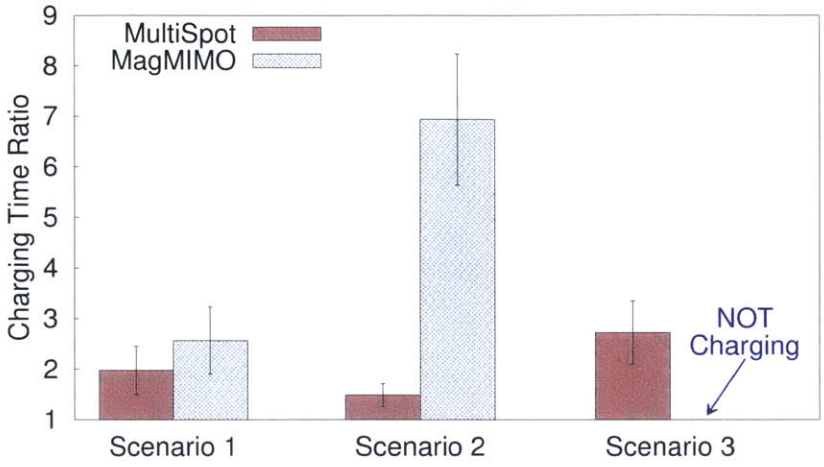

Figure 8-4: **Comparison with MagMIMO:** Scenario 1: two receivers 5cm apart and both 25cm away from the transmitter; Scenario 2: two receivers 60cm apart and both 10cm away from the transmitter; Scenario 3: two receivers 60cm apart and both 20cm away. The figure shows that MagMIMO works well for co-located receivers, but can completely fail if the receivers are far apart.

twice as long as needed if plugged into the wall. The 90^{th} percentile is 4.5, which means 90% of the time the charging can be finished within 4.5x of the time needed by wall charger. Both selective-coil and single-coil have much larger charging time ratios.

8.3 Comparison with MagMIMO

MultiSpot is inspired by MagMIMO [55], which proposes magnetic beamforming to a single device. Thus, in this experiment we compare MagMIMO with MultiSpot. We separate this experiment from the other baselines since MagMIMO is not intended for charging multiple devices. Still one might wonder how MagMIMO would perform when there are multiple devices around, and how does it compare to MultiSpot.

We use the same hardware to run MultiSpot and MagMIMO. We use two receivers and run both MagMIMO and MultiSpot in three different scenarios. In the first scenario, the two receivers are co-located within 5cm from each other, and both are 25cm away from the transmitter. In the second scenario, the receivers are 60cm apart, and both 10cm away from the transmitter. In the third scenario, the two receivers

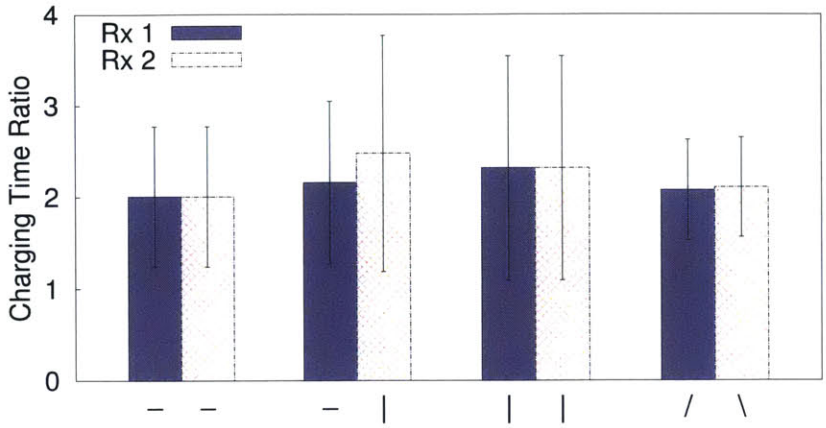

Figure 8-5: **Charging Time vs. Orientation.** We plot the charging time ratio versus different orientations. Each group of two bars represent a combination of orientations, where "–" denotes horizontal, "|" denotes vertical, while "/" and "\" denote 45°. All receivers are 25cm away from the charger.

are 60cm apart and both 20cm away from the transmitter.

Fig. 8-4 shows that MagMIMO is comparable to MultiSpot only when the two phones are co-located and hence can be considered as one device. Otherwise, MagMIMO's charging time becomes an order of magnitude longer than MultiSpot, or it fails to charge one of the phones all together. The reason is that MagMIMO has no mechanism for separating the magnetic couplings of the two receivers, and hence interprets the magnetic channels of both receivers as one channel and tries to create one beam to charge both phones. When the phones are adjacent, this technique works because one beam can charge both receivers, but as this distance increases, the charging time ratio inevitably goes up. MultiSpot on the other hand, creates two beams for both receivers and is able to power both phones regardless of the distance between them.

8.4 Charging Time vs. Orientation

We investigate MultiSpot's performance with different receiver orientations. For all experiments, the distances of both receivers is fixed at 25cm, while their orientations are varied. We test four scenarios: both phones horizontal, one horizontal and one vertical, both vertical, and both at 45° tilt.

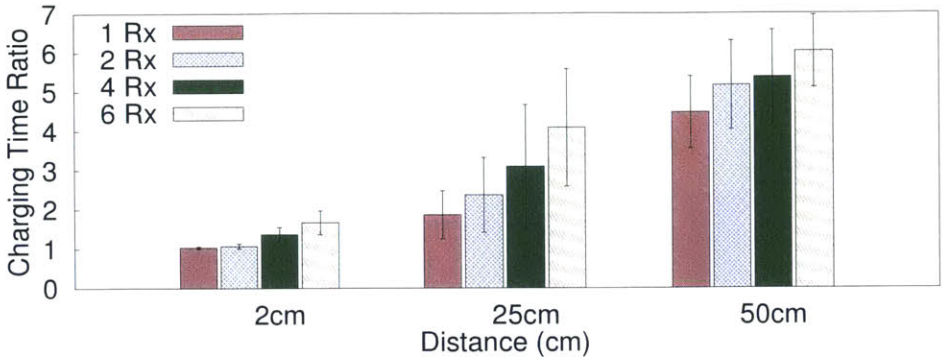

(a) Charging Time Ratio vs. Number of Rxs

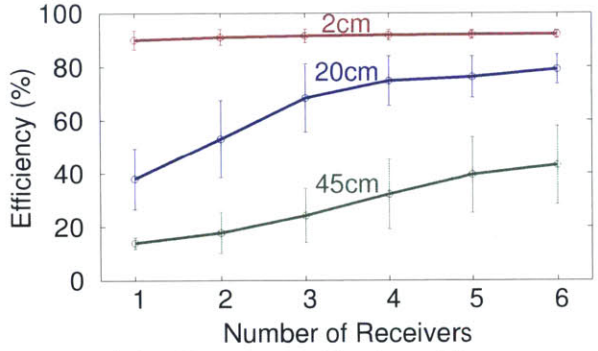

(b) Efficiency vs. Number of Rxs

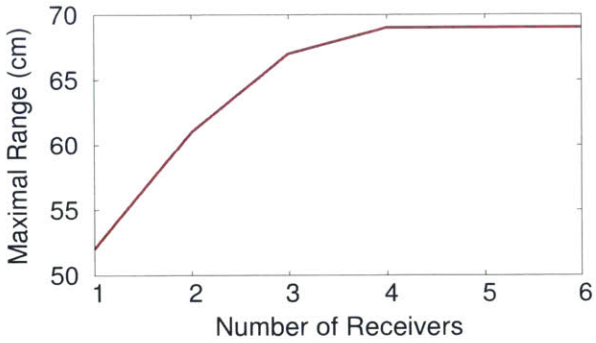

(c) Maximal Range vs. Number of Rxs

Figure 8-6: **MultiSpot's Performance with Number of Receivers.** (a) MultiSpot's charging time ratio with up to 6 receivers; (b) MultiSpot's efficiency as a function of receiver number and distance to the charger. (c) MultiSpot's maximal charging range increases with receivers.

The results in Fig. 8-5 show that the time that MultiSpot's performance is almost orientation agnostic. Although there are some variations in the charging time ratio between different orientation scenarios, the difference remains relatively small. For example, charging two horizontal phones takes about 2x the wired charging time, while two vertical phones takes 2.3x the wired charging time.

8.5 Performance vs. Number of Receivers

Next, we evaluate MultiSpot's performance along a few dimensions as the number of receivers increases.

8.5.1 Charging Time vs. Number of Receivers

We evaluate MultiSpot's ability to charge different numbers of receivers. We run experiments with 1, 2, 4, and 6 receivers. In each experiment, all of the receivers are placed at the same distance from the charger, but at random positions and orientations. To show the results we pick three representative distances, 2cm (near range), 25cm (mid range) and 50cm (far range). Fig. 8-6a shows the charging time ratio versus number of receivers. In all cases MultiSpot is able to charge all of the phones. However, the charging time increases with distance and number of receivers. This is because MultiSpot needs to split more beams when there are more receivers, so the power that is carried in each beam will go down with more receivers.

8.5.2 Efficiency vs. Number of Receivers

We test MultiSpot's efficiency with different locations and number of receivers. The distance of all receivers to the transmitter is fixed while the number of receivers is increased. For a given distance and number of receivers, the positions and orientations are varied across runs. We evaluate MultiSpot's efficiency. Similar to past work [55], we define efficiency as the ratio between the total received power at all receiving coils divided by the total input power at the transmitting coils. The experiment is repeated with three different distances: near range (2cm), mid range (25cm) and far range (45cm). For each range we repeat the experiments for different numbers of receivers.

Based on Fig. 8-6b, we make a few observations:

- For a single device, MultiSpot has similar or better efficiency compared with state-of-the-art systems. For example, MagMIMO [55] reports 89% and 34% efficiency with a single receiver at 2cm and 20cm, while MultiSpot's efficiencies are 90% and 38% at 2cm and 20cm, At near range, MultiSpot's efficiency is better than commercial systems. For example, WiTricity WiT-5000 [17] reaches its best efficiency (90%) at 0.6cm, while MultiSpot has 90% efficiency at a larger distance (2cm).

- We also find it interesting that the system efficiency increases with the number of receivers. For example, at 45cm the efficiency increases from 14% with single device to 43% with 6 receivers. This effect is more apparent when the receivers are at mid-range and far-range. The reason is that the more receivers that are around, the more magnetic flux can be picked up by the receivers. This happens because the beams are relatively wide, and hence when there are more receivers, they can collectively pick up more energy.

8.5.3 Maximal Range vs. Number of Receivers

As the number of receivers increases, the efficiency of MultiSpot increases. With this increased efficiency, it may be possible to charge a receiver at a larger distance when more receivers are in the system. Therefore, this experiment aims to find the maximum distance from the transmitter at which a phone receiver can still charge, given a number of other receivers simultaneously in the environment. To get a feel for how the range increases with the number of devices, we put all phones horizontally above the coils and find the maximal z distance. Different phones are aligned and spaced vertically.

Fig. 8-6c shows the maximal charging range vs. the number of receivers. The maximum range does indeed increase with the number of receivers. From one receiver to two receivers, the distance increases by 10cm. With 4 phones, the extension of range is 17cm.

In particular, because of the magnetic coupling between the receivers, one receiver might induce power on another receiver. In this case the receiver acts as a power relay, extending the maximal range of power delivery.

8.5.4 Efficiency When Rxs Have Different Distances to Tx

Previously, we have shown how the efficiency changes when multiple receivers have the same distance to the transmitter. In this experiment, we want to see how efficiency changes when receivers have different distances to the transmitter.

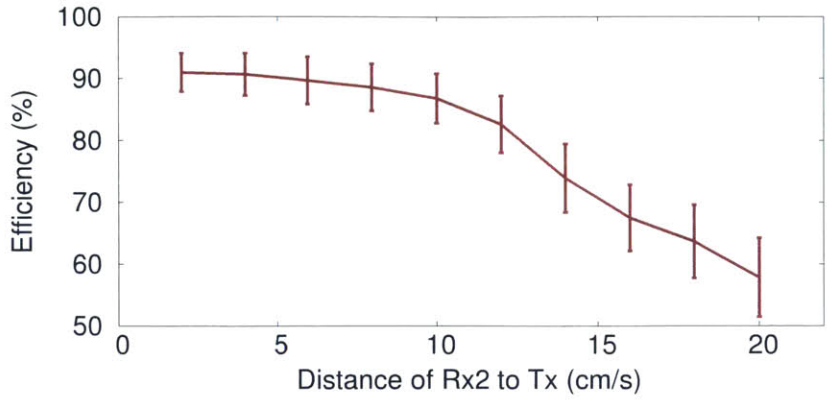

Figure 8-7: **Efficiency When Rxs Have Different Distances to Tx**: We fix the distance between Rx1 and the Tx to be 2cm, and vary the distance between Rx2 and the Tx (x-axis).

Specifically, we run the experiment with two receivers. We fix Rx1 to be 2cm away from the transmitter, and vary the distance of Rx2. We record the efficiency from the transmitter coils to the receiver coils. Fig. 8-7 shows the result.

- As expected, the efficiency goes down as Rx2 is further away from the Tx.
- The efficiency is dominated by the receiver that is further away from the Tx. Specifically, the efficiency when both receivers are at 20cm is about 53% (Fig. 8-6b); when Rx1 is at 2cm and Rx2 is at 20cm, the efficiency is about 58% (Fig. 8-7). This is because the amount of transmit current needed is dominated by the receiver that is further away (i.e., having weaker coupling). Therefore, the efficiency is dominated by the receiver that is further away.

8.6 User Experiment

The goal of this experiment is two-fold: first, we want to ensure that MultiSpot works with a diversity of devices; second, we want to show that MultiSpot could charge all devices while the user is interacting with them or moving them.

We use the same setup as used by other experiments. However, we involve a variety of receiver devices. Specifically, we have tested cell phones (iPhone 4s/5s/6, Nexus 4, Samsung Galaxy S4/S5, HTC Evo and Motorola Droid X2), tablets (Samsung

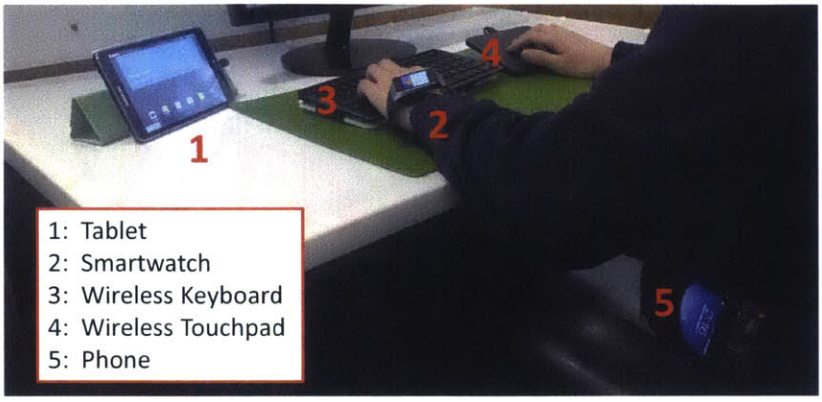

(a) The Experimental Setup

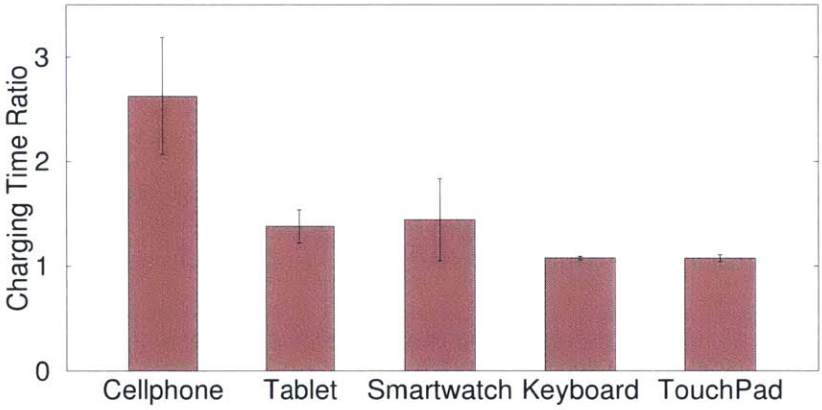

(b) Charging Time Result

Figure 8-8: **User Experiment:** MultiSpot can charge multiple types of devices concurrently in an office desk scenario as shown in (a).

Glaxy Tab 4 and Kindle Paperwhite), smartwatch (Samsung Gear Live Smartwatch), wireless keyboard (Logitech K810) and wireless touchpad (Logitech T650). In each experiment, we place the keyboard and touchpad flat on the desk, and place the tablet against a stand. We then ask the user to sit in front of the desk and type on the keyboard, with a cellphone in her pocket and a smartwatch on her wrist (see Fig. 8-8a for a photo while the experiment is running). We measure the charging time ratio for each type of devices. We repeat the experiment with three different users.

Fig. 8-8b shows the charging time ratio of the various device types. MultiSpot can charge all of the devices, however the charging time ratio of each of them is different. The cellphone and smartwatch have relatively higher charging time ratios and standard deviations. This is because they are carried by the user, while the other

devices are static on the desk resulting in them being further from the transmit coils than the other devices. Also, according to Fig. 8-8b, the cell phone takes longer than the smartwatch to charge. This is because as the user works, their wrist is moving above the desk while the phone is in their pocket, so naturally the phone is on average farther away from the coils.

Finally, we have use a temperature gun infrared thermometer [11] to monitor the temperature of the devices during the experiment. The maximal temperature increase we measured was 4°C over a duration of 5 hours.

8.7 Power Distribution among Receivers without Communication

In this section, we select three representative scenarios to show how MultiSpot distributes power among receivers. We test MultiSpotwithout communication between transmitter and receivers, i.e., following the solution in §4. We charge two iPhones 5s, in different scenarios:

- *Same Distance and Initial Battery*: We put each of the two phones 25cm away from the charger and let them charge from a dead battery. Fig. 8-9a shows their charging curve, i.e., battery percentage vs. time. Since all factors of these two phones are almost exactly the same, the phones charge at the same rate, as shown in the figure.

- *Different Distances*: We charge two phones with dead batteries but with different distances from the transmitter (10cm and 40cm). Fig. 8-9b shows the charging rate of the two phones. The figure shows that initially, the phone closer to the transmitter (i.e., Rx1) charges faster since it has a stronger magnetic coupling with the charger. However, once this phone is fully charged, MultiSpot transfers the power to the second receiver (Rx2), increasing its charging rate. Said differently, when one phone is fully charged and has no demand for power, MultiSpot automatically re-allocates the power to serve the other receiver which

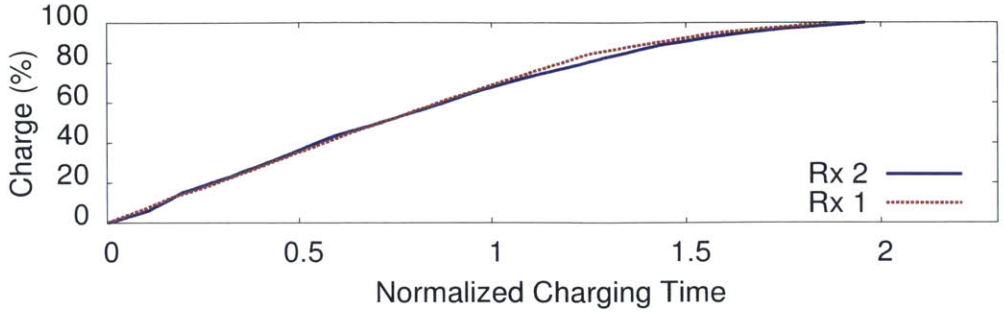

(a) Same Distance and Initial Battery

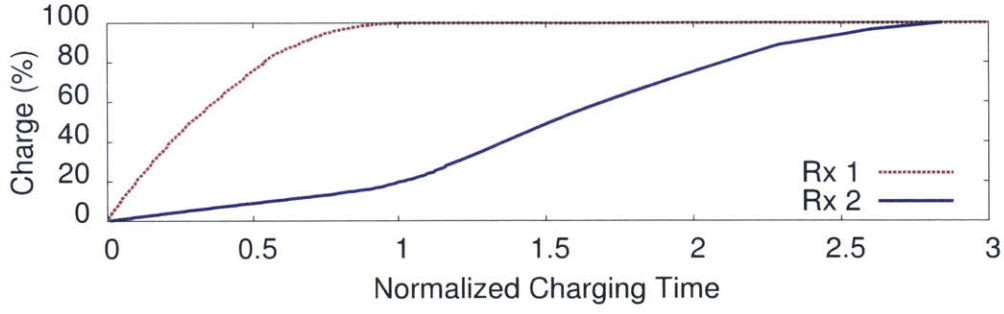

(b) Different Distances

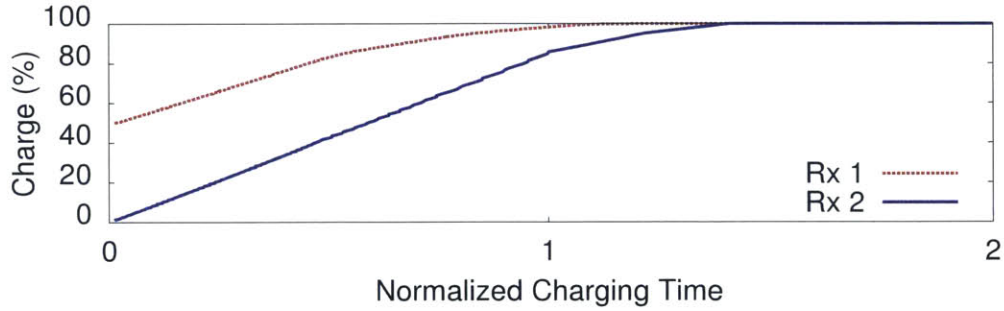

(c) Different Initial Battery

Figure 8-9: **Charging Curves of Two Phones For Three Scenarios:** The x-axis is charge time normalized by charge time of a wall plug to charge from dead battery to full. The scenarios are: (a): Charging two phones from dead batteries, with the same distance (25cm); (b): Same as (a), but with different distances (Rx1: 10cm, Rx2: 40cm). (c): Same as (a) but the two phones start with different battery levels (0%, 50%).

still has demands.

- *Different Initial Batteries*: We repeat the previous experiment, with different battery levels (0% and 50%). The results presented in Fig. 8-9c show that the phone with a lower battery level charges faster. Thus, when all other factors are the same, MultiSpot allocates more power to the device that has a lower battery level, i.e., the device with higher demands for power.

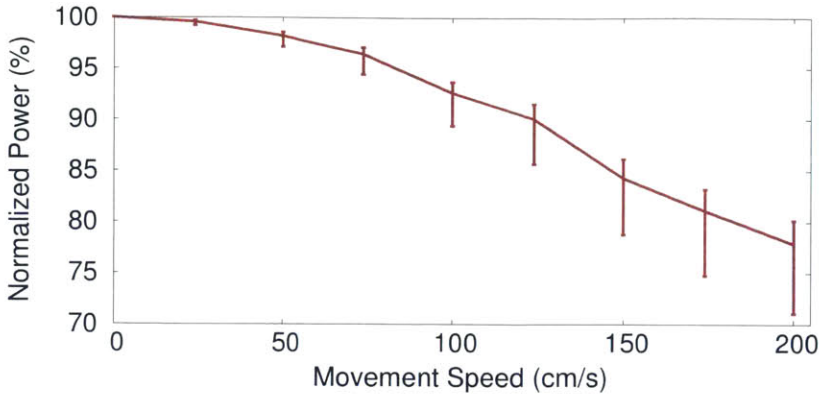

Figure 8-10: **Normalized Power vs. Motion Speed.** We plot the normalized received power versus different movement speed of the receiver. The reduction of received power is less than 3% when the speed is less than 50cm/s; it goes up to 20%-30% when the receiver moves at 200cm/s.

8.8 Performance vs. Motion

In this experiment, we aim to evaluate MultiSpot's performance with regard to the motion of the receiver. We use the same setup as other experiments, but add controlled movements to the receiver. Specifically, we attach the receiver to a motor which moves across the table where the charger is mounted, and vary the speeds across different experiments. During the experiments, the receiver is always 15cm above the table.

To measure MultiSpot's performance, we pick five evenly distanced locations in the motion's path, measure the received power at each location, and average them. We then normalize it by the power when there is no motion. Fig. 8-10 shows the normalized power versus motion speed. We can see that MultiSpot works well with mild receiver motion, and degrades if the speed increases. Various surveys [73, 35, 30] have suggested that the average speed of natural human arm movements is under 50cm/s, in which case the received power is almost unaffected (<3% degradation). If the speed reaches 200cm/s, the reduction of power is around 20%-30%.

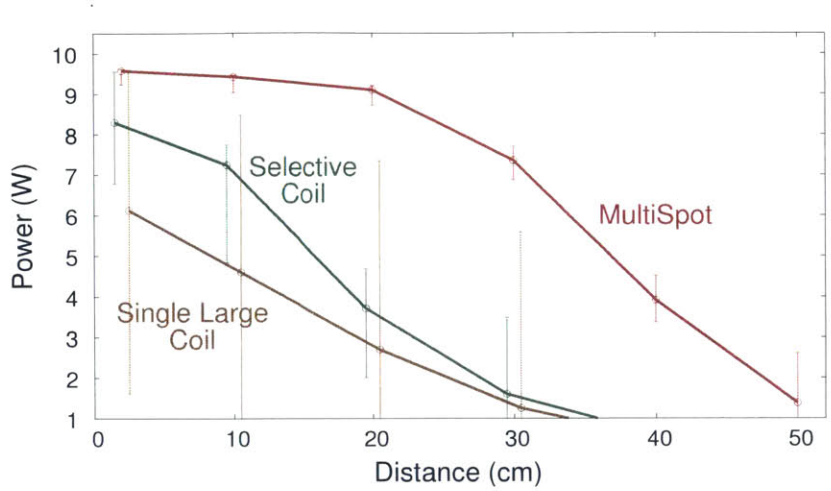

Figure 8-11: **Power Delivery Capability vs. Distance** The MultiSpot prototype can deliver constantly up to 10W below 10cm; afterwards it starts to degrade gradually with longer charging distances.

8.9 Power Delivery Capability vs. Distance

In this experiment, we want to evaluate the power delivery capability of the implemented MultiSpot prototype as an end-to-end system. We keep 20W as the maximum input power; instead of phones, we use a resistor as the load. At each location, we tune the resistance of the resistor until it receives the maximal amount of power, which we defined as *power delivery capability*. We repeat the same experiment for different locations, and across different systems.

Fig. 8-11 shows the results. We have the following observations:

- MultiSpot's power delivery has two intervals:
  - less than 20cm: The power delivery capability is almost constantly 10W, which is the rating of the power converter in the receiver circuit. In other words, the receiver circuit cannot handle more than 10W.
  - greater than 20cm: The power delivery capability degrades rapidly below 10W with distance. This occurs because the couplings between the transmitters and the receivers decay as the distances becomes larger.
- Comparing with selective coils, MultiSpot can deliver much more power. This is because at any time MultiSpot combines the magnetic field from different coils,

while selective-coil only activates a single small coil. Therefore, MultiSpot has a greater effective surface area.

- MultiSpot is also superior to a single-coil system with the same surface area. This is because for a single transmit coil, even if the receiver is near to the transmitter, it can still receive almost no power if it's orientation happens to be misaligned with the transmitter. This can also be evidenced by the much larger standard deviations of the single-coil system.

8.10 Antenna Pattern Measurements

In order to better understand how power delivery differs with spatial locations, we define (analogous to RF radiation patterns) the *antenna pattern* of a wireless charging system. Specifically, we define it as the isosurface of 3dB power loss, i.e., the surface in space where if we put the receiver on any point in the surface it receives exactly half of the total power.

One complication that a wireless power delivery system has is that the received power is a function of not only location but also orientation. Therefore, when we measure the antenna pattern, we fix the orientation of the receiver (e.g., parallel or perpendicular to the transmitter plane) and move it in the 3D space, so that the measured pattern reflects a specific orientation. We also average different orientations to get an averaged antenna pattern.

Fig. 8-12 shows our measurement result.[1] The results are organized by rows (different orientations) and columns (different systems).

We want to highlight the following observations from the result:

- A single big coil has the worst tolerance for different orientations. Visually its patterns have much more frequent rises and falls and the pattern shapes between different orientations are very different.

[1]To make sure the patterns reflect the transmitter's ability to deliver power, we scale down the total power to be below the ratings of the receiver circuit (10W in our implementation).

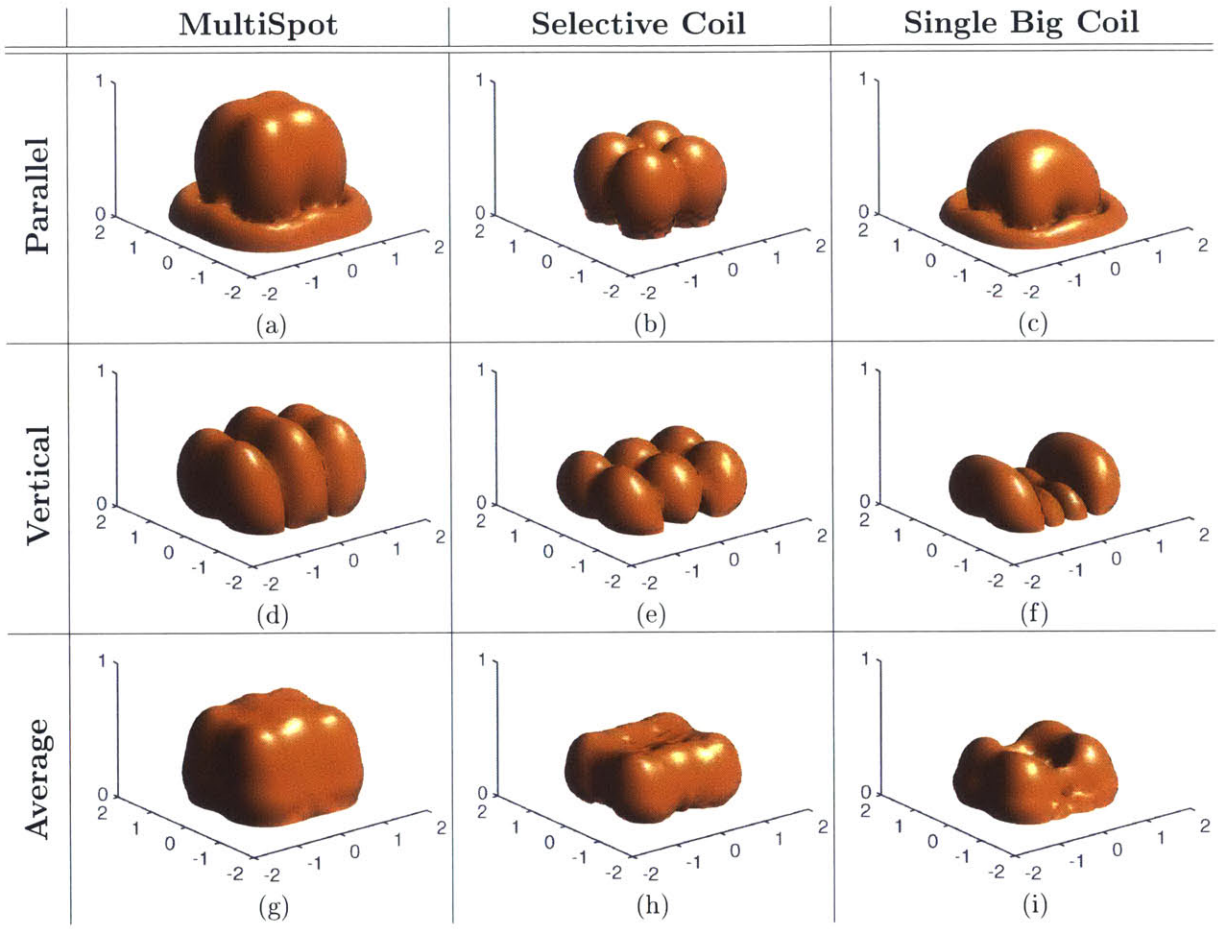

Figure 8-12: **Antenna Patterns of Different Systems & Orientations:** Different system per column, left to right: MultiSpot, selective coil, single coil; Different Rx orientation per row, top to bottom: parallel to Tx, perpendicular to Tx, averaged by different orientations. The axes are normalized by the transmitter surface area, i.e., transmitter occupies from -1 to 1 on both x and y axes.

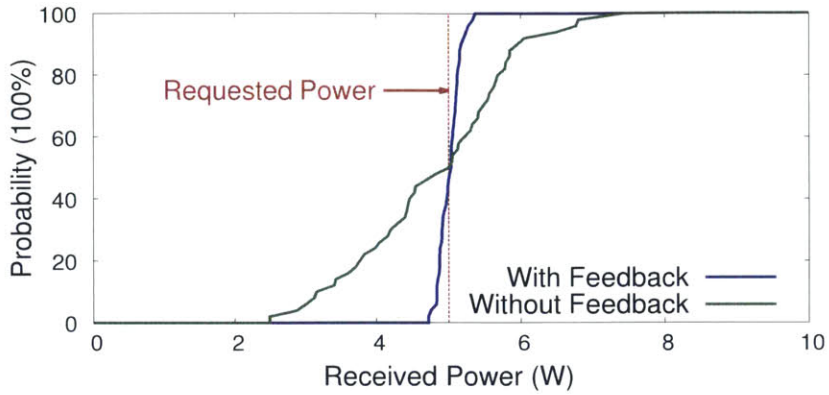

Figure 8-13: **CDF of Received Power at 5W Request Power:** Having feedback improves the accuracy of power control from 20% to 3%.

- Selective coils have much better orientation tolerance, however they have inferior range. Their maximal z projections of patterns are even smaller than the ones of a single big coil system. This is because by choosing one of multiple coils the system loses effective surface area.

- MultiSpot is able to deliver higher density power than the other systems. This is because it combines the benefits of both systems: surface area from the single big coil, and orientation tolerance from the selective coil system.

8.11 Accuracy of Power Control

In §5, we have presented how MultiSpot can have control over exactly how much power it delivers to each receiver. In this experiment, we aim to evaluate how accuate this control system is. Specifically, we ask the transmitter to deliver 5W to a resistive receiver. We measure the actual power that is delivered to the receiver, across different locations and orientations. Fig. 8-13 shows the CDF graph of how much power the receiver actually receives. Without receiver feeding back how much power it actually receives, the average control error is about 20%; adding feedback will improve this to only 3%.

Chapter 9

Conclusion

This thesis presents MultiSpot, a power hotspot that can charge multiple devices wirelessly and simultaneously in any orientation in their natural environment, at distances of up to 50cm without active user intervention. MultiSpot can be attached to an office desk, and used to charge surrounding electronic devices. It can also charge devices carried by the user once she is in the vicinity of a MultiSpot charger. This allows MultiSpot to be used in more practical scenarios, where the area of movement by the user is relatively constrained, such as desks, bed-stands, car seats, coffee shops, airports waiting seats, etc. When the user comes into the range, all of her devices will get charged automatically, including her phone in her pocket, her wearables on her wrist, and her tablet tossed on her table. We believe MultiSpot delivers the first wireless charging technology that really allows the user to forget about charging and delivers the real user experience promised by the vision of wirelss charging.

To achieve this, the thesis sets up a new theoretical framework, designs a new system architecture and implements a real-time prototype. The theoretical framework includes algorithms proven to be optimal to deliver maximal amount of power to the receivers, as well as to adapt to motion in smallest possible number of steps. It also includes an algorithm to manipulate the exact amount of power delivered to each receiver. On the system and implementation side, the thesis includes power circuit and sensing circuit design, coil design, and empirical evaluations that shows MultiSpot delivers the wireless power hotspot vision.

We also list a few challenging issues that this thesis does not address. They are not fundamental issues of MultiSpot, but rather potential improvements or extensive features that we believe are solvable under the MultiSpot framework. We leave them as directions for future work.

- *Designing transmitter coils in three dimensions*: in the thesis we have discussed the issue of designing the transmitter coils in two dimensions. One interesting question is, if we allow each coil to be three-dimensional, and we can lay out these coils freely in the three-dimensional space, what would be the optimal coil design? And how much improvement can such design have over the two-dimensional solution presented in this thesis?

- *Dealing with large foreign objects*: we have assumed in this thesis that there are no big metallic objects around the transmitter, e.g., the surface that the transmitter is mounted to is not entirely made of metal. The question is, how can we detect the existence of such metallic objects and what to do once we detect them? One possible solution would be, we can compare the total power transmitted by the transmitter, to the summation of power delivered to each receiver. If they are not equal, it means there might be metallic objects around. We could then nullify the magnetic field at their locations.

- *Interaction among different transmitters*: Imagine there are a few transmitters co-existing in the same environment. Their magnetic fields will interact with each other if they are not separated too far away. The best strategy would be for them to detect the existence of each other and cooperatively add up the magnetic fields at the receivers. In order to do so, we need to know how to detect the existence of other transmitters, how to communicate between the transmitters, and how to collectively decide the currents of all transmitters.

- *Soft-tuning of the receiver impedance*: the impedance of the receiver circuit is changing as a function of the mobile device battery percentage and the induced voltage on the receiver coil. As a result, a passive impedance matching circuit

used in this thesis can not ensure the impedances are always matched perfectly at all possible scenarios. An alternative solution is to employ active circuits like capacitive switching circuit. We propose as future work to address the tradeoff between the complexity these active impedance matching circuits require and the improvements of how well the impedances are matched.

Appendix A

Algorithm Pseudo-Code

The following pseudo-code summarizes the final algorithm running on the transmitter.

---

procedure MULTISPOT($\boldsymbol{Z}_T$)
  $\{\widetilde{\boldsymbol{M}}, \widetilde{\boldsymbol{Z}_R}\} \leftarrow$ BOOTSTRAP($\boldsymbol{Z}_T$)
  while true **do**
    Rx requests power $P_{R1}, P_{R2}, \cdots, P_{Rm}$
    Rx sends Tx its battery percentage $\eta_1, \cdots, \eta_m$
    Rx sends Tx its load function $f_1, \cdots, f_m$
    $\forall u$, solve V_{Ru} from $P_{Ru} = |V_{Ru}|^2 / f(V_{Ru}, \eta_u)$
    $\forall u$, the u-th diagonal entry of $\boldsymbol{Z}_R \leftarrow f(V_{Ru}, \eta_u)$
    $\vec{\boldsymbol{v}}_T^{\,c} \leftarrow$ CALCTXCONTROLVOLTAGE($\widetilde{\boldsymbol{Z}_R}, \widetilde{\boldsymbol{M}}, P_{R1}, \cdots, P_{Rm}$) ▷Alg. 3
    Apply $\vec{\boldsymbol{v}}_T^{\,c}$ ▷Try to deliver $P_{R1}, \cdots, P_{Rm}$ to receivers
    Measure $\vec{\boldsymbol{i}}_T$ on the transmitter
    Get $\vec{\boldsymbol{i}}_R$ communicated from Rx
    $\forall u$, the u-th diagonal entry of $\boldsymbol{Z}_R \leftarrow$ Impedance sent back from Rx
    $\forall u$, the u-th diagonal entry of $\widetilde{\boldsymbol{Z}_R} \leftarrow$ Impedance sent back from Rx
    if $\{\vec{\boldsymbol{i}}_R \neq j\omega \boldsymbol{Z}_R^{-1} \boldsymbol{M} \vec{\boldsymbol{i}}_T\}$ **then** ▷if the channel changes
      $\Delta\vec{\boldsymbol{u}} \leftarrow \frac{j}{\omega}\left(\vec{\boldsymbol{v}}_T^{\,c} - \boldsymbol{Z}_T \vec{\boldsymbol{i}}_T\right) - \widetilde{\boldsymbol{M}^\top} \vec{\boldsymbol{i}}_R$
      $\Delta\widetilde{\boldsymbol{M}} \leftarrow$ SOLVEA($\Delta\vec{\boldsymbol{u}}, \{\frac{\sqrt{P_{R1}}}{R_{R1}}, \cdots, \frac{\sqrt{P_{Rm}}}{R_{Rm}}\}$)
      $\widetilde{\boldsymbol{M}} \leftarrow \widetilde{\boldsymbol{M}} + \Delta\widetilde{\boldsymbol{M}}$
      $\widetilde{\boldsymbol{Z}_R} \leftarrow \widetilde{\boldsymbol{Z}_R} + \frac{\Delta\vec{\boldsymbol{y}} \Delta\vec{\boldsymbol{y}}^\top}{\Delta\vec{\boldsymbol{y}}^\top \vec{\boldsymbol{x}}}$ where $\Delta\vec{\boldsymbol{y}} = \omega^2 \widetilde{\boldsymbol{M}} \vec{\boldsymbol{i}}_T - \widetilde{\boldsymbol{Z}_R} \left(\boldsymbol{M}^\top\right)^\dagger \left(\vec{\boldsymbol{v}}_T - \boldsymbol{Z}_T \vec{\boldsymbol{i}}_T\right)$
      ▷ update $\widetilde{\boldsymbol{Z}_R}$
    end if
  end while
end procedure

procedure SOLVEA($\vec{\boldsymbol{y}}$, $\{a_1, \cdots, a_m\}$)
  ▷Solving $\min\{\|\boldsymbol{A}\|^2\}$, s.t. $\boldsymbol{A}\vec{\boldsymbol{x}} = \vec{\boldsymbol{y}}$
  ▷where $\vec{\boldsymbol{y}}$ is known,
  ▷but we only know the entrywise amplitude of $\vec{\boldsymbol{x}}$: $\{a_1, \cdots, a_m\}$
  $\forall i, y_i \leftarrow i$-th entry of $\vec{\boldsymbol{y}}$
  $\forall i, x_i \leftarrow e^{j\theta_i} a_i$
  repeat
    for $i = 2$ to m **do** ▷m is the length of vector $\vec{\boldsymbol{x}}$ and $\vec{\boldsymbol{y}}$
      $\theta_i \leftarrow \angle\left\{\sum_{k\neq i} x_k \overline{y_i}\right\} + \pi$
      $x_i \leftarrow e^{j\theta_i} a_i$
    end for
  until Changes in θ_i's are small
  $\vec{\boldsymbol{x}} \leftarrow [x_1, \cdots, x_m]^\top$
  $\boldsymbol{A} \leftarrow \frac{\vec{\boldsymbol{y}}\vec{\boldsymbol{x}}^*}{\vec{\boldsymbol{x}}^*\vec{\boldsymbol{y}}}$
  return $\boldsymbol{A}$
end procedure

procedure CALCTXCONTROLVOLTAGE($\boldsymbol{Z}_R$, $\boldsymbol{M}$, $P_{R1}, \cdots, P_{Rm}$)
  $\boldsymbol{H} \leftarrow j\omega \boldsymbol{Z}_R^{-1} \boldsymbol{M}$
  $\forall i,\ \vec{\boldsymbol{a}}_i \leftarrow i$-th column of $\boldsymbol{H}^\dagger$ multiplied by $\frac{\sqrt{P_{Ri}}}{R_{Ri}}$
  $\theta_1 \leftarrow 0$ ▷ We only care about relative phases so fix θ_1
  $\forall i \neq 1,\ \theta_i \leftarrow \text{rand}(0, 2\pi)$
  $\forall i,\ \vec{\boldsymbol{\xi}}_i \leftarrow e^{j\theta}\vec{\boldsymbol{a}}_i$
  repeat
    for $i = 2$ to m **do** ▷m is number of receivers
      $\theta_i \leftarrow \angle\left\{\sum_{k\neq i} \vec{\boldsymbol{\xi}}_k \vec{\boldsymbol{a}}_i^*\right\} + \pi$ ▷ Update according to Lemma 5.2.2
      $\vec{\boldsymbol{\xi}}_i \leftarrow e^{j\theta}\vec{\boldsymbol{a}}_i$
    end for
  until Changes in θ_i's are small
  $\forall u, I_{Ru} \leftarrow e^{j\theta_u}\sqrt{P_{Ru}/R_{R_u}}$
  $\vec{\boldsymbol{i}}_T \leftarrow \boldsymbol{H}^\dagger \vec{\boldsymbol{i}}_R$ ▷Lemma 5.2.1
  $\vec{\boldsymbol{v}}_T \leftarrow (\boldsymbol{Z}_T + \omega^2 \boldsymbol{M}^\top \boldsymbol{Z}_R^{-1} \boldsymbol{M})\vec{\boldsymbol{i}}_T$
  return $\vec{\boldsymbol{v}}_T$
end procedure

procedure BOOTSTRAP($\boldsymbol{Z}_T$)
  $i \leftarrow 1$ ▷i is the iteration counter
  while true **do**
    Apply $\vec{\boldsymbol{v}} \propto (i \mod N)$-th column of $\boldsymbol{Z}_T$ ▷ Diagonalize the current
    Measure $\vec{\boldsymbol{i}}_T$ on the transmitter
    $\Delta\vec{\boldsymbol{v}}_T \leftarrow \vec{\boldsymbol{v}} - \boldsymbol{Z}_T\vec{\boldsymbol{i}}_T$
    if $\Delta\vec{\boldsymbol{i}}_T \neq \vec{\boldsymbol{0}}$ **then** ▷if rx is detected
      $\boldsymbol{Z}_R \leftarrow$ impedance sent from the Rx

68: $\boldsymbol{M} \leftarrow \frac{\boldsymbol{Z}_R}{\omega^2 \Delta \vec{\boldsymbol{v}}_T \vec{\boldsymbol{i}}_T} \Delta \vec{\boldsymbol{v}}_T$
69: **end if**
70: $i \leftarrow i + 1$
71: **end while**
72: **return** $\widetilde{\boldsymbol{Y}}$
73: **end procedure**

Appendix B

Schematics

In this appendix we show the schematics of MultiSpot's implementation.

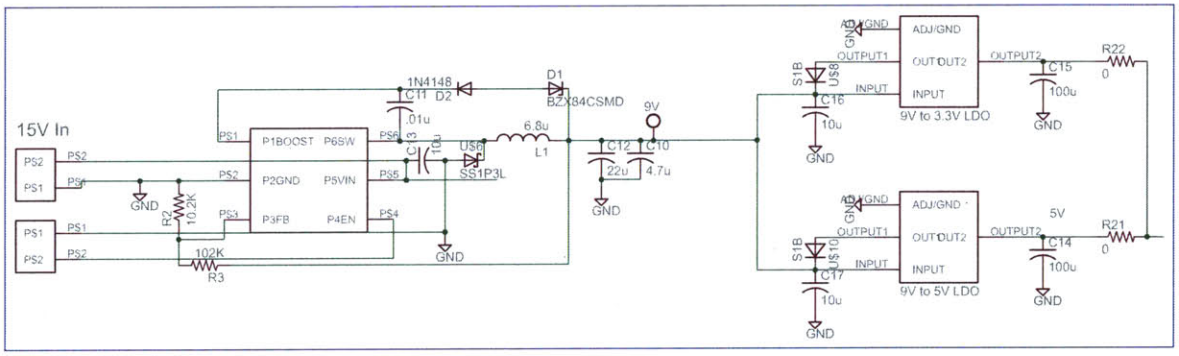

Figure B-1: **Tx Schematics, Part 1**

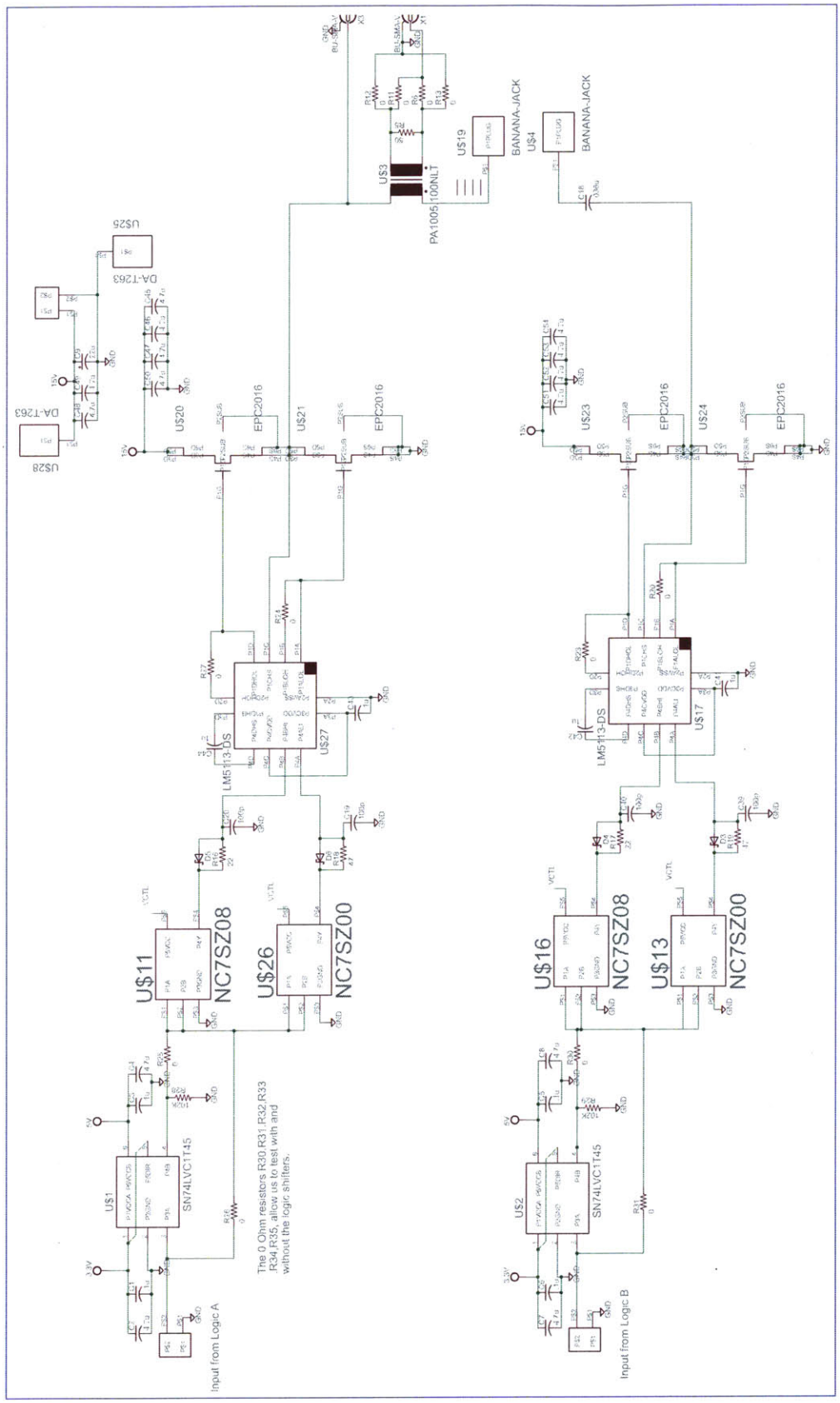

Figure B-2: **Tx Schematics, Part 2**

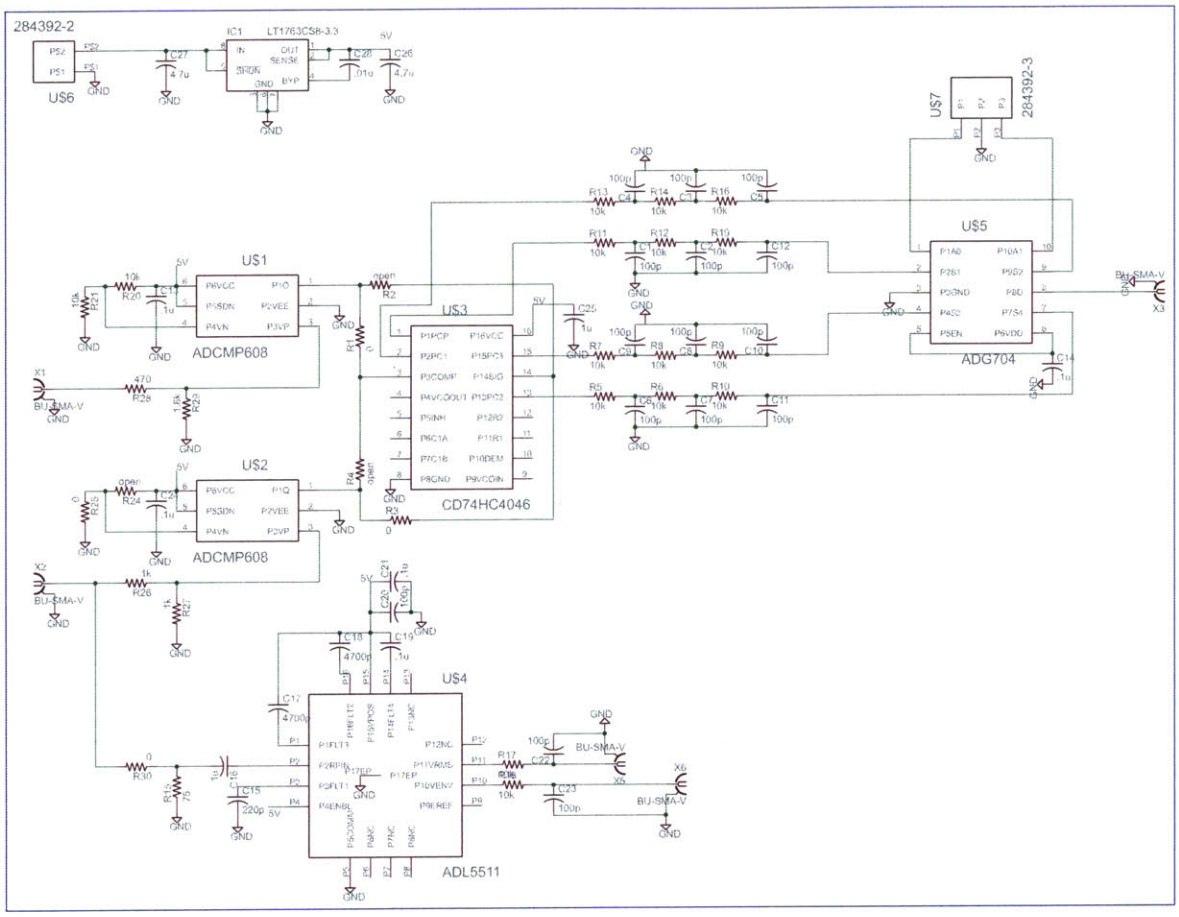

Figure B-3: **Tx Schematics, Part 3**

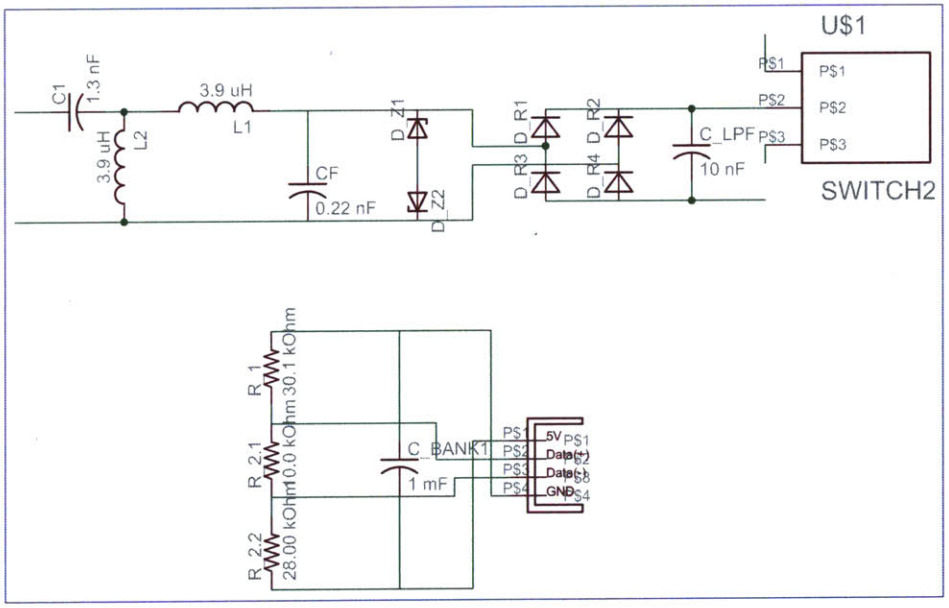

Figure B-4: **Rx Schematics, Part 1**

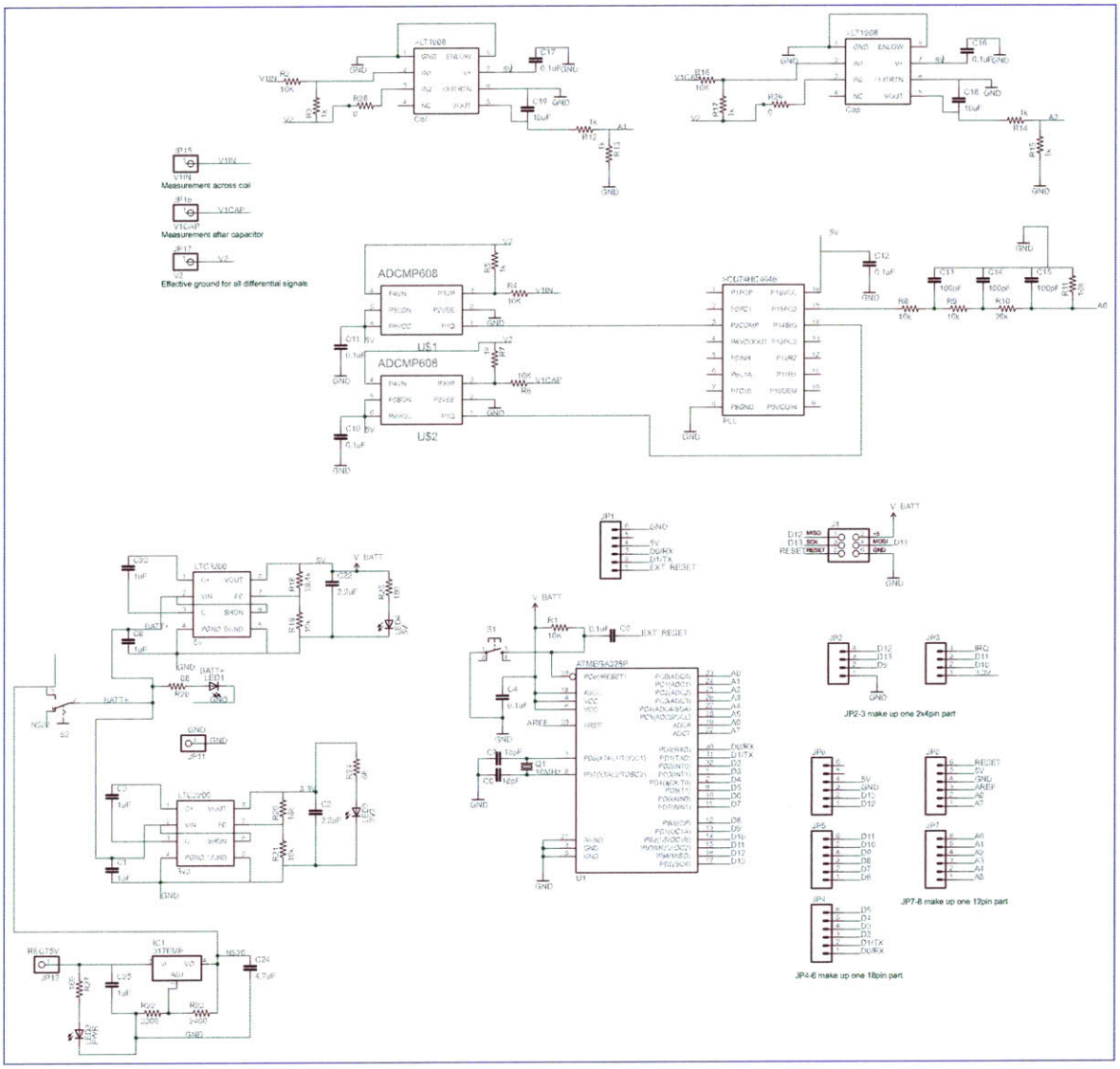

Figure B-5: **Rx Schematics, Part 2**

Bibliography

[1] Can witricity technology transfer power through walls or obstructions? http://witricity.com/technology/witricity-faqs/.

[2] Cota wireless power. Ossia Inc.

[3] Datasheet for Qi-enabled charger. RAV Power.

[4] Duracell powermat for 2 devices. Duracell Corp.

[5] Energizer dual inductive charger. Energizer.

[6] Hi-q high rf power mlc surface mount capacitors. AVX.

[7] Nokia wireless charging plate. Nokia Corp.

[8] Performance standards for microwave and radio frequency emitting products. Title 21, Part 1030, U.S. Food and Drug Administration.

[9] Proxi-point transmitter for the LTC4120. PowerByProxi.

[10] Rezence specification. Alliance for Wireless Power.

[11] Temperature gun infrared thermometers. Omega Inc.

[12] TX-200 dual wireless charging pad. LUXA2.

[13] AD8302: LF –2.7 GHz RF/IF gain and phase detector. Analog Devices.

[14] AD8333: DC to 50 MHz, dual I/Q demodulator and phase shifter data sheet (Rev. E). Analog Devices.

[15] Wattup. Energous Corp.

[16] Wi-charge. http://www.wi-charge.com/about.php.

[17] WiT-5000 development kit data sheet. WiTricity Corporation.

[18] Zynq-7000 all programmable soc (z-7010, z-7015, and z-7020): Technical reference manual. Xlin.

[19] Understanding li+ battery operation lessens charging safety concerns. Technical Report APP 4169, Maxim Integrated Products, Inc., 2008.

[20] Battery charging specification. Technical report, USB Implementers Forum, Inc., 2010.

[21] Low power wireless charger transmitter design using mc56f8006 dsc. Technical report, 2013.

[22] Rechargeable li-based batteries, 2013. Apple Inc.

[23] nRF51822 multiprotocol bluetooth low energy/2.4 GHz RF system on chip, 2014. Nordic Semiconductor.

[24] Prodigy: a hands-on demonstration system, 2014. Witricity Corp.

[25] Qi specification 1.1.2, 2014. Wireless Power Consortium.

[26] Wireless charging, at a distance, moves forward for ubeam, 2014. The New York Times.

[27] Enhancement-mode gallium nitride power transistor technology. Technical Report TB001, Efficient Power Conversion Corporation, 2015.

[28] Omid Abari, Hariharan Rahul, Dina Katabi, and Mondira Pant. Airshare: Distributed coherent transmission made seamless. In *IEEE INFOCOM*, 2015.

[29] Omid Abari, Deepak Vasisht, Dina Katabi, and Anantha Chandrakasan. Caraoke: An e-toll transponder network for smart cities. In *ACM SIGCOMM*, 2015.

[30] W. Abend, E. Bizzi, and P. Morasso. Human arm trajectory formation. *Brain*, 1982.

[31] Dukju Ahn and Songcheol Hong. Effect of coupling between multiple transmitters or multiple receivers on wireless power transfer. *Industrial Electronics, IEEE Transactions on*, 60(7), 2013.

[32] Dukju Ahn and Songcheol Hong. A study on magnetic field repeater in wireless power transfer. *Industrial Electronics, IEEE Transactions on*, 2013.

[33] Dukju Ahn and Songcheol Hong. A study on magnetic field repeater in wireless power transfer. *Industrial Electronics, IEEE Transactions on*, 60(1):360–371, 2013.

[34] Dukju Ahn and Songcheol Hong. A transmitter or a receiver consisting of two strongly coupled resonators for enhanced resonant coupling in wireless power transfer. *Industrial Electronics, IEEE Transactions on*, 2014.

[35] Christopher Atkeson and John Hollerbach. Kinematic features of unrestrained vertical arm movements. *The Journal of Neuroscience*, 5(9), 1985.

[36] Constantine A. Balanis. *Antenna Theory: Analysis and Design.* Wiley-Interscience, 2005.

[37] T.W. Barton, J.M. Gordonson, and D.J. Perreault. Transmission line resistance compression networks and applications to wireless power transfer. *Emerging and Selected Topics in Power Electronics, IEEE Journal of*, 3(1), 2014.

[38] Ken Binmore and Joan Davies. *Calculus Concepts and Methods.* Cambridge University Press, 2007.

[39] Daniel W. Bliss, Keith W. Forsythe, and Amanda M. Chan. Mimo wireless communication. *Lincoln Laboratory Journal*, 15(1), 2005.

[40] M. Borage, K.V. Nagesh, M.S. Bhatia, and S. Tiwari. Resonant immittance converter topologies. *Industrial Electronics, IEEE Transactions on*, 58(3), 2011.

[41] R. Bosshard, J. Muhlethaler, J.W. Kolar, and I. Stevanovic. Optimized magnetic design for inductive power transfer coils. In *Applied Power Electronics Conference and Exposition (APEC), 2013 Twenty-Eighth Annual IEEE*, pages 1812–1819, 2013.

[42] Stephen Budiansky. *Truth about Dogs.* 2000.

[43] Mike Butcher. Nikola labs launches iphone 6 case which harvests electricity from the air, 2015.

[44] Benjamin L Cannon, James F Hoburg, Daniel D Stancil, and Seth Copen Goldstein. Magnetic resonant coupling as a potential means for wireless power transfer to multiple small receivers. *Power Electronics, IEEE Transactions on*, 2009.

[45] J.J. Casanova, Zhen Ning Low, and Jenshan Lin. A loosely coupled planar wireless power system for multiple receivers. *Industrial Electronics, IEEE Transactions on*, 56(8), 2009.

[46] Jonathan Cassell. http://press.ihs.com/press-release/technology/apple-watch-spurs-rapid-growth-market-wireless-charging-wearable-technology.

[47] Scott Dearborn. Charging li-ion batteries for maximum run times. *Power Electronics Technology*, 2005.

[48] François C Delori, Robert H Webb, and David H Sliney. Maximum permissible exposures for ocular safety (ansi 2000), with emphasis on ophthalmic devices. 2007.

[49] P.L. Dowell. Effects of eddy currents in transformer windings. *Electrical Engineers, Proceedings of the Institution of*, 113(8), 1966.

[50] Yehui Han, O. Leitermann, D.A. Jackson, J.M. Rivas, and D.J. Perreault. Resistance compression networks for radio-frequency power conversion. *Power Electronics, IEEE Transactions on*, 22(1):41–53, 2007.

[51] James Harlow. *Electric Power Transformer Engineering.* CRC Press, 2004.

[52] James A. Harrington. Overview of power delivery and laser damage in fibers. In *Proc. SPIE 2966, Laser-Induced Damage in Optical Materials*, 1997.

[53] S. Hasanzadeh, S. Vaez-Zadeh, and A.H. Isfahani. Optimization of a contactless power transfer system for electric vehicles. *Vehicular Technology, IEEE Transactions on*, 61(8), 2012.

[54] Takehiro Imura, Hiroyuki Okabe, and Yoichi Hori. Basic experimental study on helical antennas of wireless power transfer for electric vehicles by using magnetic resonant couplings. In *Vehicle Power and Propulsion Conference, IEEE*, 2009.

[55] Jouya Jadidian and Dina Katabi. Magnetic MIMO: How to charge your phone in your pocket. In *ACM MobiCom*, 2014.

[56] Prateek Jain, Praneeth Netrapalli, and Sujay Sanghavi. Low-rank matrix completion using alternating minimization. In *Proceedings of the Forty-fifth Annual ACM Symposium on Theory of Computing*, STOC '13, pages 665–674, 2013.

[57] O. Kazanc, F. Maloberti, and C. Dehollain. High-q adaptive matching network for remote powering of uhf rfids and wireless sensor systems. In *Wireless Sensors and Sensor Networks (WiSNet), 2013 IEEE Topical Conference on*, pages 10–12, 2013.

[58] Marian K Kazimierczuk. Class d voltage-switching mosfet power amplifier. In *Electric Power Applications, IEEE*, 1991.

[59] Dr. Morris Kesler. Highly resonant wireless power transfer: Safe, efficient, and over distance. Technical report, WiTricity Corp, 2012.

[60] J. Kim, D. Kim, and Y. Park. Analysis of capacitive impedance matching networks for simultaneous wireless power transfer to multiple devices. *Industrial Electronics, IEEE Transactions on*, 2014.

[61] Jin-Wook Kim, Hyeon-Chang Son, Do-Hyun Kim, Kwan-Ho Kim, and Young-Jin Park. Analysis of wireless energy transfer to multiple devices using cmt. In *Microwave Conference Proceedings, IEEE*, 2010.

[62] Jiseong Kim, Jonghoon Kim, Sunkyu Kong, Hongseok Kim, In-Soo Suh, Nam Pyo Suh, Dong-Ho Cho, Joungho Kim, and Seungyoung Ahn. Coil design and shielding methods for a magnetic resonant wireless power transfer system. *Proceedings of the IEEE*, 101(6), June 2013.

[63] Sanghoek Kim, John S Ho, and Ada SY Poon. Wireless power transfer to miniature implants: Transmitter optimization. *Antennas and Propagation, IEEE Transactions on*, 2012.

[64] Anil Kumar, Shahriar Mirabbasi, and Mu Chiao. Resonance-based wireless power delivery for implantable devices. In *Biomedical Circuits and Systems Conference*. IEEE, 2009.

[65] André Kurs, Aristeidis Karalis, Robert Moffatt, J. D. Joannopoulos, Peter Fisher, and Marin Soljačić. Wireless power transfer via strongly coupled magnetic resonances. 317(5834), 2007.

[66] Andre Kurs, Robert Moffatt, and Marin Soljacić. Simultaneous mid-range power transfer to multiple devices. *Applied Physics Letters*, 2010.

[67] David Lay. *Linear Algebra and Its Applications*. Addison Wesley, 2002.

[68] B.J. Lee, A. Hillenius, and D.S. Ricketts. Magnetic resonant wireless power delivery for distributed sensor and wireless systems. In *Wireless Sensors and Sensor Networks (WiSNet), 2012 IEEE Topical Conference on*, Jan 2012.

[69] Pengfei Li and Rizwan Bashirullah. A wireless power interface for rechargeable battery operated medical implants. *Circuits and Systems II, IEEE Transactions on*, 2007.

[70] Udaya K Madawala and Duleepa J Thrimawithana. A bidirectional inductive power interface for electric vehicles in V2G systems. *Industrial Electronics, IEEE Transactions on*, 2011.

[71] Mariella Moon. uBeam demo video. http://www.engadget.com/2014/08/07/ubeam-wireless-charger-ultrasound/.

[72] T.K. Moon and W.C. Stirling. *Mathematical Methods and Algorithms for Signal Processing*. Prentice Hall, 2000.

[73] P. Morasso. Spatial control of arm movements. *Experimental Brain Research*, 42(2), 1981.

[74] Marco Panizza. Input-source impedance affects dc-dc converter performance. *Power Electronics*, 2010.

[75] Joseph A. Paradiso and Thad Starner. Energy scavenging for mobile and wireless electronics. *IEEE Pervasive Computing*, 4(1):18–27, 2005.

[76] Aaron N. Parks, Angli Liu, Shyamnath Gollakota, and Joshua R. Smith. Turbocharging ambient backscatter communication. In *Proceedings of the 2014 ACM Conference on SIGCOMM*, SIGCOMM '14, pages 619–630, 2014.

[77] Winfield Hill Paul Horowitz. *The Art of Electronics*. Cambridge University Press, 1989.

[78] Zoya Popovic and Branko Popovic. *Introductory Electromagnetics*. Prentice-Hall, 1999.

[79] Vijay Raghunathan, Aman Kansal, Jason Hsu, Jonathan Friedman, and Mani Srivastava. Design considerations for solar energy harvesting wireless embedded systems. In *Proceedings of the 4th International Symposium on Information Processing in Sensor Networks*, IPSN '05, 2005.

[80] A.K. RamRakhyani and G. Lazzi. Multicoil telemetry system for compensation of coil misalignment effects in implantable systems. *Antennas and Wireless Propagation Letters, IEEE*, 11, 2012.

[81] L. Roslaniec, A.S. Jurkov, A. Al Bastami, and D.J. Perreault. Design of single-switch inverters for variable resistance/load modulation operation. *Power Electronics, IEEE Transactions on*, 30(6), 2015.

[82] A.P. Sample, B.H. Waters, S.T. Wisdom, and J.R. Smith. Enabling seamless wireless power delivery in dynamic environments. *Proceedings of the IEEE*, 101(6), 2013.

[83] Lixin Shi, Paramvir Bahl, and Dina Katabi. Beyond sensing: Multi-ghz realtime spectrum analytics. In *12th USENIX Symposium on Networked Systems Design and Implementation (NSDI 15)*, 2015.

[84] Lixin Shi, Zach Kabelac, Dina Katabi, and David Perreault. Wireless power hotspot that charges all of your devices. In *ACM Mobicom*, 2015.

[85] C.R. Sullivan. Computationally efficient winding loss calculation with multiple windings, arbitrary waveforms, and two-dimensional or three-dimensional field geometry. *Power Electronics, IEEE Transactions on*, 16(1), 2001.

[86] Tsuyoshi Takagi. On an algebraic problem related to an analytic theorem of Carathéodory and Fejér and on an allied theorem of landau. *Japan. J. Math*, 1, 1924.

[87] Vamsi Talla, Bryce Kellogg, Benjamin Ransford, Saman Naderiparizi, Shyamnath Gollakota, and Joshua R. Smith. Powering the next billion devices with wi-fi. *arXiv:1505.06815v1*.

[88] Aaron Tilley. http://www.forbes.com/sites/aarontilley/2014/10/02/drayson-wireless-reemo.

[89] Bin Tong, Zi Li, Guiling Wang, and Wensheng Zhang. How wireless power charging technology affects sensor network deployment and routing. In *Distributed Computing Systems, IEEE*, 2010.

[90] David Tse and Pramod Viswanath. *Fundamentals of Wireless Communication*. Cambridge University Press, 2005.

[91] Gustav Hansson Marcus Uussalu. Analysis of the output impedance from switched dc/dc converters. Master's thesis, Chalmers University Of Technology, 2014.

[92] André Van Bezooijen, Maurice A. De Jongh, Freek Van Straten, Reza Mahmoudi, and Arthur H. M. Van Roermund. Adaptive impedance-matching techniques for controlling l networks. *Trans. Cir. Sys. Part I*, 57(2):495–505, 2010.

[93] Bingnan Wang, W. Yerazunis, and Koon Hoo Teo. Wireless power transfer: Metamaterials and array of coupled resonators. *Proceedings of the IEEE*, 101(6), 2013.

[94] Hao Wang. Multiple-resonator magnetic resonant coupling wireless power transfer. Master's thesis, University of Pittsburgh, Pittsburgh, PA, 2012.

[95] Benjamin Waters, Brody Mahoney, Vaishnavi Ranganathan, and Joshua Smith. Power delivery and leakage field control using an adaptive phased-array wireless power system. *(Accepted and Pre-Published) IEEE Transactions on Power Electronics.*

[96] Benjamin H. Waters, Alanson P. Sample, and Joshua R. Smith. Adaptive impedance matching for magnetically coupled resonators. In *Progress In Electromagnetics Research Symposium*, 2012.

[97] Liguang Xie, Yi Shi, Y Thomas Hou, and A Lou. Wireless power transfer and applications to sensor networks. *Wireless Communications, IEEE*, 2013.

[98] E. M. Yeatman. Advances in power sources for wireless sensor nodes. In *Proc. of BSN 2004*, pages 6–7, 2004.

[99] Markus Zahn. *Electromagnetic Field Theory: A Problem Solving Approach.* Krieger Pub Co, 2003.